# Evaluate, Modify, and Adapt the ConcreteWorks Software for Iowa's Use, Phase II

**Final Report**
**June 2025**

IOWA STATE UNIVERSITY
Institute for Transportation

**Sponsored by**
Iowa Highway Research Board
(IHRB Project TR-712)
Iowa Department of Transportation
(InTrans Project 16-581)

## About the Institute for Transportation

The mission of the Institute for Transportation (InTrans) at Iowa State University is to save lives and improve economic vitality through discovery, research innovation, outreach, and the implementation of bold ideas.

## Iowa State University Nondiscrimination Statement

Iowa State University does not discriminate on the basis of race, color, age, ethnicity, religion, national origin, pregnancy, sexual orientation, gender identity, genetic information, sex, marital status, disability, or status as a U.S. Veteran. Inquiries regarding non-discrimination policies may be directed to Office of Equal Opportunity, 2680 Beardshear Hall, 515 Morrill Road, Ames, Iowa 50011, telephone: 515-294-7612, email: eooffice@iastate.edu.

## Disclaimer Notice

The contents of this report reflect the views of the authors, who are responsible for the facts and the accuracy of the information presented herein. The opinions, findings and conclusions expressed in this publication are those of the authors and not necessarily those of the sponsors.

The sponsors assume no liability for the contents or use of the information contained in this document. This report does not constitute a standard, specification, or regulation.

The sponsors do not endorse products or manufacturers. Trademarks or manufacturers' names appear in this report only because they are considered essential to the objective of the document.

## Iowa DOT Statements

Iowa DOT ensures non-discrimination in all programs and activities in accordance with Title VI of the Civil Rights Act of 1964. Any person who believes that they are being denied participation in a project, being denied benefits of a program, or otherwise being discriminated against because of race, color, national origin, gender, age, or disability, low income and limited English proficiency, or if needs more information or special assistance for persons with disabilities or limited English proficiency, please contact Iowa DOT Civil Rights at 515-239-7970 or by email at civil.rights@iowadot.us.

The preparation of this report was financed in part through funds provided by the Iowa Department of Transportation through its "Second Revised Agreement for the Management of Research Conducted by Iowa State University for the Iowa Department of Transportation" and its amendments.

The opinions, findings, and conclusions expressed in this publication are those of the authors and not necessarily those of the Iowa Department of Transportation.

## Technical Report Documentation Page

| 1. Report No. | 2. Government Accession No. | 3. Recipient's Catalog No. |
|---|---|---|
| IHRB Project TR-712 | | |

| 4. Title and Subtitle | 5. Report Date |
|---|---|
| Evaluate, Modify, and Adapt the ConcreteWorks Software for Iowa's Use, Phase II | June 2025 |
| | 6. Performing Organization Code |

| 7. Author(s) | 8. Performing Organization Report No. |
|---|---|
| Kejin Wang (orcid.org/0000-0002-7466-3451), Kyle Riding (orcid.org/0000-0001-8083-554X), Anand Anand (orcid.org/0000-0001-9980-3038), Yogiraj Sargam (orcid.org/0000-0001-9980-3038), Jay Shen (orcid.org/0000-0002-8201-5569), and Charles Jahren (orcid.org/0000-0003-2828-8483) | InTrans Project 16-581 |

| 9. Performing Organization Name and Address | 10. Work Unit No. (TRAIS) |
|---|---|
| Institute for Transportation<br>Iowa State University<br>2711 South Loop Drive, Suite 4700<br>Ames, IA 50010-8664 | 11. Contract or Grant No. |

| 12. Sponsoring Organization Name and Address | 13. Type of Report and Period Covered |
|---|---|
| Iowa Highway Research Board<br>Iowa Department of Transportation<br>800 Lincoln Way<br>Ames, IA 50010 | Final Report |
| | 14. Sponsoring Agency Code |

**15. Supplementary Notes**

Visit https://intrans.iastate.edu for color pdfs of this and other research reports.


**16. Abstract**

This Phase II project contained two parts. Part A focused on the investigation of the characteristics and thermal properties of commonly used slags in Iowa cementitious materials and their effects on adiabatic temperature rise (ATR) in Iowa mass concrete structures. A new hydration model for slag-containing cementitious materials and a three-parameter ATR prediction model were developed and validated. These models were incorporated into the ConcreteWorks software, significantly improving its thermal predictions for mass concrete with slag. Part B focused on the development of a new seal slab component in the ConcreteWorks software. This new component is simple, user friendly, and well-integrated into the existing ConcreteWorks software and enables the prediction of the temperature profile of a bridge footing placed on a seal slab.

In Part A, the research included the following: (1) characterizing physical and chemical properties of slags and concrete materials, (2) studying slag's effect on cement hydration using isothermal calorimetry, (3) evaluating temperature rise in mass concrete with various slag types and dosages using semi-adiabatic calorimetry, (4) testing large concrete blocks with various slag replacements, (5) developing and validating the ATR prediction model for slag concrete, and (6) integrating the models into the ConcreteWorks software. In Part B, the research included the following: (1) developing a new seal slab component in the ConcreteWorks software and (2) conducting trial analyses to investigate the effects of the time of footing placement, the sizes of the footing and seal slab, and environmental conditions on the temperature profile of a bridge footing placed on a seal slab.

The updated ConcreteWorks software now features enhanced input parameters and equations for better heat prediction, confirmed through thermal and sensitivity analyses. The improved slag hydration model, which accurately incorporates slag's chemical properties, enhances temperature prediction accuracy for concrete containing slag. The maximum core temperature of a footing placed on a seal slab was generally found to be higher than that of a footing with no seal slab. In addition, it was found that a seal slab generally enhances the capacity for heat retention in the footing, keeping the core temperature of the footing high for a longer period.


| 17. Key Words | 18. Distribution Statement |
|---|---|
| 4C-Temp&Stress—ConcreteWorks—mass concrete—slag-containing mixes—thermal analysis | No restrictions. |

| 19. Security Classification (of this report) | 20. Security Classification (of this page) | 21. No. of Pages | 22. Price |
|---|---|---|---|
| Unclassified. | Unclassified. | 119 | NA |

**Form DOT F 1700.7 (8-72)** **Reproduction of completed page authorized**

# EVALUATE, MODIFY, AND ADAPT THE CONCRETEWORKS SOFTWARE FOR IOWA'S USE, PHASE II

**Final Report**
**June 2025**

**Principal Investigator**
Kejin Wang, Professor
Department of Civil, Construction, and Environmental Engineering, Iowa State University

**Co-Principal Investigators**
Kyle Riding, Professor
Department of Civil and Coastal Engineering, University of Florida

Charles T. Jahren, Emeritus Morrill Professor
Jay Shen, Associate Professor
Department of Civil, Construction, and Environmental Engineering, Iowa State University

**Research Assistants**
Anand Anand and Yogiraj Sargam

**Authors**
Kejin Wang, Anand Anand, Kyle Riding, Yogiraj Sargam, Jay Shen, and Charles Jahren

Sponsored by
Iowa Highway Research Board and
Iowa Department of Transportation
(IHRB Project TR-712)

Preparation of this report was financed in part
through funds provided by the Iowa Department of Transportation
through its Research Management Agreement with the
Institute for Transportation
(InTrans Project 16-581)

A report from
**Institute for Transportation**
**Iowa State University**
2711 South Loop Drive, Suite 4700
Ames, IA 50010-8664
Phone: 515-294-8103 / Fax: 515-294-0467
https://intrans.iastate.edu

## TABLE OF CONTENTS

## LIST OF FIGURES

## LIST OF TABLES

## ACKNOWLEDGMENTS

The authors would like to thank the Iowa Department of Transportation (DOT) and Iowa Highway Research Board (IHRB) for sponsoring this research.

The technical advisory committee (TAC) for this project included Curtis Carter, James Nelson, Wayne Sunday, Todd Hanson, James Hauber, and Ahmad Abu-Hawash. The authors gratefully acknowledge their valuable suggestions throughout the course of this project. Special thanks are also extended to Curtis Carter for leading an outstanding effort to review and provide valuable comments on the project report.

The authors also greatly appreciate the frequent help provided by Iowa State University staff and students, including laboratory managers Doug Wood and Owen Steffens of the Structural Engineering Research Laboratory, research technician Jeremy McIntyre of the Portland Cement Concrete Research Laboratory, and graduate students Bharath Melugiri Shankaramurthy, Kwangwoo Wi, and Siraj Al Qunaynah of the Department of Civil, Construction and Environmental Engineering, during the casting and testing of large concrete blocks.

## EXECUTIVE SUMMARY

This Phase II project contained two parts. Part A focused on the investigation of the characteristics and thermal properties of commonly used slags in Iowa cementitious materials and their effects on adiabatic temperature rise (ATR) in Iowa mass concrete structures. In this part, a new hydration model for slag-containing cementitious materials and a three-parameter (3P) ATR prediction model were developed and validated. These models were incorporated into the ConcreteWorks software, significantly improving its thermal predictions for mass concrete with slag. Part B focused on the development of a new seal slab component in the ConcreteWorks software. This new component is simple, user friendly, and well-integrated with the existing software and enables the prediction of the temperature profile of a bridge footing placed on a seal slab.

The sections below summarize the tasks, activities, and major findings of each part of the project.

### Part A: Improving Thermal Prediction for Mass Concrete Containing Slags

*Task A-1: Characterization of slags and other concrete materials used*

The characterization included analyzing the fineness, chemical composition, and crystalline/glass phases of the slags commonly used in Iowa, and the characteristics of the slags were analyzed through Blaine's method, X-ray fluorescence (XRF), and X-ray diffraction (XRD), respectively.

*Task A-2: Study of the effect of the slags on cement hydration using isothermal calorimetry measurements*

In this task, binary mixes made with portland cement and different slags (Grade 100 or 120) with various slag replacement levels (0%, 20%, 50%, and 75% by weight of binder) were investigated. For each paste mix, isothermal calorimetry tests were performed at four different temperatures (10°C, 20°C, 30°C, and 40°C). Based on the measurements, the apparent activation energy ($E_a$) of the mix was determined, and the results were also used for the development of the slag hydration model.

*Task A-3: Evaluation of the effect of slag types and replacement dosages on the temperature rise in mass concrete using semi-adiabatic calorimetry tests*

In this task, mass concrete mixes, made with Iowa Department of Transportation (DOT) C4 mix proportion and binary cementitious materials, containing 0%, 25%, 50%, and 75% of slag replacements for cement, were evaluated. The fresh properties of these concrete mixes were tested for slump, unit weight, air content, and initial temperature measurement. Their thermal and hardened properties were tested for semi-adiabatic calorimetry, compressive strength, and maturity. The temperature development of each concrete mix was monitored using the semi-

adiabatic calorimeter drum built in the previous phase of this research. The measured data were then converted to true adiabatic temperature.

*Task A-4: Temperature monitoring from large concrete blocks containing various slag replacements*

Four large concrete block specimens, with dimensions of 3 ft × 3 ft × 4 ft, were built to obtain the ATR of concrete containing various levels of slag replacements for cement (0, 25, 50, and 75 wt.%). Six temperature sensors were installed in different locations of each specimen. The sensors recorded the concrete temperature data for a period of 28 days. The recorded temperature profile data were used in Task A-6 for validation of the newly developed ATR model.

*Task A-5: Establishment of a new slag hydration model*

In this task, a thorough literature search was conducted to collect the temperature data of concrete mixes containing slag-cement binary binder for the development of a slag hydration model. The collected data include the dimensions of the mass concrete structures, slag and cement chemical and physical properties, concrete mix design, thermal properties (such as ATR profiles and activation energy), and fresh and hardened concrete properties. These data were processed, filtered, and refined. Statistical regression analysis was performed to generate prediction equations for the heat parameters in the slag hydration model. These models/equations were further validated in Task A-6.

*Task A-6: Development and validation of ATR prediction model for concrete containing slag*

In this task, 4C Stress&Temp software (4C) was used to convert the measured concrete block temperature data (with limited heat loss) into true adiabatic temperatures (with zero heat loss). To convert the measured temperature data from the concrete blocks, made with 0%, 25%, 50%, and 75% slag replacement for cement as described in Chapter 4 into true adiabatic temperature, the team's approach was to change the heat parameters ($Q_\infty$, $\tau_e$, $\alpha$) in 4C so that the concrete block temperature profile simulated using 4C matched the temperature rise and the maximum temperature profile measured from the large concrete block tests. Using the obtained heat parameters, 4C simulated the true adiabatic temperatures of these large concrete blocks, and the results were compared with the true adiabatic temperatures of these blocks predicted using the ATR model in ConcreteWorks modified with the new slag hydration model developed in Task A-5.

Six concrete mixes, three of which were the large concrete block mixes containing 25%, 50%, and 75% slag and three of which were from the literature, were used for the model validation. Refinements were made on the heat parameters so that the adiabatic temperature profiles of the six mixes predicted using the refined heat parameter equations were comparable to their measured temperature profiles that were obtained from the above-mentioned 4C analyses. The model refinement was completed when the absolute error of the prediction from the newly modified ConcreteWorks software decreased to about 15%.

*Task A-7: Incorporation of the new models in ConcreteWorks*

In this task, the refined and validated hydration and ATR models for slag-containing concrete were summarized and then incorporated into the ConcreteWorks software. Using the updated version of the ConcreteWorks software, some trial analyses were performed, and the temperature profiles of the trial mixes predicted by the new and older version of the ConcreteWorks software were compared. Finally, a sensitivity study was conducted, and some limitations of the new models in the updated (new) ConcreteWorks software were identified.

The updated ConcreteWorks software now features enhanced input parameters and equations for better heat prediction, confirmed through thermal and sensitivity analyses. The improved slag hydration model, which accurately incorporates slag's chemical properties, enhances temperature prediction accuracy for concrete containing slag.

The following **observations** were made during the present study:

- Based on the isothermal calorimetry measurements, it was observed that slag replacement does not necessarily decrease the total heat of hydration. When the slag replacement increases from 25% to 75%, the initial rate of heat generation (about 7 to 20 hours after testing) decreases. However, at a later age (40 to 80 hours), depending on the temperature and percent replacement), the rate of heat generation and the accumulated heat of slag mixes surpassed that of the control mix (0% slag replacement for cement), indicating the late-age reactivity of slag is high. The surpassing effect occurred earlier as the testing temperature increased, indicating higher reactivity and sensitivity of slag at high temperatures.
- In this study, the major difference between the slag with two different grades, Grade 100 (S1) and Grade 120 (S2) is their fineness. The finer slag (Grade 120) had a significantly higher rate of heat and total heat of hydration compared to Grade 100 slag mixes. This effect was increased at higher temperatures, suggesting that the mass concrete slag physical properties (such as fineness) can be a key factor that influences the maximum temperature rise.
- Literature data were collected to get the ATR, slag and cement compositions, and mix designs of mass concrete structures. These data were used in the 3P and six-parameter (6P) models to get the best-fit hydration parameters. Based on the fit ($R^2$ value), the 3P model was chosen for further advancement.
- The previous ConcreteWorks model was modified using regression analysis to include slag replacement dosages as well as slag chemical properties. Slag fineness was excluded due to the lack of availability in the literature data. A second-order polynomial regression was fitted to get the best $R^2$ fit, and cases of over-fitting (on higher order polynomial) were avoided.
- The model was verified using 4C analysis and large concrete block measurements. The true adiabatic temperature was obtained using the 4C software, and then it was plotted in the 3P model. The new model was also used to model the temperature rise. Both results were compared, and the newly developed model showed a 20% reduction (from 35% to 15.6%) in absolute error.
- Overall, the new ConcreteWorks model predicts the early-age temperature profile with higher accuracy and predicts the maturity and strength of Iowa mass concrete quite well.

The features in the updated (new) ConcreteWorks software include the following:

- The default input values in the ConcreteWorks software have been updated to contain slag chemical compositions based on the results obtained from this research project (both laboratory and modeling). They are available for use when analyzing Iowa mass concrete and can also be changed when measured data are available.
- The new slag hydration model includes the chemical properties of the slag, which makes the predictions of the new version of ConcreteWorks more accurate.
- The temperature prediction of the concrete has improved in the newly modified ConcreteWorks software, when compared with the previous version of ConcreteWorks. The absolute error of the prediction from the newly modified ConcreteWorks software decreased from 35% (resulting from the previous ConcreteWorks software) to 15.6%.
- The newly developed model includes the hydration parameter equations for both the Bogue and Rietveld methods, and these equations are easy to implement.

The following are **recommendations** for effective use of the new ConcreteWorks software and for further research:

- This study shows that slag replacement dosage significantly influences maximum and 28-day concrete temperatures. Adiabatic temperature sensitivity is highest for slag replacement dosage, followed by slag aluminum and calcium contents. These factors are crucial for future mass concrete material selection, mix design, and thermal control.
- When extreme inputs, such as 80% slag replacement dosage, were used, the adiabatic temperature profile predicted by the new ConcreteWorks software shows a sudden temperature drop. This occurs due to limitations in the software models, which were developed with a relatively small amount of data. As a result, the prediction may perform poorly when applied to unseen data.
- The modified ConcreteWorks software has a newly developed hydration model, which includes slag chemical properties, but it still does not include slag physical properties (fineness). In the future, this model can be modified by considering fineness as an input parameter (when enough literature data are available to conduct the analysis).
- The modified version of ConcreteWorks does not take the chemical properties of any other supplementary cementitious materials, such as fly ash and silica fume, into account. In the future, based on literature and available data, the model can be further improved, and a new model can be developed for tertiary cementitious systems.
- In this study, only binary slag cement with slag was studied. Low-carbon cement, such as limestone cement, which has been increasingly used in Iowa, calcined clay—containing cement and ternary cement, which are increasingly used in Iowa, were not included in the present study. Investigation into the thermal behavior of mass concrete containing low-carbon cement, especially limestone cement, may be necessary in the very near future.
- The modified version of ConcreteWorks can be used to generate a temperature development profile at any point and the temperature differential between any two points in the mass concrete member. In the future, the generated results can be compared with the Iowa DOT temperature differential limits, and the information on the comparison can be incorporated into the software.

**Part B: Developing a New Component in ConcreteWorks for Seal Slab–Footing Thermal Analysis**

As explained in Chapter 8, the team originally proposed to perform this part of the project through a field investigation. However, a suitable bridge construction site was not available during the project timeframe. Therefore, without the use of field data, the team simply developed a new component capable of modeling concrete seal slabs placed underneath rectangular footings. This new component has been incorporated into the existing ConcreteWorks software.

*Task B-1: Developing a new seal slab component in ConcreteWorks*

In this task, seal slabs were simply modeled in two-dimensional analysis cases for rectangular footings. Before the footing is virtually placed on the seal slab, the seal slab is modeled the same as a rectangular footing without a seal slab placed underneath. After a user-defined seal slab curing period, the curing material on top of the seal slab is removed, and the footing is virtually placed on top of the seal slab. The input parameters of the seal slab component include seal slab and footing dimensions, mix design, time of footing placement, environmental conditions, and so on. The output parameters are the same as those for a footing with no seal slab. In the software, the user can select a footing with or without a seal slab for temperature analysis. By comparing the temperature profiles of the footing with and without a seal slab, the user can understand the effects of the seal slab on the temperature profile of the footing above.

*Task B-2: Conducting trial analyses using the new seal slab component in ConcreteWorks*

Using the updated ConcreteWorks software from Task B-1, a series of trial analyses were conducted. These trial analyses investigated the effects of (1) the time of footing placement, (2) the sizes of the seal slab and footing, and (3) the construction season or environmental temperature on the temperature profile of a footing with a seal slab.

The following **observations** were made from the Part B study:

- The new component is simple, user friendly, and well integrated with the existing ConcreteWorks software.
- The maximum core temperature of a footing placed on a seal slab is generally higher than that of a footing with no seal slab (by approximately 3°C).
- The maximum core temperature of a footing placed on a seal slab drops much more slowly than that of a footing without seal slab. That is, a seal slab enhances the capacity for heat retention in the footing, keeping the core temperature of the footing high for a longer period.
- The temperature profile of a footing placed on a seal slab can be affected by factors like seal slab and footing dimensions, time of footing placement, environmental temperature, the mix design of the seal slab and footing, and so on. Additional sensitivity studies can be conducted to investigate the effects of various seal slab mix designs on the temperature profile of the footings placed above.

# 1. INTRODUCTION

This Phase II project contained two parts.

Part A focused on the investigation of the characteristics and thermal properties of commonly used slags in Iowa cementitious materials and their effects on adiabatic temperature rise (ATR) in Iowa mass concrete structures. A new hydration model for slag-containing cementitious materials and a three-parameter ATR prediction model were developed and validated. These models were incorporated into the ConcreteWorks software, significantly improving its thermal predictions for mass concrete with slag.

Part B focused on the development of a new seal slab component in the ConcreteWorks software. This new component is simple, user friendly, and well integrated into the existing ConcreteWorks software and enables the prediction of the temperature profile of a bridge footing placed on a seal slab.

## 1.1. Background

### *1.1.1. Part A – Background*

In Phase I of Iowa Highway Research Board (IHRB) Project TR-712 (Wang et al. 2020), the researchers found that concrete mixes containing slag, especially at a high replacement level (≥50%), might undergo a higher ATR than concrete with the same amount of fly ash (Figure 1-1a) or even concrete with pure portland cement (Moon et al. 2018). According to the literature, a key reason for this is that the pretreatments used for modern slags alter their fineness, particle size distribution, and calcium sulfate content, and such slags affect the hydration of cement differently from those used in previous years (Barnett et al. 2005, Chini and Parham 2005, Gruyaert et al. 2010). These changes in slag characteristics have not been addressed in the current ConcreteWorks software. In addition, two adjacent peaks are commonly seen in the heat generation curve of cement containing slag, but only a single peak is seen in the heat generation curve of ordinary portland cement (OPC) and OPC-fly ash cement (Figure 1-1b) (Barnett et al. 2005). Prior to the present study, the prediction models in ConcreteWorks did not consider the occurrence of the two hydration peaks, thus leading to an inaccurate estimation of the temperature of concrete containing slag.

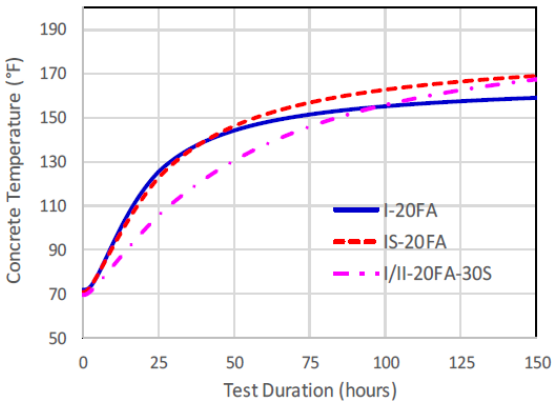


(a) Adiabatic temperature

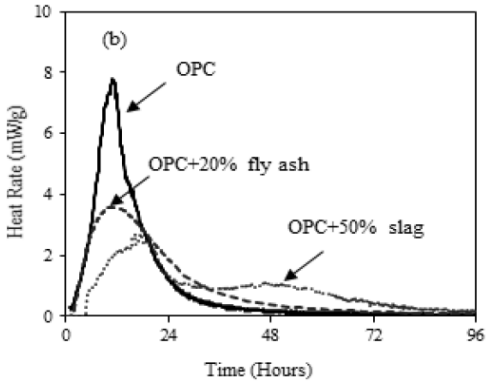


(b) Semi-isothermal calorimetry curve

Wang et al. 2020

**Figure 1-1. Temperature rise and heat generation of concrete containing different cementitious materials**

Later, the research team used ConcreteWorks to conduct a preliminary thermal analysis for a mass concrete project on I-74 in Iowa, where slag was used in the concrete mix. The results showed that all of the maximum and differential temperatures predicted using ConcreteWorks were more than 10°F higher than those measured during the project. Because slag is commonly used in Iowa mass concrete mixes, additional study is necessary to modify ConcreteWorks to further improve the thermal predictions for Iowa mass concrete containing slag.

### *1.1.2. Part B – Background*

Mass concrete is often associated with large structures like bridge foundations. During the construction of bridge foundations, cofferdams are built to form watertight enclosures surrounding excavations. These enclosures typically consist of sheet piling driven around the perimeter of the excavation. A concrete seal coat is placed within the sheet piling, and the bridge footing is then built on the seal coat slab. Usually, a lean concrete mix is used for the seal coat slab, and thermal cracking due to the heat of cement hydration is not much of a concern in this concrete component. Therefore, the concrete mixes used for the seal coat slabs are usually not considered mass concrete, and no temperature control of the seal coat slab concrete is believed as necessary. However, a major concern is that the heat development in an underwater seal coat slab can consequently affect the early-age temperature development in the footing placed above it, and the current ConcreteWorks software does not have a component for predicting the concrete temperature of the seal coat slabs.

## 1.2. Goals and Objectives

### *1.2.1. Part A – Objectives*

The present research project (TR-712, Phase IIA) aimed to provide a better understanding of the hydration of slag and its effects on temperature development in the mass concrete used in Iowa.

The goal of the study was to improve the thermal predictions made by ConcreteWorks for Iowa mass concrete containing slag.

The specific objectives of the Part A study were as follows:

- Investigate the characteristics of the slags commonly used in Iowa and their effects on the ATR in Iowa mass concrete structures
- Establish hydration model of binary and ternary cementitious materials containing slag
- Develop an appropriate ATR prediction model that will be incorporated into ConcreteWorks
- Validate the ATR prediction model and improve the thermal prediction of ConcreteWorks for Iowa mass concrete containing slag

#### *1.2.2. Part B – Objectives*

The objective of the Part B study was to develop a new component in the ConcreteWorks software that enables the following:

- Prediction of the temperature profile of seal coat concrete slabs in bridge foundations
- Analysis of the effect of the temperature of seal coat concrete slabs on the temperature behavior of bridge footings placed above them

### 1.3. Project Tasks

#### *1.3.1. Part A – Tasks*

The following tasks were conducted for the Part A study of this research project:

*Task A-1: Characterization of slags and other concrete materials used*

Two nationally available slags (Grades 100 and 120, Lafarge Holcim) and one locally available slag (Grade 100, Manatt's, Inc.) were collected with the help of the project's technical advisory committee (TAC) members. The fineness, chemical composition, and crystalline/glass phases of the slags were analyzed through Blaine's method, X-ray fluorescence (XRF), and X-ray diffraction (XRD), respectively. The XRF testing was performed at the Iowa Department of Transportation (DOT) facilities in Ames, Iowa, and the fineness of the slag was provided by the manufacturer.

*Task A-2: Study of the effect of the slags on cement hydration using isothermal calorimetry measurements*

To obtain the parameters needed for the development of the heat of cement hydration model, isothermal calorimetry measurements for the corresponding cement pastes are necessary. In this

task, isothermal calorimetry measurements were conducted for eight paste mixes prepared using the materials collected in Task A-1. Selected binary mixes made with portland cement and different slags (Grade 100 or 120) with various slag replacement levels (0%, 20%, 50%, and 75% by weight of binder) were investigated. For each paste mix, isothermal calorimetry tests were performed at four different temperatures (10°C, 20°C, 30°C, and 40°C). Thus, over 40 tests were run, and each test was run for 7 to 10 days, depending upon the thermal behavior of the pastes. Based on the measurements, the apparent activation energy ($E_a$) of the mix, indicating the sensitivity of the hydration reaction to temperature, was determined, and the results were used to understand how slag replacement alters cement hydration and to provide a necessary component for the development of the slag hydration model.

*Task A-3: Evaluation of the effect of slag types and replacement dosages on the temperature rise in mass concrete using semi-adiabatic calorimetry tests*

To develop the model for the prediction of the true ATR, eight mass concrete mixes were evaluated using the semi-adiabatic calorimetry device that was built in TR-712 Phase I. These concrete mixes had the same mix proportions as those used in TR-712 Phase I (Iowa DOT C4 mix) but with the same paste compositions as those used in Task A-2. The fresh properties of the laboratory-prepared/ready mix plant-delivered mixes were tested for slump, unit weight, air content, and placement temperature. Hardened and thermal properties were tested using semi-adiabatic calorimetry, compressive strength, and maturity. Compressive strength and maturity tests were performed at the concrete age of 3, 7, 28, and 56 days. The temperature development of each concrete mix was monitored using the semi-adiabatic calorimeter drum built in the previous phase of this research. The measured data were then converted to true adiabatic temperature.

*Task A-4: Temperature monitoring from large concrete blocks containing various slag replacements*

Four large concrete block specimens, with dimensions of 3 ft × 3 ft × 4 ft, were built to obtain the ATR of concrete containing various levels of slag replacements for cement (0, 25, 50, and 75 wt.%). Six temperature sensors were installed in different locations of each specimen. The sensors recorded the concrete temperature data for a period of 28 days. The recorded temperature profile data were used in Task A-6 for validation of the newly developed ATR model.

*Task A-5: Establishment of a new ATR prediction model for concrete mixes containing slag*

In the previous ConcreteWorks hydration model, the heat generation of cement and that of slag are simply superimposed under an assumption that there is no interaction between these materials. This task examined this assumption using two steps as follows:

1. To develop a model that simulates the two peaks as observed in the rate of the heat generation curve of slag-containing mixes, as shown in Figure 1-1b, which is referred to as the slag hydration model

2. To develop a model that predicts the true ATR of concrete containing slag based on the parameters obtained from the slag hydration model and semi-adiabatic calorimetry measurements (Task A-3)

Because true ATR (with zero heat loss) is almost impossible to measure in laboratory testing, semi-adiabatic calorimetry tests (allowing a small amount of heat loss), which provide an estimate of the heat generation characteristics of a concrete mixture, are often performed in practice because of their relative simplicity. During the semi-adiabatic calorimetry tests, the small amount of heat loss was measured. By adding the measured heat loss back to the heat generated during the test, the measured temperature values of the tested concrete were then corrected. Finally, the concrete temperature rise that would occur under fully adiabatic conditions, i.e., ATR, was backcalculated based on the hydration model parameters.

To develop the slag hydration and true adiabatic temperature prediction models, data for slag-containing mixes were collected from the literature. The collected data include the dimensions of the mass concrete structures, slag and cement chemical and physical properties, concrete mix design, thermal properties (such as ATR profiles and activation energy), and fresh and hardened concrete properties. These data were processed, filtered, and refined to develop the model. Statistical regression analysis was performed to generate prediction equations for the model parameters in terms of the physical and chemical properties of cement and slag. These models/equations were further validated in Task A-6.

*Tasks A-6: Development and validation of the developed prediction model using large concrete block specimens*

In this task, 4C Stress&Temp software (4C) was used to convert the measured concrete block temperature data (with limited heat loss) into true adiabatic temperatures (with zero heat loss). To convert the measured temperature data from the concrete blocks, made with 0%, 25%, 50%, and 75% slag replacement for cement as described in Chapter 4 into true adiabatic temperature, the team's approach was to change the heat parameters ($Q_\infty$, $\tau_e$, $\alpha$) in 4C so that the concrete block temperature profile simulated using 4C matched the temperature rise and the maximum temperature profile measured from the large concrete block tests. Using the obtained heat parameters, 4C simulated the true adiabatic temperatures of these large concrete blocks, and the results were compared with the true adiabatic temperatures of these blocks predicted using the ATR model in ConcreteWorks modified with the new slag hydration model developed in Task A-5.

Six concrete mixes, three of which were the large concrete block mixes containing 25%, 50%, and 75% slag and three of which were from the literature, were used for the model validation. Refinements were made on the heat parameters so that the adiabatic temperature profiles of the six mixes predicted using the refined heat parameter equations developed in Task A-5 were comparable to their measured temperature profiles that were obtained from the above-mentioned 4C analyses. The model refinement was completed when the absolute error of the prediction from the newly modified ConcreteWorks software decreased to about 15%.

*Task A-7: Incorporation of the new models in ConcreteWorks*

In this task, the refined and validated hydration and ATR models for slag-containing concrete were summarized and then incorporated into the ConcreteWorks software. Using the updated version of the ConcreteWorks software, some trial analyses were performed, and the temperature profiles of the trial mixes predicted by the new and older version of the ConcreteWorks software were compared. Finally, a sensitivity study was conducted, and some limitations of the new models in the updated (new) ConcreteWorks software were identified.

### *1.3.2. Part B – Tasks*

The following tasks were conducted for the Part B study of this research project:

*Task B-1: Developing a new seal slab component in the ConcreteWorks software*

*Task B-2: Conducting trial analyses*

Using the updated ConcreteWorks software with the new seal slab component developed in Task B-1, this task investigated the effects of the time of footing placement, the sizes of the footing and seal slab, and environmental conditions on the temperature profile of a bridge footing placed on a seal slab.

## 1.4. Report Outline

In this report, Chapter 1 is the Introduction, Chapters 2 through 7 describe the research activities and present the results for Tasks A-1 to A-7, Chapter 8 covers Tasks B-1 and B-2, and Chapter 9 provides conclusions and recommendations from both Part A and Part B.

## 2. MATERIAL CHARACTERIZATION (TASK A-1)

### 2.1. Concrete Materials Used

Three different ground granulated blast furnace slags (GGBFS) were collected. Two of them, Grade 100 and Grade 120, were from the LafargeHolcim (LH) plant in the South Chicago neighborhood of Chicago, Illinois, and were named S1 (LH Grade 100) and S2 (LH Grade 120), respectively. The third was collected from the Manatt's (M) ready mixed concrete plant in Ames, Iowa, and was named S3 (M Grade 100). Type I/II portland cement was collected from Continental Cement Co. of Ames, Iowa. Photos of these cementitious materials are shown in Figure 2-1. In addition, river sand from Hallett Materials in Ankeny, Iowa, was used as fine aggregate, and crushed limestone from Martin Marietta in Ames, Iowa, was used as coarse aggregate.

(a) Type I/II (b) S1 (c) S2 (d) S3

**Figure 2-1. Cementitious materials collected**

### 2.2. Material Characterization Methods and Results

*2.2.1. Cementitious Materials*

X-ray diffractometer Siemens D500 XRD, with a copper X-ray tube at 40 kV and 35 mA, was used to identify the crystalline phases of the cementitious materials. The XRD data were collected over the range of 0º to 70º with scanning rate of 2º per minute and step size of 0.02º.

The fineness of the materials was measured using a Blaine apparatus in compliance with ASTM C204. (The test results were provided by the Iowa DOT in Ames, Iowa.) In the present study, XRF analysis was conducted to determine the chemical composition of the cementitious materials used.

Table 2-1 shows the chemical and physical properties of the slags, along with those of Type I/II cement, obtained using XRF analysis. Figure 2-2 shows the XRD pattern of S1. The results indicate that the chemical properties of all three slags received are similar, but the fineness of S2 (LH Grade 120) is higher than that of S1 or S3 (Grade 100). This suggests that S3 (M Grade 100) was possibly from the same source as S1, because the Manatt's ready mixed concrete plant

primarily sources its slag from LafargeHolcim. Therefore, S3 (M Grade 100) was not studied further.

**Table 2-1. Chemical and physical properties of the cementitious materials**

| Oxide (%) | OPC Type I/II | S1 (LH Grade100) | S2 (LH Grade120) | S3 (M Grade100) |
|---|---|---|---|---|
| $SiO_2$ | 22.802 | 35.635 | 35.860 | 33.104 |
| $Al_2O_3$ | 5.355 | 10.052 | 10.109 | 9.402 |
| $Fe_2O_3$ | 3.512 | 0.894 | 0.889 | 1.719 |
| CaO | 64.186 | 38.907 | 38.881 | 42.803 |
| MgO | 2.704 | 10.004 | 10.713 | 8.611 |
| $SO_3$ | 1.641 | 0.965 | 1.015 | 1.220 |
| $Na_2O$ | 0.154 | 0.254 | 0.245 | 0.358 |
| $K_2O$ | 0.624 | 0.428 | 0.416 | 0.384 |
| $TiO_2$ | 0.257 | 0.415 | 0.388 | 0.473 |
| $P_2O_5$ | 0.048 | 0.015 | 0.014 | 0.074 |
| $Mn_2O_3$ | 0.082 | 0.293 | 0.259 | 0.230 |
| SrO | 0.099 | 0.038 | 0.044 | 0.162 |
| ZnO | 0.018 | 0.009 | 0.009 | 0.012 |
| BaO | 0.092 | 0.103 | 0.107 | 0.150 |
| Specific Gravity | 3.150 | 2.930 | 2.950 | 2.930 |
| Blaine Fineness ($m^2/kg$) | 300 | 443 | 552 | 443 |

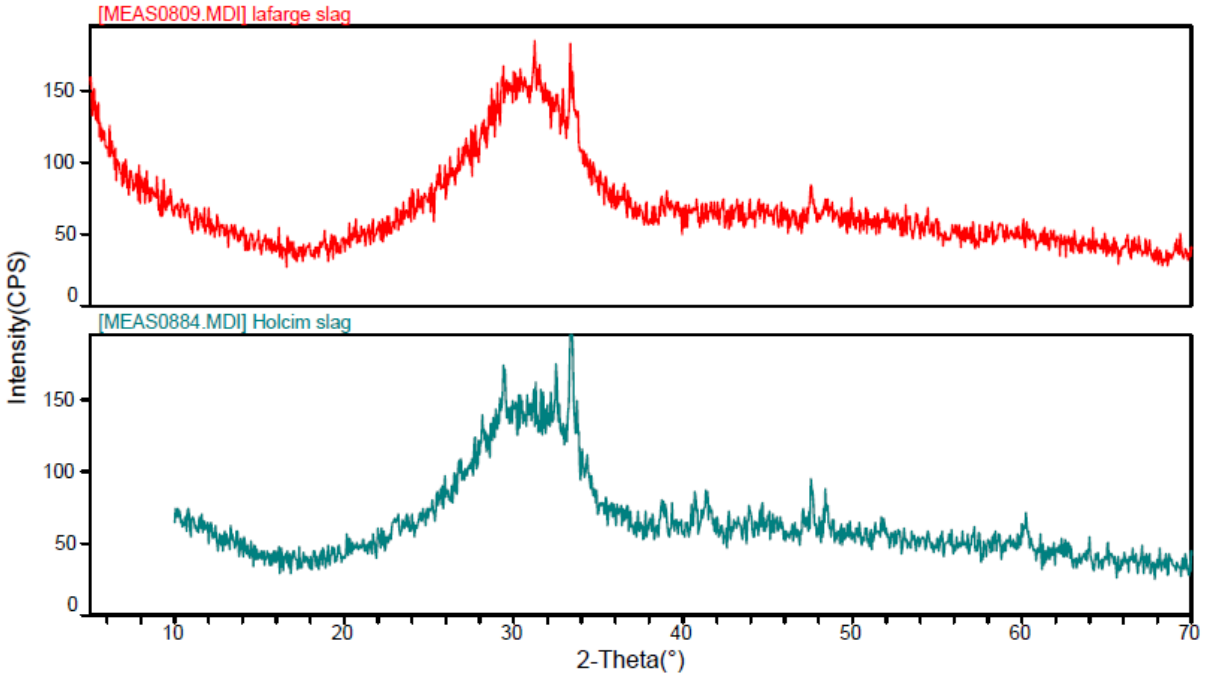


**Figure 2-2. XRD pattern of S1 (LH Grade 100) and S2 (LH Grade 120)**

As shown in Figure 2-2, S1 and S2 display a major amorphous hump in the range of 18º to 38º, indicating the presence of a significant amount of amorphous or glassy material in the slag.

### *2.2.2. Concrete Aggregates*

For all concrete mixes studied, 1 in. nominal maximum size aggregate (NMSA) limestone sourced from Martin Marietta in Ames, Iowa, was used as coarse aggregate, and river sand from Hallett Materials in Ankeny, Iowa, was used as the fine aggregate. The properties of the aggregates, such as gradation, specific gravity, absorption, dry rodded unit weight (DRUW), fineness modulus, etc., were measured in the Phase I project (Wang et al. 2020), and the results are shown in Table 2-2.

**Table 2-2. Properties of aggregate materials**

| | **Specific Gravity** | **Absorption, %** | **Moisture Content, %** | **DRUW, lb/ft$^3$** | **Fineness Modulus** |
|---|---|---|---|---|---|
| Limestone CA | 2.7 | 0.71 | 0.13 | 98.2 | - |
| River Sand | 2.68 | 1.1 | 1.15 | - | 2.92 |

### *2.2.3. Chemical Admixtures*

A low-range water reducer (LRWR), Euclid WR 91, and an air entraining agent (AEA), Euclid AEA-92, which are commonly used in Iowa pavement concrete, were used as admixtures for concrete slump and freeze-thaw durability control, both of which were provided by Manatt's ready mixed concrete plant.

## 3. ISOTHERMAL CALORIMETRIC STUDY OF SLAG CEMENT HYDRATION (TASK A-2)

To understand the effects of the different slags on cement hydration, and the hydration of pure slag, various paste mixes were prepared to conduct the isothermal calorimetry measurements.

### 3.1. Materials and Proportions

The pastes were prepared using 0, 20, 50, 75, and 100 wt.% of S1 (LH Grade 100) and S2 (LH Grade 120) to replace Type I/II cement and at a water-to-binder (w/b) ratio of 0.43. The LRWR admixture Euclid WR 91 was used at the recommended dosage of 5 fl oz per 100 kg of cementitious material.

### 3.2. Test Methods

An eight-channel semi-isothermal calorimeter (shown in Figure 3-1) was used (Ge et al. 2009, Ge and Wang 2009). As illustrated in Figure 3-1, each unit has an aluminum sample holder, which rests on a heat flow sensor (Peltier) that is placed on a common heat sink of a large block of aluminum. On the other side of the heat sink is another heat flow sensor and a 129 g aluminum block. The aluminum block is used as a reference to reduce the noise signal in this conduction calorimeter. When a sample is placed in the unit, the heat produced by hydration flows rapidly to its surroundings. The main route for heat exchange between the sample and its surroundings is through the heat flow detector. The heat flow, caused by the temperature difference across the sensor, creates a voltage signal proportional to the amount of heat flow. This voltage signal is then converted to the rate of heat evolution by applying a calibration factor based on the reference material (aluminum).

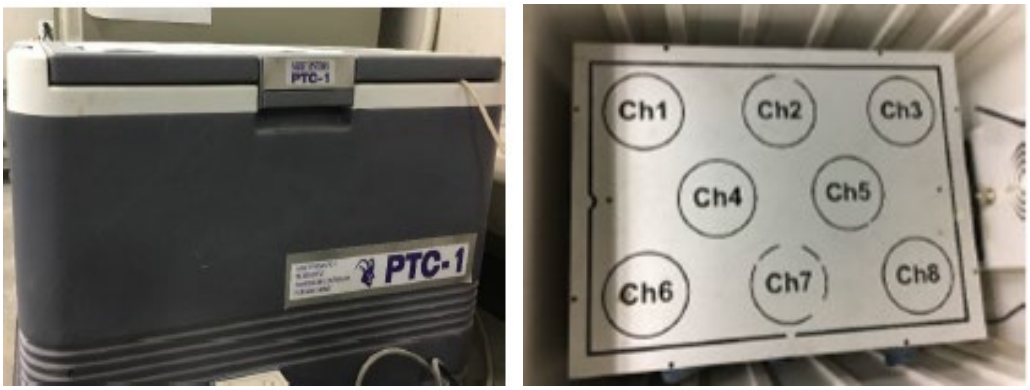


**Figure 3-1. Isothermal calorimetry (left) and channels for holding samples (right)**

Before performing the calorimetry tests, the calorimeter was calibrated. The calibration procedure aimed to obtain the baseline of the calorimeter and the calibration factors for each of the eight cells at each of four temperatures 10°C, 20°C, 30°C, and 40°C. The steps for the calibration procedure followed the process described in Wang et al. (2020), Poole (2007), and

Riding et al. (2011). After the calibration factors were determined, calorimetry tests were conducted following the procedure previously discussed. The data were recorded in millivolts (mV) at every 1-minute interval for approximately 100 hours. Then, equation 3-1 was used to determine the rate of heat generation in megawatts per gram (mW/g) of cement.

$$P = \frac{(R-B)*CFWs}{(1+sc+wc)} \tag{3-1}$$

Where *P* is the rate of heat generation (mW/g), *R* is the data reading (mV), *B* is the calibrated baseline (mV), *CF* is the calibration factor (mW/mV), *Ws* is the weight of the sample (g), *s* is the weight of sand (g), *c* is the weight of cement (g), and *w* is the weight of water (g). The rate of heat generation (mW/g) at every 15-minute interval was converted to the total heat generated in joules per hour (J/h), and the cumulative heat is then calculated by adding the heat generated in each interval.

The calorimetry tests were performed at testing temperatures of 10°C, 20°C, 30°C, and 40°C. To bring the temperature of the constituent materials to the designed testing temperature, all the materials (cement, GGBFS, water, and water-reducing admixture) were first kept in separate containers in the calorimeter for approximately 24 to 48 hours (depending on the time needed to achieve a constant temperature reading). When the temperature of the materials had reached the designed testing temperature, they were taken out for mixing.

During the paste mixing, the water-reducing admixture was first added into water and stirred well for 15 seconds. Then, the binder (slag and cement) was added in the water and mixed with a plastic non-stick spoon for 2 minutes. The homogenous mixed paste was then divided equally into two cups, and the respective weight was recorded. The paste specimens, weighing nearly 50 g each, were then placed into eight different channels in the aluminum chamber of the isothermal calorimeter. After the samples were placed, the preprogrammed calorimeter started taking readings at an interval of 15 minutes until the heat generation became stable. For 20°C, 30°C, and 40°C, the samples were tested for 7 days, and for 10°C, the samples were measured for 10 days. A total of 40 mixtures (including the different temperature combinations) were tested in the isothermal calorimeter.

All the tests were done by the same person, and the cups were placed in the chamber at the same time to maintain consistency and to improve the accuracy of the results. The number of tests done for the given mixtures at the selected temperature are shown in Table 3-1.

**Table 3-1. Mixes used for isothermal calorimetry tests**

| Testing Temperature (°C) | Slag Replacement (%) | Mix ID (S1 series) | Mix ID (S2 series) |
|---|---|---|---|
| 10°C | 0 | S1-10C-0% | S2-10C-0% |
| | 25 | S1-10C-25% | S2-10C-25% |
| | 50 | S1-10C-50% | S2-10C-50% |
| | 75 | S1-10C-75% | S2-10C-75% |
| | 100 | S1-10C-100% | S2-10C-100% |
| 20°C | 0 | S1-20C-0% | S2-20C-0% |
| | 25 | S1-20C-25% | S2-20C-25% |
| | 50 | S1-20C-50% | S2-20C-50% |
| | 75 | S1-20C-75% | S2-20C-75% |
| | 100 | S1-20C-100% | S2-20C-100% |
| 30°C | 0 | S1-30C-0% | S2-30C-0% |
| | 25 | S1-30C-25% | S2-30C-25% |
| | 50 | S1-30C-50% | S2-30C-50% |
| | 75 | S1-30C-75% | S2-30C-75% |
| | 100 | S1-30C-100% | S2-30C-100% |
| 40°C | 0 | S1-40C-0% | S2-40C-0% |
| | 25 | S1-40C-25% | S2-40C-25% |
| | 50 | S1-40C-50% | S2-40C-50% |
| | 75 | S1-40C-75% | S2-40C-75% |
| | 100 | S1-40C-100% | S2-40C-100% |

### 3.3. Test Results

The paste mixes (with varying amounts of slag replacement) were tested at different temperatures (10°C, 20°C, 30°C, and 40°C) using isothermal calorimetry. The heat of hydration and total heat were measured using isothermal calorimetry for 7 days (168 hours) at intervals of 15 minutes. This section discusses the results obtained from isothermal calorimetry.

Figure 3-2 presents the rate of heat generated from a typical cement paste, showing several peaks associated with hydration of various cement components (Ballard et al. 2011). For example, the second peak, or the main peak, is associated with $C_3S$ hydration, which can be seen in almost all cement hydration heat flow curves, while the third peak is associated with the secondary $C_3A$ reaction, which is commonly seen in Type I/II cement and cement with supplementary cementitious materials (SCMs), like slag and fly ash.

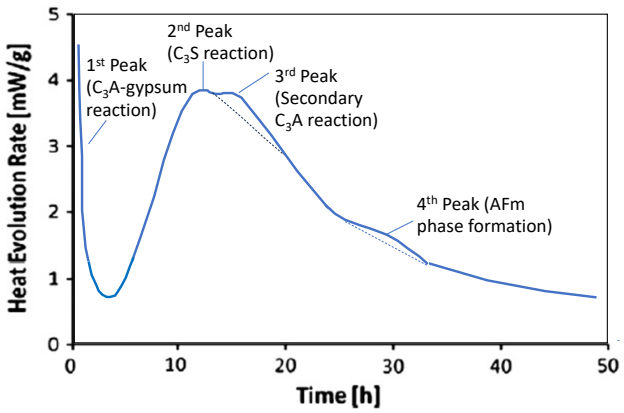


**Figure 3-2. Rate of heat generation of a typical cement paste**

*3.3.1. Mixes Containing Grade 100 Slag (S1)*

Figure 3-3 and Figure 3-4 illustrate the heat of hydration and total accumulated heat released during the hydration of different paste mixes studied at various temperatures. The heat of hydration is calculated based on the weight of the total binder content (cement + slag weight). Observations are made from the obtained heat flow curve to identify the effect of slag replacement on the hydration from the peak type, height, and occurring time as well as the total heat generated.

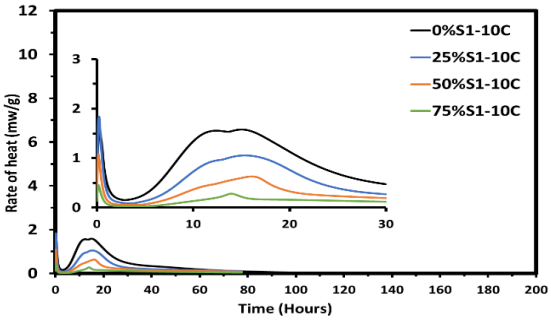


(a) Rate of heat of hydration for mix S1–10°C

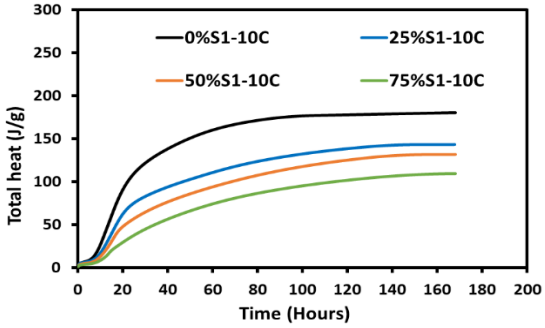


(b) Total heat accumulated for mix S1–10°C

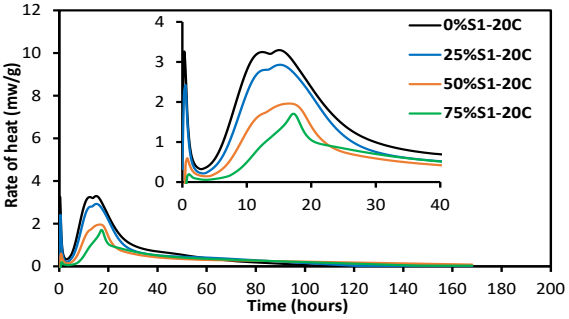


(c) Rate of heat of hydration for mix S1–20°C

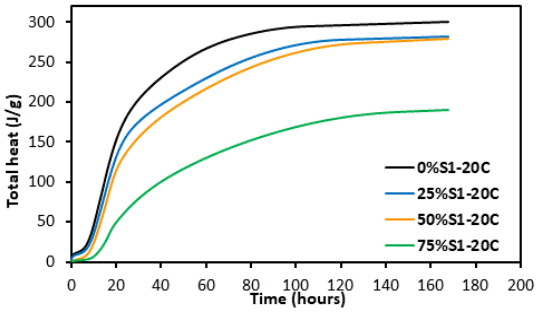


(d) Total heat accumulated for mix S1–20°C

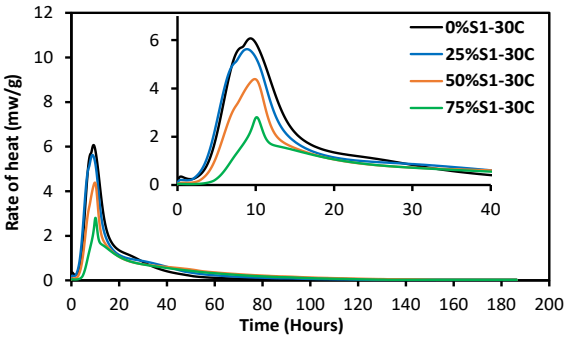


(e) Rate of heat of hydration for mix S1–30°C

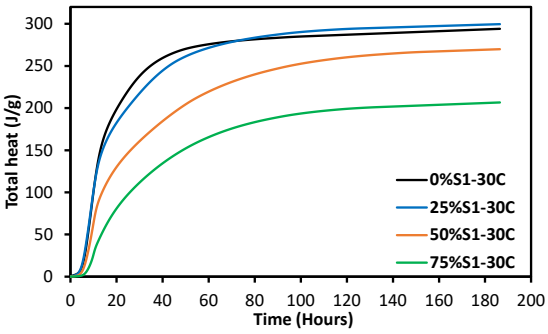


(f) Total heat accumulated for mix S1–30°C

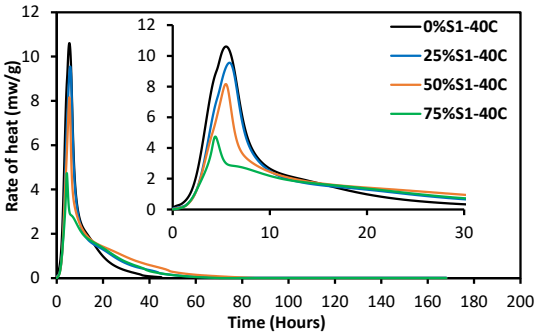


(g) Rate of heat of hydration for mix S1–40°C

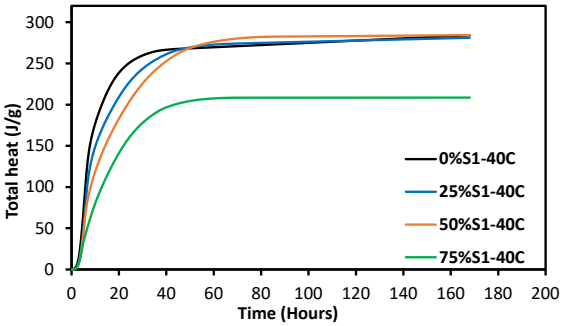


(h) Total heat accumulated for mix S1–40°C

**Figure 3-3. Rate of heat of hydration and total heat for S1 at different temperatures**

Figures 3-3a and 3-3b show the results of the calorimetry tests conducted at the testing temperature of 10°C. It can be seen from Figure 3-3a that as the slag replacement increases, all

peaks of the rate of heat generation decrease. When compared with the second peak resulting from the $C_3S$ reaction, the third peak resulting from the secondary $C_3A$ reaction was relatively enhanced with slag content in the binder system. This is mainly because the slag replacement for cement reduces calcium silicate content and increases calcium aluminate content in the binder system. As a result, the initiation of the second peak is also delayed, suggesting a delayed binder set time. Thus, it can be inferred that as the slag replacement increases, the rate of heat of hydration decreases and the hydration slows (Poole et al. 2007, Woo et al. 2018). Similar trends are observed in Figures 3-3c, 3-3e, and 3-3g, where the calorimetry testing temperature is 20°C, 30°C, and 40°C, respectively. However, as the testing temperature increases, the peak of heat generation rate occurs earlier. This signifies that the slag-cement hydration is accelerated by the environmental (testing) temperature, and subsequently, the set time of the binder is reduced. Also, at nearly 60 hours for the testing temperature of 20°C, 30 hours for the testing temperature of 30°C, and 15 hours for the testing temperature of 40°C, the rate of heat generation of the slag mixes (25%, 50%, and 75% slag replacement) was higher than that of the Type I/II portland cement paste mix. This trend reveals an accelerated slag hydration after the $C_3S$ hydration peak occurs, especially under a high testing temperature.

Figure 3-3b shows that the total accumulated heat of hydration decreases as the slag replacement increases. For 0% slag, the total heat of hydration is around 165 J/g; for 25% slag, it is 125 J/g; for 50% slag, it is 118 J/g; and for 75% slag, it is 98 J/g at the testing temperature of 10°C, which again is evidence of the reduced heat generation and decelerated binder hydration with increasing slag content of the pastes tested at 10°C. However, different trends are seen in Figures 3-3d, 3-3f, and 3-3h, where the calorimetry testing temperature is 20°C, 30°C, and 40°C, respectively. Figure 3-3d shows that under the testing temperature of 20°C, the total heat generation values of pastes with 25% and 50% slag get much closer to that of control paste (0% slag) at the end of the tests (168 hours). Figure 3-3f shows that under the testing temperature of 30°C, the total heat generation value of the paste with 25% slag exceeds that of control paste after 70 hours of testing. Figure 3-3h shows that under the testing temperature of 40°C, the total heat generation values of pastes with both 25% and 50% slag exceeds that of control paste after about 50 hours of testing. This trend is contradictory to the widely held conception that concrete temperature resulting from the heat of cement hydration can be reduced by use of slag replacement for cement. This trend occurs because increasing temperature can significantly accelerate not only cement hydration but also, more significantly, the pozzolanic reaction provided by the slag.

As mentioned in Section 1.1, the excess heat contributed by slag replacement for cement has not been considered in concrete temperature prediction models, computer programs, and field concrete temperature control measures. The present study is to bridge this research gap.

### *3.3.2. Mixes Containing Grade 120 Slag (S2)*

Isothermal calorimetry measurements of the S2 mixes (Lafarge Grade 120) are presented in Figure 3-4.

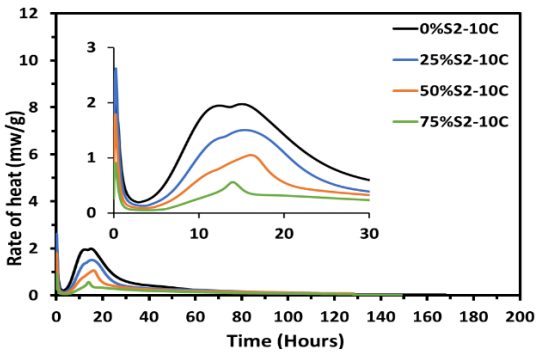


(a) Rate of heat of hydration for mix S2–10°C

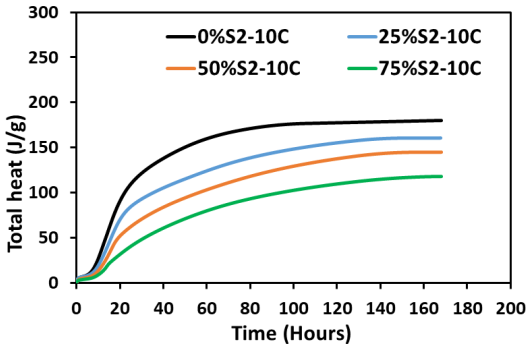


(b) Total heat accumulated for mix S2–10°C

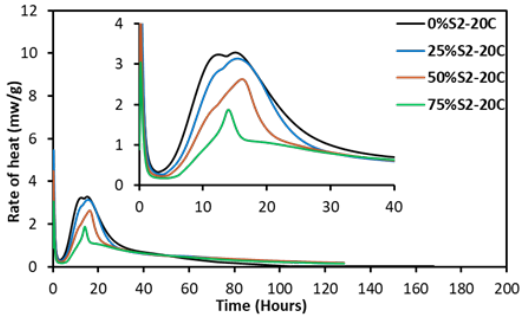


(c) Rate of heat of hydration for mix S2–20°C

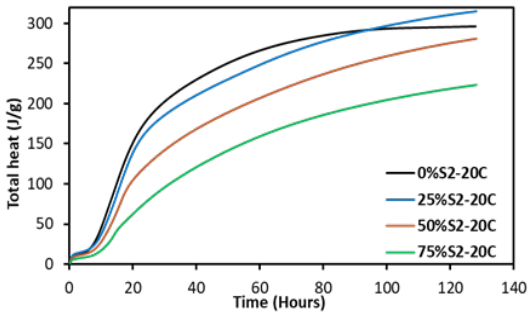


(d) Total heat accumulated for mix S2–20°C

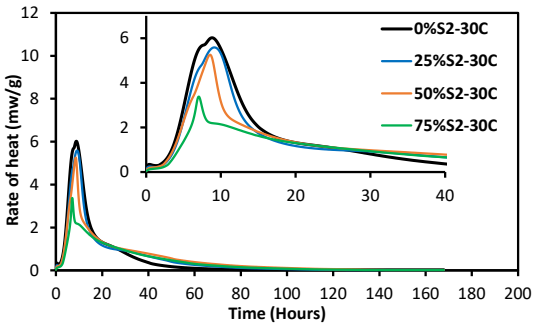


(e) Rate of heat of hydration for mix S2–30°C

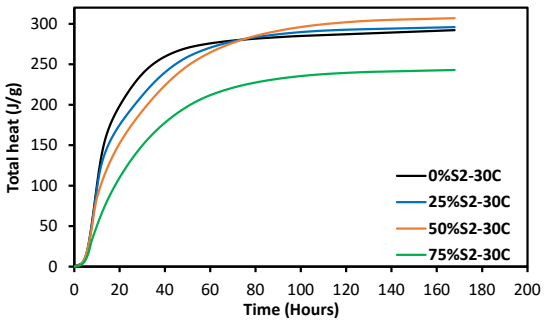


(f) Total heat accumulated for mix S2–30°C

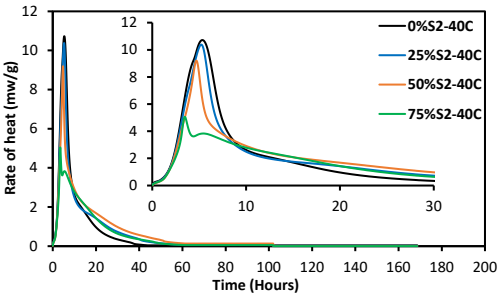


(g) Rate of heat of hydration for mix S2–40°C

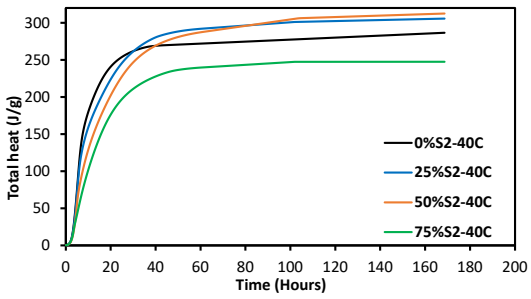


(h) Total heat accumulated for mix S2–40°C

**Figure 3-4. Rate of heat of hydration and total heat for S2 at different temperatures**

The overall trends of the rate of heat generation and the total accumulated heat of the mixes made with Grade 120 slag (in Figure 3-4) are similar to those of the mixes made with Grade 100

slag (in Figure 3-3). However, Grade 120 slag shows a higher reactivity than Grade 100 slag, evidenced by the following observations:

- The corresponding values of the rate of heat generation and accumulated heat of mixes made with Grade 120 slag are higher than those of the corresponding mixes made with Grade 100 slag.

- At the testing temperature of 10°C, the rate of heat generation of all mixes containing Grade 120 slag starts to exceed that of the control mix (0% slag) at about 100 hours of testing, although the total accumulated heat of the mixes containing slag was still lower than that of control mix (no slag) during the testing time.

- At the testing temperature of 20°C, the rate of heat generation of all mixes containing Grade 120 slag starts to exceed that of the control mix at about 50 hours of testing. After about 95 hours, the total accumulated heat of the mix with 25% Grade 120 slag exceeds that of the control mix.

- At the testing temperature of 30°C, the rate of heat generation of all mixes containing Grade 120 slag starts to exceed that of the control mix at about 25 hours of testing. After about 75 hours, the accumulated heat of the mixes with both 25% and 50% Grade 120 slag exceeds that of the control mix.

- At the testing temperature of 40°C, the rate of heat generation of all mixes containing Grade 120 slag starts to exceed that of the control mix (0% slag) at about 10 hours of testing. After about 35 hours, the accumulated heat of the mixes with both 25% and 50% Grade 120 slag exceeds that of the control mix. After 80 hours, the total accumulated heat of the mix with 50% Grade 120 slag exceeds that of the mix with 25% Grade 120 slag.

- Although the rate of heat generation and accumulated heat of the mix containing 75% slag do not exceed those of control mix, they get closer to the values of the control mix as the testing temperature increases, suggesting an accelerated slag hydration.

These results further suggest the importance of considering slag type, content, and reactivity in the prediction of the heat generation of concrete containing slags.

### *3.3.3. Mixes Containing 100% Slags*

To further understand the reactivity of the slags used, a few paste mixes made of 100% slag were tested at different temperatures using isothermal calorimetry. Figure 3-5 shows the rate of heat generation and accumulated heat for S1 (Grade 100) and S2 (Grade 120) mixes at different temperatures (10°C, 20°C, 30°C, and 40°C).

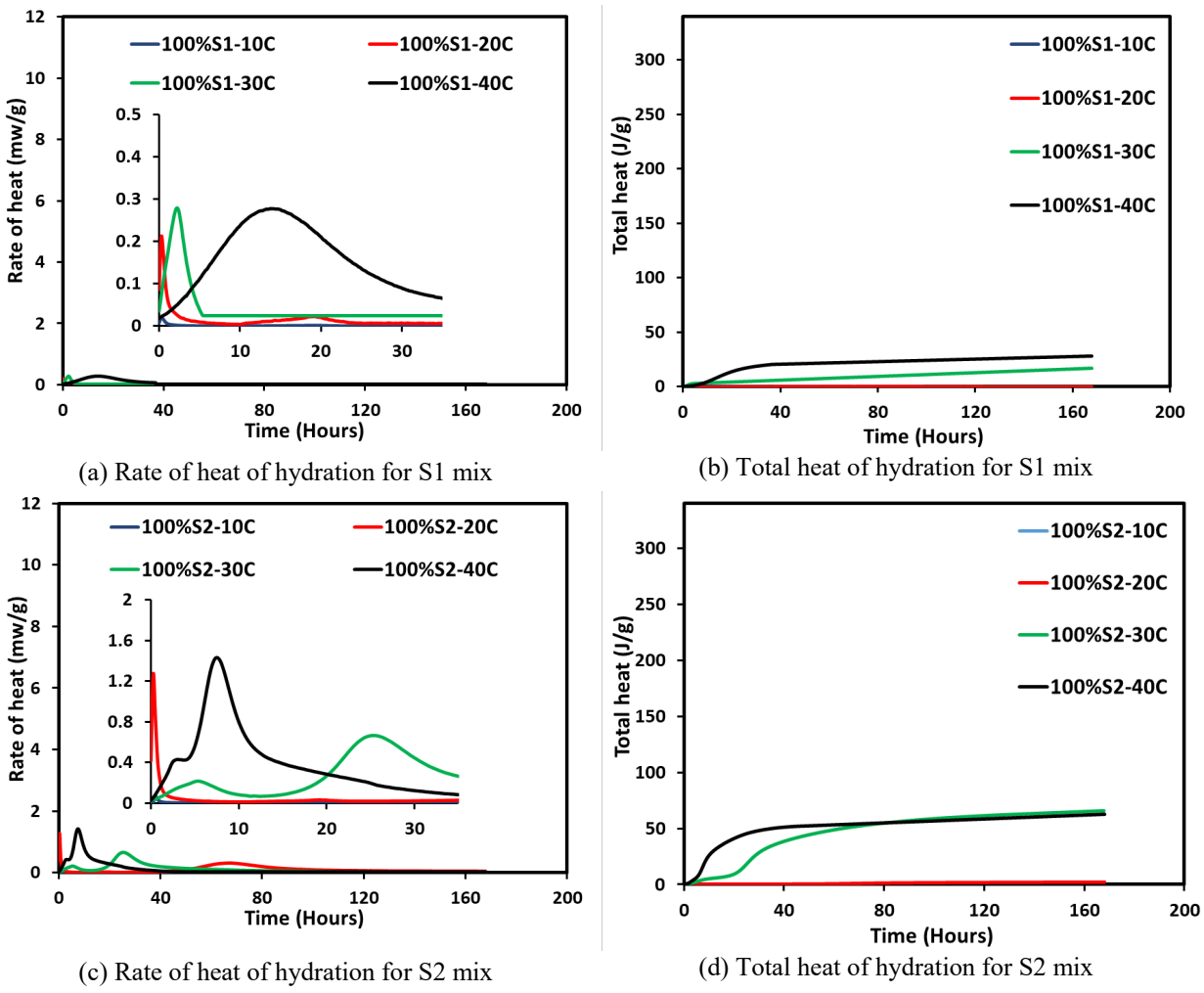


(a) Rate of heat of hydration for S1 mix

(b) Total heat of hydration for S1 mix

(c) Rate of heat of hydration for S2 mix

(d) Total heat of hydration for S2 mix

**Figure 3-5. Rate of heat and total heat of hydration for 100% S1 and S2 mixes at different temperatures**

Figure 3-5 shows that at the testing temperature of 10°C, little/no hydration reactivity is seen for both S1 and S2. At the testing temperature of 20°C, a rate of heat generation is seen for both S1 and S2, but their total heat generation is still very limited. At the testing temperatures of 30°C and 40°C, S1 and S2 hydration can be clearly seen from both their rate of heat generation and total heat generation curves, and S2 generated about twice the amount of heat as S1 at the end of the test, approximately 50 J/g at 160 hours, which is about 20% of the total heat generated by 100% portland cement paste. This implies that if simply superimposed, the total heat of hydration of pastes containing slag would not exceed the control paste were it not for the addition of slag. In Figures 3.3 and 3.4, the total heat generated by some pastes containing slag was higher than the control paste, implying the synergetic effect existed in the pastes due to the cement-slag reaction, such as accelerated cement hydration and pozzolanic reaction. It is noted that most heat generation of the 100% S2 paste occurred between 20 and 75 hours at the testing temperature of 30°C, while it was during the first 30 hours at the testing temperature of 40°C. This confirms the significant temperature effect on pure slag hydration.

Table 3-2 shows the hydration peak for the 100% S2 paste mix at different testing temperatures and the corresponding time to obtain these hydration peaks.

**Table 3-2. Calorimetry parameters of pastes made with 100% S2 slag**

| Slag 120 | | | | | |
|---|---|---|---|---|---|
| **Temp.** | **Slag Replacement (%)** | **H1 (1st peak height)** | **T1 (time to reach H1)** | **H2 (2nd peak height)** | **T2 (time to reach H2)** |
| 10ºC | 0 | 1.89 | 7.80 | 1.94 | 16.00 |
| | 25 | 1.60 | 11.80 | 1.70 | 17.60 |
| | 50 | 1.20 | 16.00 | NA | NA |
| | 75 | 0.60 | 12.00 | NA | NA |
| 20ºC | 0 | 3.24 | 12.25 | 3.29 | 15.25 |
| | 25 | 2.83 | 12.33 | 3.14 | 15.50 |
| | 50 | 1.85 | 11.33 | 2.61 | 16.41 |
| | 75 | 1.86 | 14.08 | 1.07 | 18.91 |
| 30ºC | 0 | 5.65 | 7.41 | 6.02 | 8.75 |
| | 25 | 4.64 | 7.08 | 5.57 | 9.33 |
| | 50 | 3.18 | 6.00 | 5.17 | 8.75 |
| | 75 | 3.32 | 7.16 | 2.14 | 9.91 |
| 40ºC | 0 | 8.60 | 4.08 | 10.71 | 5.41 |
| | 25 | 10.32 | 5.33 | NA | NA |
| | 50 | 9.17 | 4.75 | NA | NA |
| | 75 | 4.90 | 3.58 | 3.82 | 5.58 |

### *3.3.4. Summary of Calorimetry Test Results*

#### 3.3.4.1. Effect of Slag Content on Heat Generation

Based on Figures 3-3 and 3-4, it was evident that as the slag replacement increases from 25% to 75%, the initial rate of heat generation (about 7 to 20 hours of testing) decreases for both S1 and S2 mixes. The difference in the rate of heat generation was not exactly proportional; the difference between 25% slag and 0% slag replacement was higher than the difference between 50% slag and 25% slag replacement. However, at a later age (40 to 80 hours, depending on the temperature and percent replacement), the rate of heat generation and the accumulated heat of slag mixes surpassed that of the control mix (0% slag replacement for cement), indicating the late-age reactivity of slag was high (Gajda et al. 2014). The surpassing effect occurred earlier as the testing temperature increased.

#### 3.3.4.2. Effect of Testing Temperature

As the testing temperature increased, the rate of heat generation increased. The time to achieve the hydration peak decreased with increasing temperature, indicating higher reactivity of slag at higher temperatures. The acceleration period lasted longer at a lower temperature than at a higher temperature. The differences in peaks across the samples are more prevalent at higher

temperatures than at lower temperatures. The rate and degree of hydration increase with an increase in the testing temperature (Gajda and Vangeem 2002).

3.3.4.3. Effect of Slag Type/Fineness

In this study, slag with two different grades, Grade 100 (S1) and Grade 120 (S2), was used. The XRF and XRD analyses indicate little difference in chemical compositions of these slags. However, S2 had a Blaine fineness of 552 $m^2$/kg, while S1 had a Blaine fineness of 443 $m^2$/kg. Mixes containing S2 showed a slightly higher rate of heat generation and a significantly higher total heat of hydration at a later age than the mixes containing S1, indicating that S2 had higher reactivity than S1. The difference between these two corresponding slag mixes became more obvious with increasing the testing temperature.

Therefore, in addition to slag content, slag reactivity, affected by chemical and physical characteristics of the slag, should also be considered in the prediction models for the heat generation or the temperate rise of concrete containing slags.

# 4. EVALUTION OF EFFECT OF SLAG ON ATR FROM LARGE CONCRETE BLOCK TESTING (TASKS A-3 AND A-4)

## 4.1. Configuration of Large Concrete Block Specimens and Sensor Locations

Large concrete block specimens were built at the Structural Engineering Research Laboratory, Iowa State University (ISU), to obtain the ATR of concrete with various levels of slag replacement for cement in a typical Iowa mass concrete mix. As indicated in Figure 4-1, the large concrete block specimens had dimensions of 3 ft × 3 ft × 4 ft, or 1 $yd^3$ in volume, and they were insulated with 6 in. of Styrofoam and plywood around all surfaces. Six temperature sensors were installed to monitor the concrete temperature rise at critical locations. Three sensors were installed at the top, bottom, and side centers, 3 in. from the surfaces, respectively. One sensor was placed at the core, one at the corner, and one on the outside of the specimens.

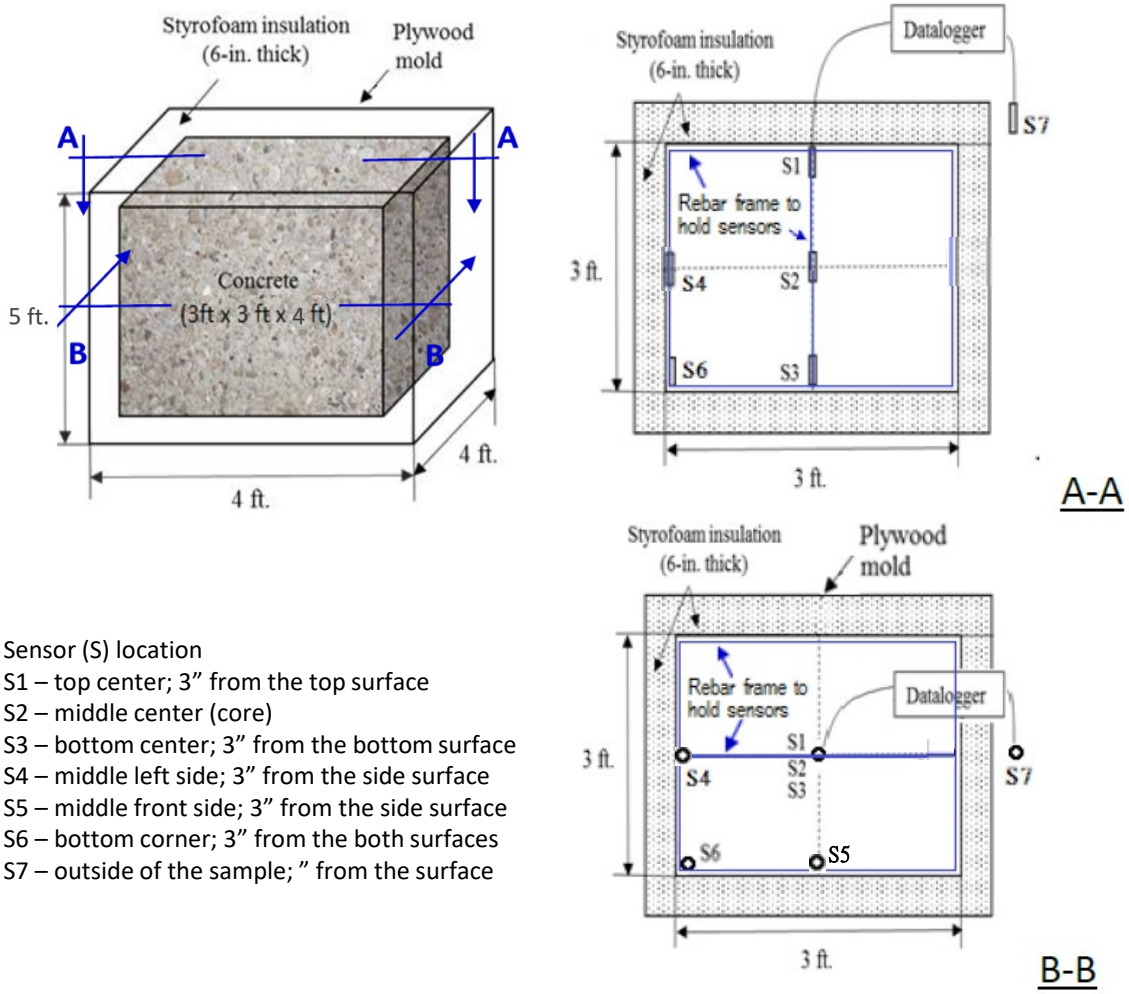


Sensor (S) location
S1 – top center; 3” from the top surface
S2 – middle center (core)
S3 – bottom center; 3” from the bottom surface
S4 – middle left side; 3” from the side surface
S5 – middle front side; 3” from the side surface
S6 – bottom corner; 3” from the both surfaces
S7 – outside of the sample; ” from the surface

**Figure 4-1. Large block measurement setup**

Due to the limited space in the laboratory, the large samples were cast and tested one by one in the laboratory. This test setup was used to obtain the concrete adiabatic temperature rise. The large blocks had a high thermal mass and high amounts of insulation that could be simulated to fit the concrete adiabatic temperature rise. The temperature data were recorded for a period of 30 days. The measured data were compared with those obtained from ConcreteWorks analyses (Task A-4), thus validating and refining the new ATR model.

### 4.2. Materials and Mix Proportions Used

The ready mixed concrete mixtures were prepared by Manatt's, Inc. of Ames, Iowa, and delivered to the ISU structures laboratory. Table 4-1 presents the mix proportions of the mixes studied, where the binder content and water-to-binder ratio (w/b) were constant for all four mixtures. The AEA content of concrete containing slag was 2.0 fl oz/yd$^3$ for blocks 2 and 4 and 2.5 fl oz/yd$^3$ for block 3, lower than that of control concrete, block 1 (4.0 fl oz/yd$^3$). The water reducer (WR) content of concrete containing slag was 3.0 fl oz/yd$^3$ for blocks 2 through 4, lower than that of control concrete, block 1 (5.0 fl oz/yd$^3$). The different WR and AEA contents were used to keep the concrete slump around 2 in. and air content around 6%.

**Table 4-1. Concrete mix proportion for adiabatic (large block) and semi-adiabatic testing**

| Material | Mix Proportion | | | |
|---|---|---|---|---|
| | 0% Slag (Block 1) | 25% Slag (Block 2) | 50% Slag (Block 3) | 75% Slag (Block 4) |
| Cement (lb/yd$^3$) | 593 | 445 | 296 | 148 |
| Slag (lb/yd$^3$) | 0 | 148 | 297 | 445 |
| Water (lb/yd$^3$) | 255 | 255 | 255 | 255 |
| Fine agg. (lb/yd$^3$) | 1509 | 1505 | 1523 | 1496 |
| Coarse agg. (lb/yd$^3$) | 1531 | 1526 | 1540 | 1517 |
| w/b ratio | 0.43 | 0.43 | 0.43 | 0.43 |
| Euclid AEA-92 (fl oz/yd) | 4.0 | 2.0 | 2.5 | 2.0 |
| Euclid WR 91 (fl oz/cwt) | 5.0 | 3.0 | 3.0 | 3.0 |

Note: The ready mix concrete manufacturer adjusted the mixing water based on the approximate moisture content of field aggregates; thus, the estimated w/b ratios of these mixes were near 0.43.

Immediately following the delivery, the concrete was sampled following ASTM C172/C172M-10 and then tested for its fresh properties. The fresh properties tested were slump, air content, and unit weight, measured in accordance with ASTM C143/C143M-15, ASTM C231/231M-10, and ASTM C138/C138M-13, respectively. Table 4-2 shows the fresh concrete properties of all four concrete mixes studied.

**Table 4-2. Fresh properties of concrete mixtures**

| Fresh Properties | 0% Slag Mix (Block 1) | 25% Slag Mix (Block 2) | 50% Slag Mix (Block 3) | 75% Slag Mix (Block 4) |
|---|---|---|---|---|
| Casting Date | 09/24/2020 | 03/29/2021 | 02/18/2021 | 01/08/2021 |
| Ambient Temperature (°F) | 73.10 | 48.20 | 30.10 | 17.60 |
| Slump (in.) | 2.50 | 2.75 | 2.00 | 3.75 |
| Air content (%) | 6.50 | 6.20 | 5.90 | 2.30 |
| Unit weight (lb/ft$^3$) | 142.80 | 143.50 | 144.20 | 150.70 |
| Concrete Placement Temperature (°F) | 70.20 | 68.30 | 61.30 | 50.90 |

It can be seen from Table 4-2 that the ambient and concrete placement temperatures were different as the blocks were cast on different dates. Although the same AEA content was used for slag concrete, the air content of block 4 (75% slag) was only 2.3%, much lower than designed 6%, which was probably associated with mixing under cold weather conditions. Additionally, block 4 had the highest slump among all the mixtures. As a result, the unit weight of the block 4 mixture was a little higher.

### 4.3. Strength and Maturity

In accordance with ASTM C192-16, 4 in. × 8 in. cylindrical specimens were made from fresh concrete. After approximately 24 hours, the specimens were demolded and then moist cured in a standard curing room (73.5 ±3.5°F and ≥95R.H.) until testing. The compressive strengths of the specimens prepared from the four concrete mixes were tested at 1, 3, 7, 28, 56, and 90 days according to ASTM C39. Maturity of the concrete mixes were also measured according to ASTM C1074 - Standard Practice for Estimating Concrete Strength by the Maturity Method. For the test, a temperature sensor was inserted into a 6 in. × 12 in. specimen, and the temperature of the concrete under a standard moisture curing was monitored for a total of 28 days. The concrete maturity, M(t), was then computed according to the following equation:

$$M(t) = \Sigma\,(Ta\ - To) * \Delta T \qquad (4\text{-}1)$$

where M(t) is the temperature-time factor (°C-days); $T_a$ is the average temperature (°C) measured during ΔT, $T_0$ is the datum temperature (-10°C), and ΔT is the time interval (days).

Figure 4-2 shows the strength and maturity-strength relationships of the concrete mixes studied. These results were used later as inputs of the ConcreteWorks program for the concrete thermal analysis. From Figure 4-2, it can be seen that the slope of the strength-maturity curve of the mixes containing 50% and 75% slag is much higher than that of mixes containing 0% and 25% slag, illustrating that the mixes containing 50% and 75% slag would gain strength more rapidly than the mixes with 0% and 25% slag after the concrete matures, having strength higher than 4,000 psi. For example, the mixes with 0% and 25% slag would gain the strength of 5,000 psi earlier than the mixes with 50% and 75% slag.

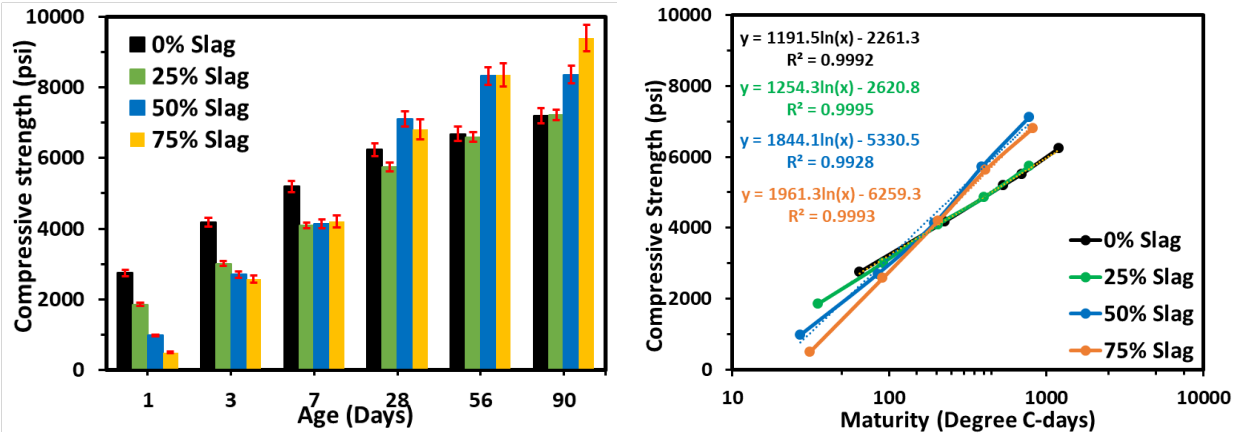


(a) Compressive strength (psi)

(b) Maturity (°C-days)

**Figure 4-2. Hardened properties of concrete mixtures**

## 4.4. Semi-Adiabatic Calorimetry and Large Block Testing

Accurate characterization of the temperature rise in a concrete element requires an estimate of the ATR of the concrete mixture. Adiabatic calorimetry requires an adiabatic process in which no heat is gained or lost to the system's surroundings. Because of the difficulty and the expensive equipment needed to eliminate heat gain or loss in an adiabatic calorimetry test, semi-adiabatic calorimetry is commonly used. From the semi-adiabatic calorimetry test results, the ATR can be calculated. Even though the semi-adiabatic calorimetry test is a common test, there is no standard test method for it.

This study followed the guidelines outlined in Poole (2007). Based on these guidelines, a semi-adiabatic calorimeter was developed in the Portland Cement Concrete (PCC) Research Laboratory at ISU. Figures 4-3a and 4-3b show a diagram with the details of the calorimeter and the finished apparatus, respectively. The semi-adiabatic calorimeter was built using a 24 in. × 34 in. cylindrical drum that was insulated with insulation foam (crack-insulating foam placed by big gaps and cracks). The top insulation lid was also prepared using the same insulation foam. In the middle of the drum, there was a 7 in. (diameter) × 14 in. (height) chamber, made with galvanized steel sheeting, for holding the tested concrete cylinder sample (6 in. in diameter and 12 in. in height).

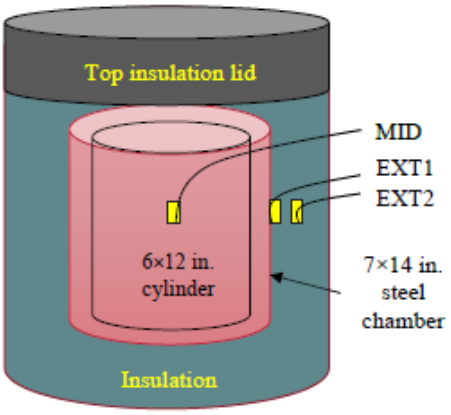


(a) Illustration of semi-adiabatic setup

(b) Actual semi-adiabatic setup

**Figure 4-3. Semi-adiabatic calorimetry setup**

Fresh concrete was poured into the 6 × 12 in. cylinder placed inside this chamber. The temperature was measured using Type T thermocouples at three locations: one at the center of the concrete specimen (MID), one at the surface of the steel chamber (EXT1), and one at 1 in. away from the chamber surface in the insulation (EXT2). The MID thermocouple was placed 6 in. into the center of the fresh concrete specimen. A plug-in for the thermocouple was installed at the edge of the steel chamber opening. For connecting thermocouple wires to the data logger, a hole was drilled in the middle of the drum surface through which the wires were extracted.

To calibrate the semi-adiabatic chamber, water was boiled and placed in the chamber, and the temperature of the water was recorded for 160 hours at intervals of 15 minutes using Type T sensors installed in the semi-adiabatic chamber (shown in Figure 4-3a as MID, EXT1, and EXT2). The measured data were plotted in an Excel spreadsheet, and a regression analysis using the $R^2$ method with the Solver function in Excel was performed to match the modeled change in water temperature to the measured change in water temperature. The Solver function generated the best-fit calibration factors ($C_{f1}$ and $C_{f2}$) that were used to model the change in water temperature. These calibration factors ($C_{f1}$ and $C_{f2}$) were later used to convert the semi-adiabatic temperature to true adiabatic temperature. The detailed process of the calibration and semi-adiabatic to true adiabatic conversion was described by Zhu et al. (2022). Using the calibration factors ($C_{f1}$ and $C_{f2}$), the true ATR of the concrete tested with semi-calorimetry can then be calculated (Appendix A).

For the large block testing, an experimental setup was prepared to mimic the mass concrete behavior. A concrete block of 3 ft × 3 ft × 4 ft was constructed, and sensors were installed. Figure 4-4 shows the steps followed in the experimental setup to measure the temperature profile at different locations. To measure the temperature of the block at various locations, Type T sensors with high accuracy (0.01°C) were used. These sensors were installed using reinforcement, and a cage/framework was built to keep the sensors in place. At each location of interest, a minimum of two sensors were installed. These sensors were isolated to prevent direct contact with the rebar to avoid any discrepancy with data.

(a) Rebar and sensor ties

(b) Sensor and insulation setup

(c) Actual experimental setup in process

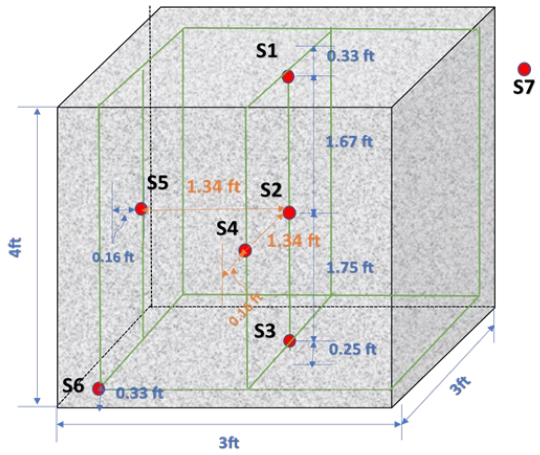


(d) Sensor locations


(e) Large block experimental setup

(f) Final large block after casting

**Figure 4-4. Large block test setup and casting procedures**

Figure 4-4a shows the reinforcement bars (No. 4, 9/16 in. diameter rebar) and sensor ties. The rebars were tied using Type 2 stirrups. Figure 4-4b shows the insulation used to prevent the sensor from interacting with the rebar. Figure 4-4c shows the rebar frame built to keep the sensor in place. Figure 4-4d shows the locations of the various sensors. After the sensors were placed, the rebar frame was ready to be placed in the steel formwork containing insulation Styrofoam.

The insulation Styrofoam (Foamular 250, R-10) was installed to prevent or minimize heat dissipation during testing. The Styrofoam was triple-layered in a staggered form as shown in Figure 4-4e. The thickness of each Styrofoam layer is 2 in., and the total thickness of the Styrofoam insulation was 6 in. on each side. To prevent heat loss at the joints, aluminum foil, with a high-reflective index, was used to seal the joints.

Once the steel formwork with the Styrofoam was ready, the rebar frame with the sensors was placed inside, on small plastic chairs to keep the rebar frame in the center of the formwork. After all the sensors were checked using a data logger (Pico Tech), the designed concrete was poured in a continuous manner to make a large concrete block specimen. An electrical internal vibrator was used for concrete consolidation. Right after casting, the top surface of the concrete block was covered with three layers of Styrofoam. Spray foam insulation (Great Stuff Gaps & Cracks, 1 in. sealing) was used to fill the gaps, and extra weights were added on the top to keep the Styrofoam sheet in place, as shown in Figure 4-4f. Then, the entire concrete block was covered with an insulation blanket. The temperatures at different locations recorded by the Type T sensors were monitored using a data logger for 30 days.

### 4.5. Temperature Profiles Measured from Large Concrete Blocks

A total of four large concrete blocks were cast with different slag replacement levels (0%, 25%, 50%, and 75%). The obtained temperature at each location was the average of the readings from two sensors (as noted previously); the measured temperature data are presented in Figure 4-5. As shown in Figure 4-5, S1, S2, and S3 were located at the top, middle (core), and bottom of the block, respectively; S4 and S5 were located at the middle side of the block, and S6 was located at the bottom corner of the block. It was noted that the core temperature (measured by S2) and the temperature at the bottom corner (measured by S6), which presents the largest difference from the core temperature, were the two points of interest.

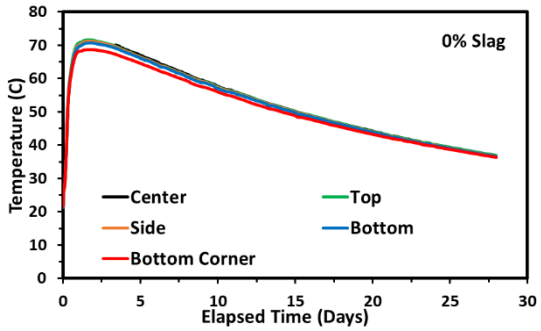


(a) Large block tests: 0% slag

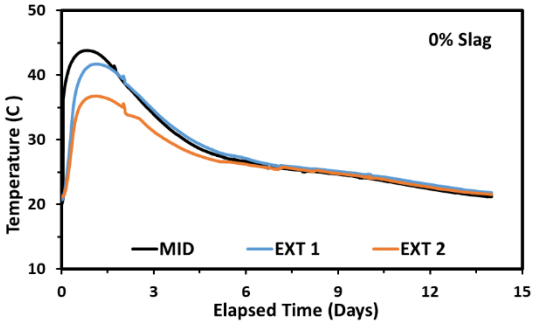


(b) Semi-adiabatic tests: 0% slag

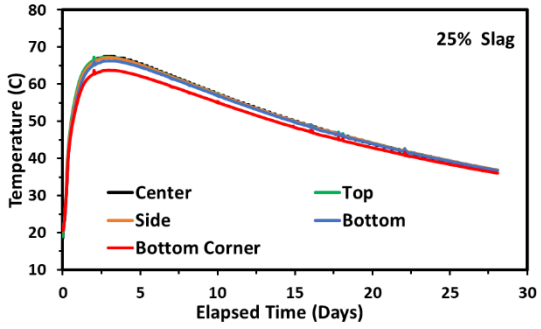


(c) Large block tests: 25% slag

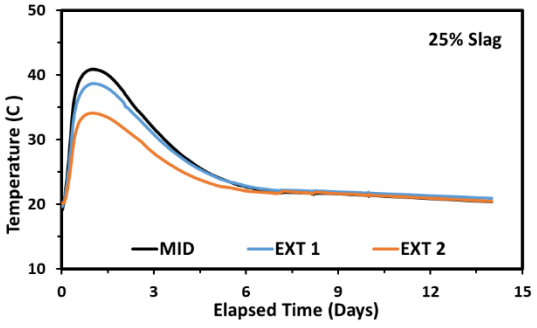


(d) Semi-adiabatic tests: 25% slag

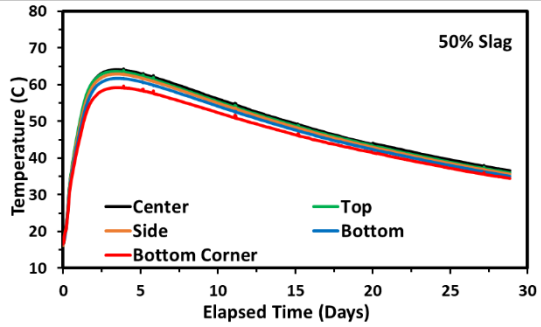


(e) Large block tests: 50% slag

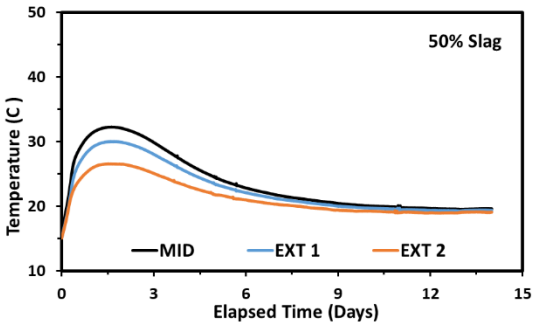


(f) Semi-adiabatic tests: 50% slag

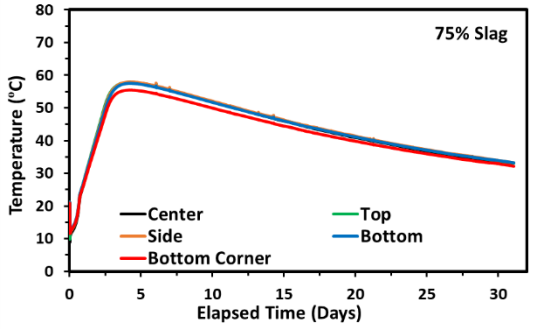


(g) Large block tests: 75% slag

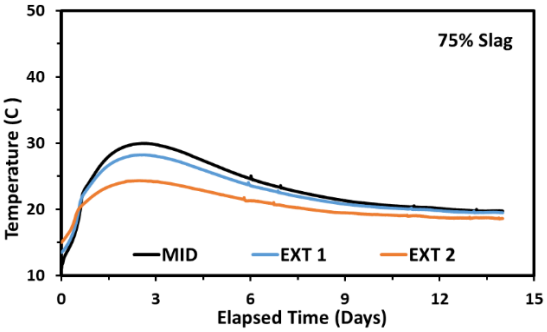


(h) Semi-adiabatic tests: 75% slag

**Figure 4-5. Temperature profile measured by sensors at different locations from large block tests (3 × 3 × 4 ft samples) and from semi-adiabatic tests (6 × 12 in. samples) of concrete mixes**

Figures 4-5a, 4-5c, 4-5e, and 4-5g show the temperature profile measured from the large concrete blocks at selected locations, top (S1), center (S2), bottom (S3), side (S5) and bottom corner (S6). Parallelly, Figures 4-5b, 4-5d, 4-5f, and 4-5h show the temperature profile of the corresponding concrete measured by the semi-adiabatic calorimeter.

It is found from the large block tests that: (1) the data measured by two sensors at the same location are very consistent (the difference is <5°C), indicating a good reliability of the data, (2) the difference between the core temperature (measured by S2) and the bottom corner temperature (measured by S6) is also very limited (<7°C), indicating a quality insulation of the large concrete blocks, and (3) all temperature profiles have a similar trend, increasing and reaching the peak at an early stage (0 to 72 hours, depending on the slag percentage replacement) and then slow decreasing over time until the samples reached the environmental temperature.

It is observed from the semi-adiabatic calorimetry tests that the trend of the temperature profiles of concrete containing different levels of slag replacement for cement is also similar. However, due to significant heat loss, the maximum temperatures measured from the semi-adiabatic calorimetry tests are much lower than those measured from the large block concrete tests, and the temperature drop is much more rapid and occurs at a much earlier time, especially for the mixes containing low slag content.

The temperature profiles obtained from both the large block and semi-adiabatic calorimetry tests, as shown in Figure 4-5, provide evidence that as slag replacement increases, the maximum temperature peak reduces, and the peak shifts toward the right, which indicates a reduced rate of heat of hydration due to delayed slag hydration. In addition, as the slag replacement increases, the curvature of the temperature rises, and loss decreases. For 0% slag replacement, the temperature rise curve was much steeper compared to the 75% slag replacement. Similar behavior was observed at a later age (as the temperature decreased) as well. This indicated that the rate of heat loss is proportional to the rate of heat gain. For the standard mix (0% slag replacement), the heat gain and heat loss were faster compared to other mixes.

To have a better understanding of the observed data, the observed temperature and temperature rise at the core and the bottom corner sensors of the large concrete block and semi-adiabatic chamber are presented in Figure 4-6 and Figure 4-7.

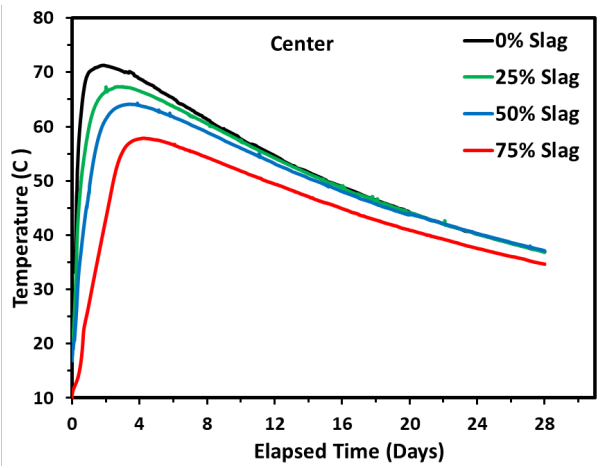


(a) Temperature profile measured by the center sensor (S2)

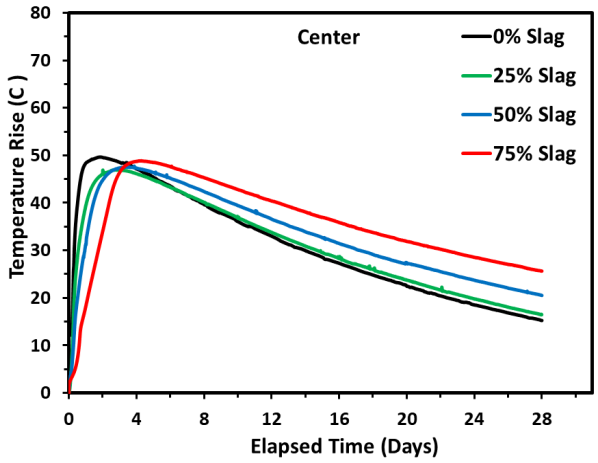


(b) Temperature rise for the center sensor (S2)

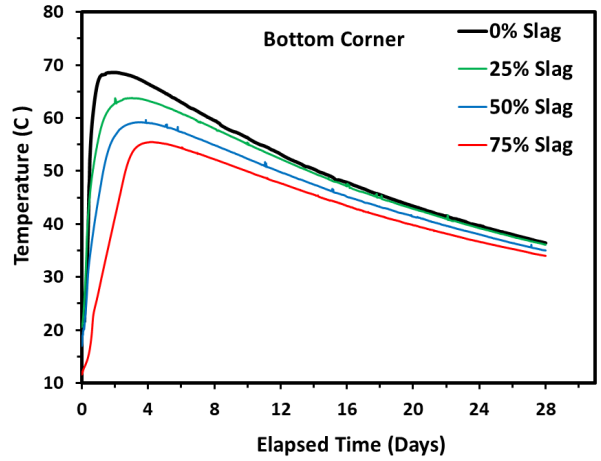


(c) Temperature profile measured by the bottom corner (S3)

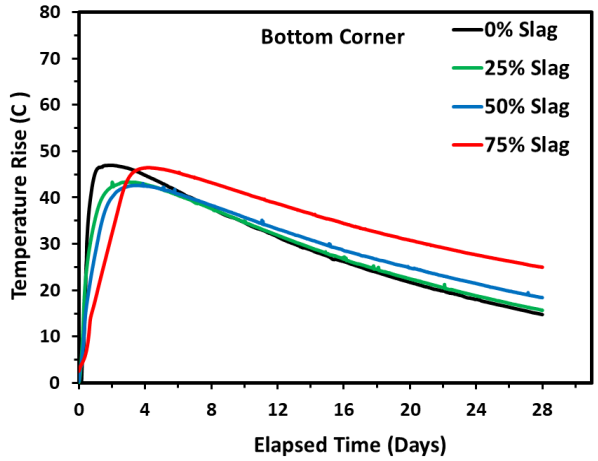


(d) Temperature rise for the bottom corner (S3)

**Figure 4-6. Temperature profile and temperature rise measured by sensors at different locations of large concrete block samples (3 × 3 × 4 ft) with different slag replacement levels**

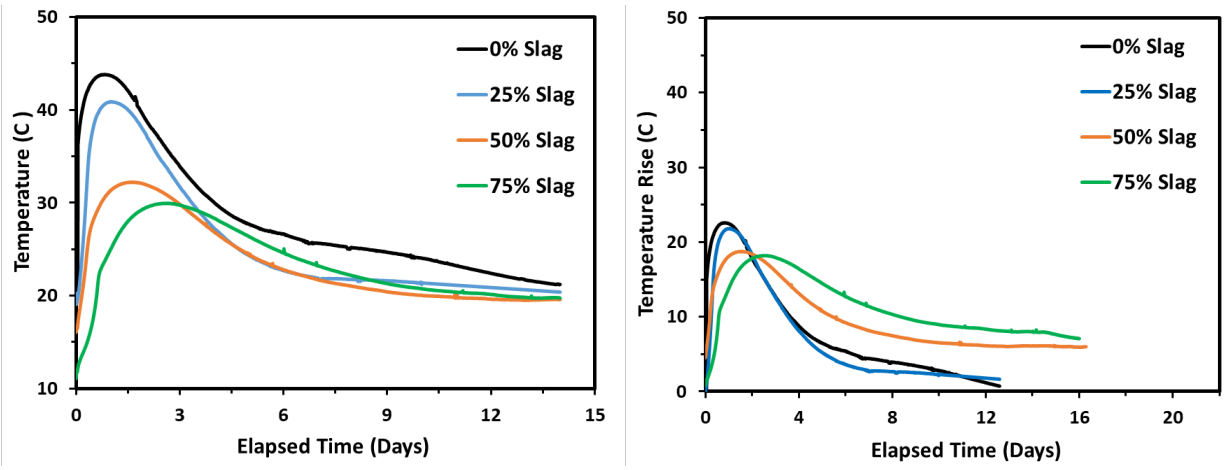


(a) Temperature profile measured at center

(b) Temperature rise profile for the center

**Figure 4-7. Semi-adiabatic temperature profiles for the slag mixes**

Figure 4-6a clearly shows a linear trend that as the slag replacement increases, the maximum temperature decreases, and the time to achieve the maximum temperature increases. Although the temperature profile in Figure 4-6a shows a clear pattern, the temperature rise (calculated by subtracting the temperature in the profile from the initial temperature) as presented in Figure 4-6b does not show a clear trend. Figure 4-6b shows the temperature rise for the standard mix (0% slag replacement) and the mix with 75% slag replacement were nearly the same. In addition to the increase in the time to achieve the maximum temperature, the temperature rise at later ages increased as the slag replacement increases because slag hydration has contributed significantly to heat generation. Similar behavior was observed in the bottom corner sensor as well (Figure 4-6c and 4-6d).

However, temperature profiles (Figure 4-7a) obtained from the semi-adiabatic tests show different trends from those of the large block tests (Figure 4-6a). The effects of the ambient temperature and initial concrete temperature are more evidenced by the semi-adiabatic test results (Figure 4-7). The broader temperature peaks and higher temperature rises in the concrete with higher levels of slag replacement for cement at the later ages again demonstrate the increasing slag hydration at later ages.

Using the data presented in Figure 4-6 and Figure 4-7, the true ATR of the concrete mixes can be calculated, which is then used to validate the slag hydration model as explained in Chapter 6.

## 5. DEVELOPMENT OF NEW SLAG HYDRATION PREDICTION MODEL (TASK A-5)

### 5.1. Basic Concept and Methodology

A wide range of study has been conducted on prediction of ATR in mass concrete (Zhu et al. 2022, Bas 2020, Dabarera et al. 2017, Riding et al. 2012, Riding et al. 2007, Riding et al. 2006, Schindler and Folliard 2005, Tam et al. 1994). Based on the published knowledge, degree of hydration (α(*t*)) can be considered as a ratio of the heat evolving at time (*t*) to the ultimate total amount of heat available from cement hydration ($H_u$), and this concept has been used in this project. The equations used for estimation of α(*t*) are shown in equations 5-1 to 5-3 (Zhu et al. 2022, Poole et al. 2007), where the degree of hydration α(*t*) varies from 0 to 1, with a value of 1 indicating complete hydration.

$$a(t) = \frac{H(t)}{H_u} \tag{5-1}$$

$$H_u = H_{cem} * P_{cem} + 461 * p_{slag} + 1800 * p_{FA-CaO} * p_{FA} \tag{5-2}$$

$$H_{cem} = 500 * p_{C_3S} + 260 * p_{C_2S} + 866 * p_{C_3A} + 420 * p_{C_4AF} + 624 * p_{SO_3} + 1186 * p_{FreeCa} + 850 * p_{MgO} \tag{5-3}$$

where $H(t)$ is the heat evolved from time 0 to time $t$ (J/g); $H_u$ is the ultimate total heat available from cement hydration (J/g); $H_{cem}$ is the total heat of cement hydration at α = 1.0 (J/g), which can be calculated using Bogue equations as shown in equation 5-3; and $p_{cem}$, $p_{slag}$, *and* $p_{FA}$ is the mass percentage of portland cement, slag, and fly ash in the total cementitious materials, respectively. $p_{FA\text{-}CaO}$ is the percentage of fly ash CaO mass in the total fly ash content. $p_{C3S}$, $p_{C2S}$, $p_{C3A}$, $p_{C3S}$, $p_{C4AF}$, $p_{SO3}$, $p_{Free\text{-}Ca}$, and $p_{MgO}$, is the percentage of $C_3S$, $C_2S$, $C_3A$, $C_3S$, $C_4AF$, $SO_3$, Free-CaO, and MgO in the cement.

To simplify the comparison of different cementitious systems or conditions, the degree of hydration at an equivalent time (α($t_e$)) is commonly used under the assumption that the cement systems will reach the same degree of hydration at time $t_e$. The degree of hydration at an equivalent time (α($t_e$)) can be calculated using the following equation 5-4:

$$a(t_e) = a_u * e^{-[\frac{\tau}{t_e}]^{\beta}} \tag{5-4}$$

where $t_e$ is equivalent age at which the degree of cement hydration is calculated; $a_u$ is ultimate degree of hydration; τ is the time to reach the hydration peak; and β is a parameter that reflects the shape or curvature of the function (α($t_e$)).

Equivalent age ($t_e$) of concrete can be assessed using equation 5-5.

$$t_e(T_r) = e^{\frac{E_a}{R}*\left(\frac{1}{T_r}-\frac{1}{T_c}\right)} \quad (5\text{-}5)$$

where $t_e(T_r)$ is the equivalent age at the reference temperature, in hours; $T_r$ is the reference temperature (23°C); and $T_c$ is the concrete temperature at the time interval $\Delta t$, in °C.

Thus, the temperature development of a concrete element under adiabatic conditions can be computed from equation 5-6.

$$Q(t) = \int_0^t \dot{q}(t)dt \text{ or } Q(t) = \sum_0^t \frac{Q_h(t)\cdot\Delta t}{\rho\, Cp} \quad (5\text{-}6)$$

where $\dot{q}$ (t) is the heat release rate at time $t$, and it can be calculated from the following equation 5-7:

$$\dot{q}\,(t) = Q_h\,(t)/(\rho C_p) \quad (5\text{-}7)$$

where ρ is the concrete density, in kg/m$^3$; $C_p$ is the concrete specific heat capacity, in (J/kg)/°C; and $Q_h(t)$ is the heat generation in concrete at time $t$, in W/m, which can be calculated using the following equation 5-8:

$$Q_h(t) = H_u * C * \left(\frac{\tau}{t_e}\right)^{\beta} * \left(\frac{\beta}{t_e}\right) * a(t_e) * e^{\frac{E_a}{R}*\left(\frac{1}{T_r}-\frac{1}{T_c}\right)} \quad (5\text{-}8)$$

where $C$ is the weight of cement in the concrete mix, in kg/m$^3$; $R$ is a heat constant; $E_a$ is the activation energy of concrete; $T_r$ is the reference temperature (23°C); and $T_c$ is the concrete temperature at the time interval of interest, in °C.

It should be noted that $a_u$, β, and $\tau$ are critical parameters in the prediction models for cement hydration and concrete ATR. In order to establish robust ATR models for slag hydration and slag concrete, the model inputs should be based on various concrete mixes. Therefore, a literature review was conducted in this study to collect the respective adiabatic temperature data of concrete mixes containing slag and cement as a binary binder. The valid data extracted from the literature reviewed were then used for developing models for predicting $a_u$, β, and $\tau$, and these parameters were further used to establish the slag-cement hydration and the slag-concrete ATR prediction models.

In this study, two types of models were initially considered for predicting slag hydration, and they are (1) the three-parameter (3P) model and (2) the six-parameter (6P) model. In the 3P model, which is the form of the cement hydration model in the current ConcreteWorks software, slag cement is considered as a one-component binder, and its hydration can be described by only one set of three parameters, $\alpha_u$, $\beta$, and $\tau$. In the 6P model, slag cement is considered as having

two-components, portland cement and slag, each of which contributes to the cement hydration separately. Thus, equation 5-6 becomes equation 5-9 given as follows:

$$Q_{total} = a * Q_{h,c}(t) + b * Q_{h,s}(t) \quad (5\text{-}9)$$

To calculate $Q_{h,c}(t)$ and $Q_{h,s}(t)$, the following equations 5-10 and 5-11 are used to replace $\alpha$ ($t_e$) in equation 5-8.

$$a_c(t_e) = a_{u,c} * e^{-[\frac{\tau_c}{t_e}]^{\beta_c}} \quad (5\text{-}10)$$

$$a_s(t_e) = a_{u,s} * e^{-[\frac{\tau_s}{t_e}]^{\beta_s}} \quad (5\text{-}11)$$

In equations 5-10 and 5-11, there are six parameters, $\alpha_{u,c}$, $\beta_c$, and $\tau_c$ for $\alpha_c(t)$ and $\alpha_{u,s}$, $\beta_s$, and $\tau_s$ for $\alpha_s(t)$.

### 5.2. Data Collection

A thorough literature search was conducted to collect the temperature data of concrete mixes containing slag-cement binary binder for the development of a slag hydration model. The following key components were collected:

- Dimensions of the structural element
- Slag physical and chemical compositions
- Cement chemical and physical compositions
- Concrete mix design
- ATR with time, ultimate heat of hydration
- Activation energy
- Fresh and hardened properties

Among the papers reviewed, 20 papers were found to contain valid data for this project (Woo et al. 2018, Zhu et al. 2022, Riding et al. 2012, Bas 2020, Han 2020, Tang et al. 2017, Zayed et al. 2015, Wang and Lee 2010, Chen et al. 2021, Schindler and Folliard 2003, Riding et al. 2019, Hamid and Chorzepa 2020, Luan et al. 2012, Tia et al. 2010, Koo et al. 2014, Abeka et al. 2017, Coole 1998, da Silva et al. 2015, Yikici and Chen 2015, Lawrence et al. 2012). More details on the papers included in the model development can be found in Appendix B.

For papers with sufficient information and valid adiabatic test results, data with concrete mixes containing slag were extracted using the WebPlotDigitizer software. A short description of the procedure used for the data extraction is given as follows:

1. Take a snapshot/picture of the graph from paper/article.
2. Paste the picture in the WebPlotDigitizer software.

3. Mark and align the axis of the graph with values and define the scale.
4. Select the trend/plot of interest.
5. Pick the data points manually one by one from the plot.
6. Pick data points as close as possible.
7. Download the data file as an Excel spreadsheet.

Figure 5-1 shows an example of the data before and after the extraction process. Figure 5-1a is the original graph from the literature, and Figure 5-1b is the graph reconstructed after plotting the extracted data, where only the mixes containing slag are the subject of interest for this project. To ensure sufficient accuracy, more than 50 points were collected from each original curve to reconstruct a new curve.

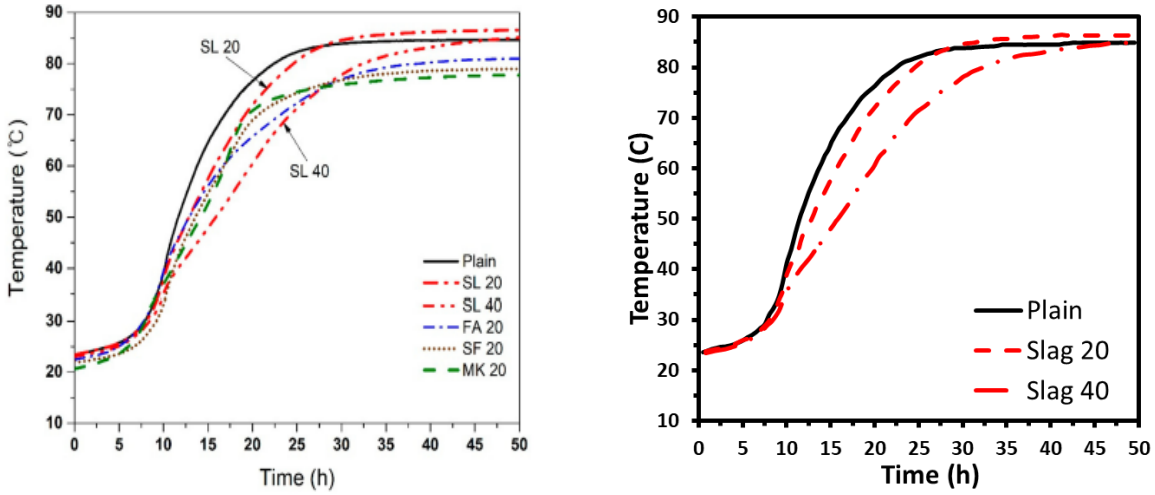


(a) Original curves in literature

(b) Reconstructed curves from extracted data

**Figure 5-1. Illustration of the data extraction using WebPlotDigitizer software**

### 5.3. Data Analysis

After the valid data were extracted, the analysis of the data was conducted using the following steps:

1. Calculate the ultimate total heat of hydration (Hu) using equations 5-2 and 5-3.
2. Obtain the concrete activation energy ($E_a$) (calculated using existing ConcreteWorks equations if not provided in the literature).
3. Calculate the equivalent time ($t_e$) using equation 5-5, and then calculate the degree of cement hydration at an equivalent time ($\alpha(t_e)$) using equation 5-4.
4. Compute the true adiabatic temperature using equations 5-6 to 5-8, where $\alpha u=0.75$, $\beta = 0.8$, and $\tau = 8$ hours were selected as a starting point.
5. Plot the concrete adiabatic temperature calculated from equation 5-6 against the true adiabatic temperature measured and published in the literature. The coefficient of determination, or R2 value, of this plot is then determined.

6. If the R2 value is not acceptable, the selected values of $\alpha_u$, $\beta$, and $\tau$ are adjusted until the R2 value becomes acceptable for further study.

Table 5-1 presents the results from the analysis of the literature data, where regression $R^2$ was maximized using the heat parameter as an independent variable ($\alpha_u$, $\beta$, $\tau$).

**Table 5-1. Hydration parameters based on 3P and 6P models with respective $R^2$ values for the selected mixes**

| Mix | | No. of | 3-Parameter Model | | | | 6-Parameter Model | | | | | | |
|---|---|---|---|---|---|---|---|---|---|---|---|---|---|
| OPC | Slag | Mixes Studied | $R^2$ | $\alpha_u$ | $\beta$ | $\tau$ | $R^2$ | $\alpha_{u,c}$ | $\beta_c$ | $\tau_c$ | $\alpha_{u,s}$ | $\beta_s$ | $\tau_s$ |
| | | | | 0.75* | 0.80 | 8.00 | | 0.75 | 0.80 | 8.00 | 0.60 | 0.65 | 30.0 |
| 80 | 20 | 1 | 0.97 | 0.62 | 0.87 | 21.57 | 0.99 | 0.92 | 0.89 | 21.13 | 0.54 | 0.75 | 31.1 |
| 70 | 30 | 5 | 0.98 | 0.45-0.6 | 0.58-1.3 | 12.4-17.5 | 0.99 | 1.00 | 1.3 | 13.5 | 1.00 | 2.9 | 23.4 |
| 65 | 35 | 1 | 0.99 | 0.69 | 0.74 | 18.86 | 0.99 | 1.00 | 1.16 | 9.51 | 1.00 | 3.47 | 51.1 |
| 60 | 40 | 8 | 0.98 | 0.52-0.71 | 0.63-1.3 | 19-28.63 | 0.99 | 1.00 | 1.30 | 14.04 | 1.00 | 2.69 | 67.3 |
| 55 | 45 | 2 | 0.99 | 0.5-0.55 | 0.6-0.72 | 18.66 | | | | | | | |
| 50 | 50 | 8 | 0.98 | 0.65-0.78 | 0.8-1.4 | 32-46 | 0.99 | 1.00 | 3.55 | 12.94 | 1.00 | 2.45 | 193.3 |
| 30 | 70 | 6 | 0.99 | 0.38-0.66 | 0.7-1.4 | 26-42 | 0.99 | 1.00 | 2.98 | 7.34 | 0.75 | 1.38 | 44.3 |
| 20 | 80 | 2 | 0.98 | 0.32-0.53 | 0.6-1.26 | 29-31.03 | | | | | | | |

Note: The $\alpha_u$, $\beta$, and $\tau$ values in the first row were assumed, and the rest of the values were adjusted to obtain a high $R^2$ value.

It can be seen from Table 5-1 that the $R^2$ values resulting from the 3P and 6P models are very close, 0.98 to 0.99, respectively. Therefore, it was concluded that simple 3P model is sufficient for the hydration heat modeling of the slag-containing concrete mixtures. Thus, it was decided to update the 3P model in the ConcreteWorks software, rather than developing a new model, for the prediction of slag cement hydration.

## 5.4. Determination of Heat Parameters of Slag Cement Hydration

As discussed in Section 5.1, the concrete adiabatic temperature can be calculated from parameters $H_u$, $E_a$, $\tau$, $\beta$, and $\alpha_u$, and these parameters can be predicted based on the concrete mixture proportions and constituent material properties.

In this project, the $\tau$, $\beta$, and $\alpha_u$ parameters are calculated from a statistical analysis based on over 300 semi-adiabatic calorimetry tests performed according to recommendations from International Union of Laboratories and Experts in Construction Materials, Systems and Structures (RILEM) technical committee 119 and validated by 18 tests conducted on concrete sampled from concrete construction sites and 44 tests conducted independently by Schindler and Folliard (2005) and Ge and Wang (2009). The data set used includes concrete containing various chemical admixtures, cement fineness and chemical compositions, and SCMs.

The apparent activation energy, $E_a$, is also calculated based on the cementitious material properties and the chemical admixtures used. A statistical analysis of 117 apparent activation energies calculated from isothermal calorimetry was developed by Poole et al. (2007).

The $H_u$ parameter is calculated from the cement chemical composition using a model developed by Schindler and Folliard (2005) and later altered to better characterize the influence of Grade 120 GGBFS by Poole et al. (2007), as described by equation 5-2.

The cement composition can be determined from either the Rietveld method determined from quantitative XRD or the Bogue method calculated according to ASTM C150.

*5.4.1. Heat Parameter Equations in the Current ConcreteWorks Software*

When the Rietveld method is used to determine the cement chemical composition, the following equations 5-12 through 5-15, which are in the existing ConcreteWorks, were used to calculate the heat of slag cement hydration parameters, $\tau$, $\beta$, $\alpha_u$, and $E_a$ in this study:

$$a_u = \frac{1.031*\frac{w}{cm}}{0.194+\frac{w}{cm}} + \exp\begin{Bmatrix} -0.0885 - 13.7 * p_{C_4AF} * p_{cem} \\ -283\ p_{Na_2O_{eq}} * p_{cem} \\ -9.90 * p_{FA} * p_{FA-CaO} \\ -339 * WRRET - 95.4 * PCHRWR \end{Bmatrix} \quad (5\text{-}12)$$

$$\beta = \exp\begin{Bmatrix} -0.464 + 3.41 * p_{C_3A} * p_{cem} - 0.846 * p_{slag} + 107 * WRRET \\ +33.8 * LRWR + 15.7 * MRWR \\ +38.3 * PCHRWR + 8.97 * NHRWR \end{Bmatrix} \quad (5\text{-}13)$$

$$\boldsymbol{\tau} = \exp\begin{Bmatrix} 2.92 - 0.757 * p_{C_3S} * p_{cem} + 98.8 * p_{Na_2O} * p_{cem} \\ +1.44 * p_{slag} + 4.12 * p_{FA} * p_{FA-CaO} \\ -11.4 * ACCL + 98.1 * WRRET \end{Bmatrix} \quad (5\text{-}14)$$

$$E_a = 41230 + 8330 * \left[\left(p_{C_3A} + p_{C_4AF}\right) * p_{cement} + p_{Gypsum} * p_{cement}\right]$$
$$-3470 * Na_2O_{eq} - 19.8 * Blaine + 2.96 * p_{FA} * p_{FA-CaO}$$
$$+162 * p_{GGBS} - 516 * p_{sf} - 30900 * WRRET - 1450 * ACCL \quad (5\text{-}15)$$

where *p-$C_3S$,* $C_3S$, $C_2S$, $C_3A$, $C_3S$, $C_4AF$, cement, slag, FA-CaO and FA is the same as that defined in equations 5-2 and 5-3. *p-$Na_2O_{eq}$*, *$Na_2O$, and Gypsum* is the percentage of $Na_2O_{eq}$, $Na_2O$, and gupsum in the portland cement, respectively. *p-GGBFS and p-SF* is the percentage of GGBFS and silica fume of the total cementitious materials, respectively. *WRRET* is the ASTM Type B and D WR/retarder dosage, *PCHRWR* is an ASTM Type F polycarboxylate-based high-range WR dosage, *LRWR* is the ASTM Type A WR dosage, *MRWR* is the mid-range WR dosage, *NHRWR* is the Type F naphthalene high-range WR dosage, and *ACCL* is the ASTM Type C accelerator dosage. The chemical admixture dosages are in percent solids by weight of cementitious materials.

In the current ConcreteWorks software, the existing model equations for the hydration parameters ($\alpha_u$, $\beta$, $\tau$) (equations 5-12 to 5-15) do not take the slag physical and chemical compositions into account but only the slag replacement level (in percentage). The main objective of the present work is to include the slag physical and chemical compositions into the

slag hydration parameter equations. To fulfil this goal, a statistical approach is used to update the hydration parameters with new equations.

Table 5-2 shows the hydration parameters calculated from the equations in ConcreteWorks (equations 5-12 to 5-14), in comparison with those obtained from the literature data using the 3P model procedure as described in Section 5.3. It can be seen from the table that the values of the hydration parameters obtained from the 3P model of the literature data and from the existing ConcreteWorks model differ greatly from each other, implying the need for updating the hydration parameter equations in the ConcreteWorks software.

**Table 5-2. Hydration parameters calculated from new 3P model vs. current ConcreteWorks equation**

| Mix | | No. of Mixes Studied | New 3P Model from Regression of Literature Data | | | | 3P Model in Current ConcreteWorks | | |
|---|---|---|---|---|---|---|---|---|---|
| OPC | Slag | | $R^2$ value | α' | β' | τ' | α | β | τ |
| – | | (45 Total) | – | 0.75 | 0.80 | 8.00 | – | | |
| 60 | 40 | 1 | 0.99 | 1.26 | 0.80 | 20.67 | 0.73 | 0.52 | 45.77 |
| 40 | 60 | 2 | 0.99 | 1.00 | 0.89 | 48.54 | 0.831 | 0.46 | 56.02 |
| 30 | 70 | 3 | 0.99 | 1.00 | 0.77 | 61.74 | 0.87 | 0.44 | 61.98 |
| 20 | 80 | 4 | 0.98 | 0.79 | 0.81 | 54.11 | 0.92 | 0.41 | 68.57 |
| 50 | 50 | 5 | 0.99 | 0.83 | 0.67 | 30.17 | 0.77 | 0.52 | 43.55 |
| 50 | 50 | 6 | 0.99 | 0.84 | 1.00 | 20.7 | 0.78 | 0.65 | 43.55 |
| 50 | 50 | 7 | 0.99 | 0.63 | 0.66 | 10.68 | 0.79 | 0.46 | 39.85 |
| 30 | 70 | 8 | 0.98 | 0.57 | 0.80 | 10.44 | 0.87 | 0.41 | 53.54 |
| 70 | 30 | 9 | 0.97 | 1.11 | 0.88 | 9.01 | 0.85 | 0.50 | 22.93 |

Note: The $\alpha_u$, $\beta$, and $\tau$ values in the first row were assumed, and the rest of the values were adjusted to obtain a high $R^2$ value.

*5.4.2. New Hydration Heat Parameter Equations Developed from the Literature Data*

Portland cement chemistry is basically well known, and it is generally consistent for cement from a given plant. Thus, it is rational to assume that the differences in hydration parameter values between cement without and with slag replacement are attributed to the slag chemistry. Therefore, a regression analysis was designed to evaluate the effect of the slag physical and chemical compositions on the hydration parameters. The hydration parameters were modeled with the slag physical and chemical properties.

The ConcreteWorks model hydration parameters are $\alpha_u$, $\beta$, and $\tau$; the new 3P hydration model hydration parameters are $\alpha_u'$, $\beta'$, and $\tau'$ . The difference between the hydration parameters calculated from the ConcreteWorks model and the new 3P hydration model are noted as Φ, which has three components, $\Phi_\alpha$, $\Phi_\beta$, and $\Phi_\tau$ for parameters α, β, τ, respectively. Equations 5-16 to 5-18 express the calculations of each Φ component.

$$\phi_\alpha = \alpha'_u - \alpha_u \quad (5\text{-}16)$$

$$\phi_\beta = \beta' - \beta \quad (5\text{-}17)$$

$$\phi_\tau = \tau' - \tau \quad (5\text{-}18)$$

Equations 5-16 through 5-18 can be rewritten in a common mathematical form as follows:

$$\phi = F(\text{slag physical and chemical properties}) \quad (5\text{-}19)$$

where $F$ represents a function.

Based on the literature review, a few components significantly influence heat generated from cement hydration, and they were slag replacement level, slag fineness, and alkali, alumina, sulphur, magnesium, and calcium contents of the slag. Therefore, the information on these slag properties was collected (Appendix C) and considered in this study. To assist with the data analysis, the collected values were represented by seven parameters: slag replacement fraction (X1), alumina content (X2), alkali content (X3), calcium content (X4), magnesium content (X5), sulphur content (X6), and slag fineness (X7). However, it was found later that slag fineness (X7) was not reported by most of the literature. Due to the very limited data on the fineness of slag, the team decided to eliminate the variable X7, resulting in six independents variables (X1–X6).

Thus, equation 5-19 can be rewritten as $\phi = F(X)$.

As described in the following section, a key task for the development of the slag cement hydration model is to find the function, *F*.

5.4.2.1. Linear Regression to Evaluate the Relationship between Hydration Heat Parameters and Slag Physical Properties

As discussed above, function *F* describes the relationship (function) of the slag chemical and physical properties (independent variables, X1–X7) with the hydration parameters (dependent variables, $\alpha_u$, $\beta$, and $\tau$) of a slag cement binder. In statistics, linear regression is a linear approach for modeling the relationship between the dependent variable and the independent variable. In the case that only one dependent variable is considered, the regression is called simple linear regression. If more than one dependent variable is considered, the regression is called multiple linear regression. This term is distinct from multivariate linear regression, where multiple correlated dependent variables are predicted, rather than a single scalar variable.

In this study, since the independent variable *X* is a matrix with seven components, the regression is multivariate linear regression as noted in this section.

$$\phi_\alpha = F_1(X_i) \quad (5\text{-}20)$$

$$\phi_\beta = F_2(X_i) \quad (5\text{-}21)$$

$$\phi_\tau = F_3(X_i) \quad (5\text{-}22)$$

In the present study, the following two groups of regression formats were used:

Group 1 (simple linear equations)

Linear regression (single variable):

$$\phi = a_0 + a_1 x_1 \quad (5\text{-}23)$$

Linear regression (multiple variables):

$$\phi = a_0 + a_1 x_1 + a_2 x_2 \ldots \quad (5\text{-}24)$$

Group 2 (log linear equations)

Linear regression (single variable in log):

$$\phi = a_0 + a_1 \log(x_1) \quad (5\text{-}25)$$

Linear regression (multiple variables in log):

$$\phi = a_0 + a_1 \log(x_1) + a_2 \log(x_2) + \ldots. \quad (5\text{-}26)$$

The regression was performed using the data set collected from the literature. Nearly 33 different data sets were used to do the regression, and each time the $R^2$ values were calculated to see the dependency on the regression. Because the information on the independent variable fineness (X7) was not reported by most of the literature, the team decided to eliminate the variable X7, resulting in six independents variables.

Multiple trials of the regression analyses were conducted. First, the single variable linear regression was conducted to see the effect of each independent parameter (for example, X1: slag replacement) on the dependable parameter (hydration parameters: $\phi_\alpha$, $\phi_\beta$, and $\phi_\tau$) and respective $R^2$ values were measured. Table 5-3 shows that the $R^2$ values for all $\phi$ ($\phi_\alpha$, $\phi_\beta$, and $\phi_\tau$) of trials 1 through 5 were always less than 0.5, indicating a poor correlation between the dependent and independent variable, or a poor regression function. Therefore, multivariate linear regression analyses (trials 6 through 29) were conducted with all possible combinations to get the best fit. It was found that as more variables were considered, the $R^2$ values increased, and the highest $R^2$ value reached 0.66 when all material parameters, X1 through X6, were included in regression. The trial analyses were done for $\phi_\alpha$ initially. After the $R^2$ value of $\phi_\alpha$ exceeded 0.5, more regressions were then performed for $\phi_\beta$ and $\phi_\tau$. As seen in Table 5-3 and Appendix D, the regression analyses suggest that the heat of slag cement hydration is governed by multiple factors.

**Table 5-3. Hydration parameters affected by the slag properties (X1–X6) considered**

| Trial | No. of Variables | Replacement (X1) | Alumina (X2) | Alkali (X3) | Ca (X4) | Mg (X5) | Sulphur (X6) | $R^2$ Value | | |
|---|---|---|---|---|---|---|---|---|---|---|
| | | | | | | | | $\phi_\alpha$ | $\phi_\beta$, | $\phi_\tau$ |
| 1 | 1 | | | | Yes | | | 0.21 | | |
| 2 | | | | | | Yes | | 0.30 | | |
| 3 | | | Yes | | | | | 0.24 | | |
| 4 | | Yes | | | | | | 0.35 | | |
| 5 | | | | | | | Yes | 0.15 | | |
| 6 | 2 | Yes | Yes | | | | | 0.24 | | |
| 7 | | Yes | | Yes | | | | 0.38 | | |
| 8 | | Yes | | | | | Yes | 0.34 | | |
| 9 | | | Yes | Yes | | | | 0.25 | | |
| 10 | | Yes | | | Yes | | | 0.29 | | |
| 11 | | Yes | | | | Yes | | 0.39 | | |
| 12 | 3 | Yes | Yes | Yes | | | | 0.36 | | |
| 13 | | Yes | | Yes | | Yes | | 0.41 | | |
| 14 | | Yes | | | Yes | Yes | | 0.19 | | |
| 15 | | Yes | | | Yes | | Yes | 0.23 | | |
| 16 | | Yes | | Yes | Yes | | | 0.27 | | |
| 17 | | Yes | | Yes | | | Yes | 0.43 | | |
| 18 | | | Yes | Yes | | Yes | | 0.14 | | |
| 19 | | | Yes | Yes | | | Yes | 0.43 | | |
| 20 | | | Yes | | Yes | Yes | | 0.36 | | |
| 21 | 4 | Yes | Yes | Yes | | Yes | | 0.48 | | |
| 22 | | Yes | Yes | Yes | Yes | | | 0.47 | | |
| 23 | | Yes | Yes | Yes | | | Yes | 0.46 | | |
| **24** | | **Yes** | **Yes** | | **Yes** | **Yes** | | **0.55** | | |
| 25 | | Yes | | Yes | Yes | Yes | | 0.53 | | |
| 26 | 5 | Yes | Yes | Yes | Yes | | Yes | 0.52 | | |
| 27 | | Yes | Yes | Yes | | Yes | Yes | 0.5 | | |
| 28 | | Yes | Yes | Yes | Yes | Yes | | 0.5 | | |
| 29 | 6 | Yes | Yes | Yes | Yes | Yes | Yes | 0.66 | 0.51 | 0.6 |

Figure 5-2 show the relationship of $\phi_{actual}$ (measured and reported in the reviewed literature) and $\phi_{model}$ (from the literature data regression) for the dependent variable X1 (slag replacement) and respective $R^2$ values.

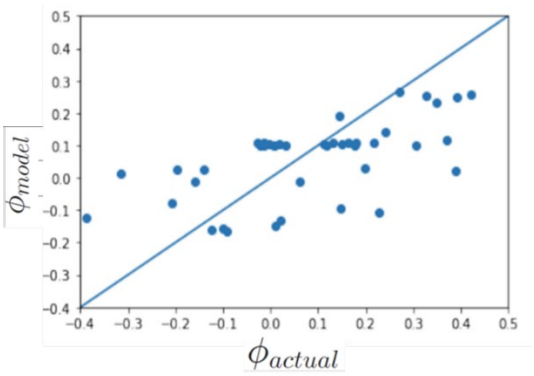


(a) $\phi_\alpha$

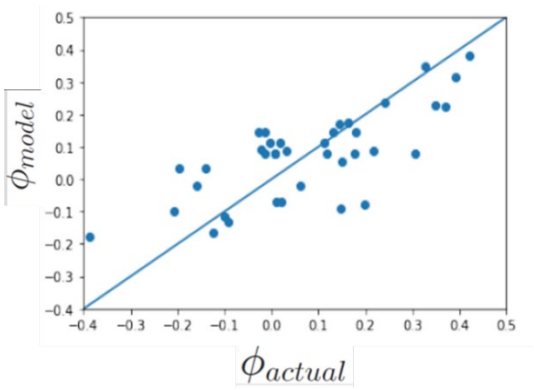


(b) $\phi_\beta$

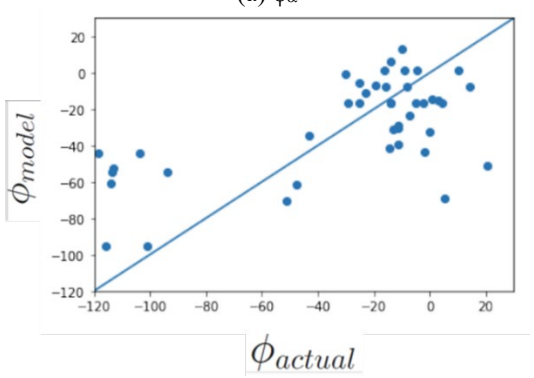


(c) $\phi_\tau$

$R^2$ values for $\phi_\alpha$ = 0.23
$R^2$ values for $\phi_\beta$ = 0.38
$R^2$ values for $\phi_\tau$ = 0.30

(d) $R^2$ values for slag replacement

**Figure 5-2. Relationship between $\phi_{actual}$ and $\phi_{model}$ for the dependent variable X1 (slag replacement)**

Similarly, the simple linear regression was performed for all six independent variables (X1 through X6), and the corresponding relationships and $R^2$ values of each independent variables can be found in Appendix D.

5.4.2.2. Model Improvement by Cross-Checking the Selective Mixture Data

An effort was made to ensure the reliability of the linear regression presented in Section 5.4.2.1. As shown in this section, this work was done by identifying the outliers and cross-checking the selective mixture data to catch any errors and redo the analysis if needed. In this approach, selective outliers were found in the highest $R^2$ value regression, the background calculations were checked, and a 10% error margin was considered.

Figure 5-3 shows the sample results from linear regression of the single variable X3 (alkali content of slag). It is clearly seen that the $R^2$ values in Figure 5-3 were improved significantly when compared with those in Figure 5-2 and Table 5-3 (as shown in trials 1 through 5).

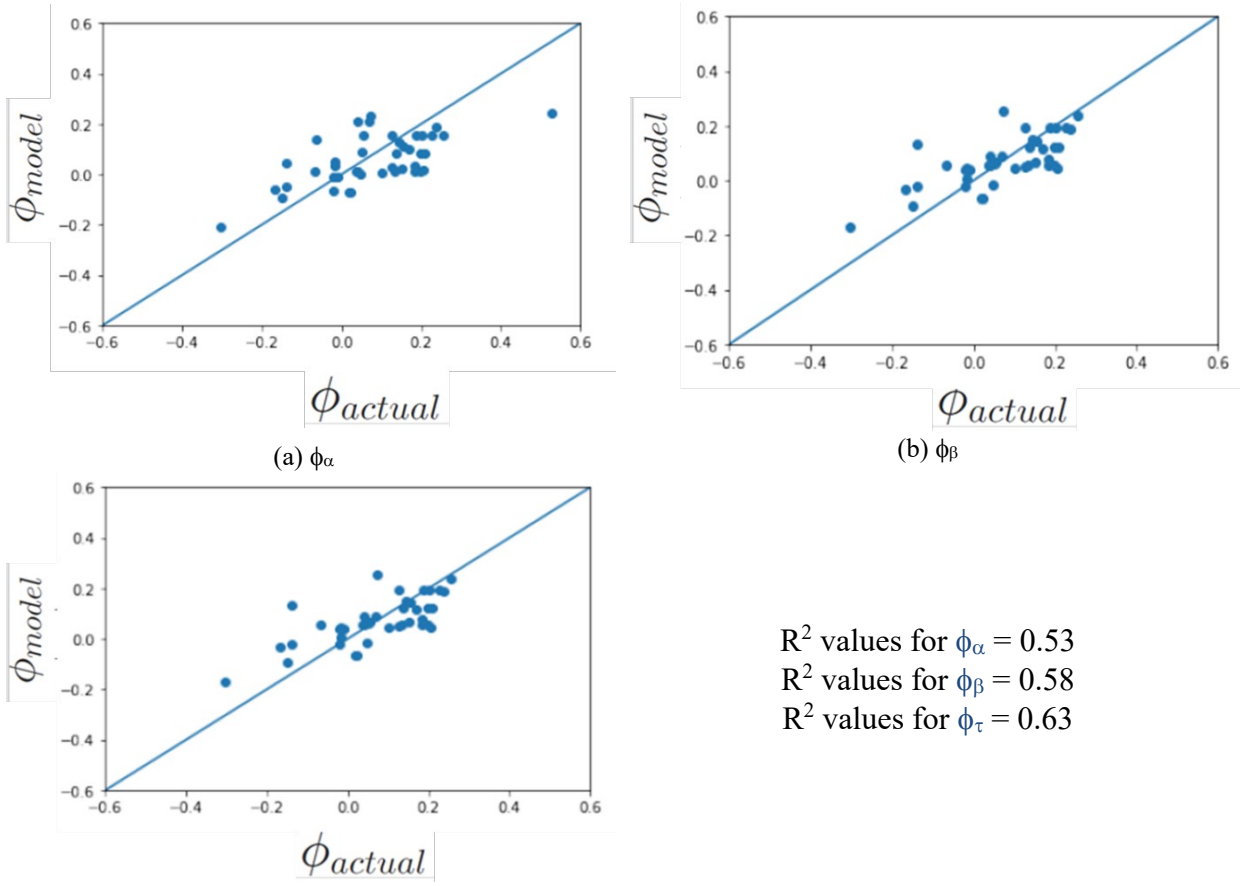


(a) $\phi_\alpha$ (b) $\phi_\beta$

(c) $\phi_\tau$

$R^2$ values for $\phi_\alpha$ = 0.53
$R^2$ values for $\phi_\beta$ = 0.58
$R^2$ values for $\phi_\tau$ = 0.63

**Figure 5-3. Relationship between $\phi_{actual}$ and $\phi_{model}$ for the dependent variable X3 (alkali content)**

5.4.2.3. Model Improvement Using Higher Order Multivariate Regression

Although gradual improvements were made with more independent variables and the error margin considered as presented in Sections 5.4.2.1 and 5.4.2.2, most $R^2$ values up to this point were still less than desired (<0.65). Therefore, some new approaches were selected as follows:

1. Examine the $R^2$ values from the predicted total heat ($H_u$) and final ATR from regression models versus measured data. This approach was based on the consideration that the combination of all hydration parameters ($\phi_\alpha$, $\phi_\beta$, $\phi_\tau$) results in overall heat or temperature rise. Thus, the total heat and final temperature from the predicted function should match the measured data collected from the corresponding literature-collected data. Based on their relationship, $R^2$ could be calculated.
2. Conduct higher order regression analysis such as second-order regression, third-order regression, etc.

   The second-order regression (multiple variables) can be expressed as follows:

$$\phi = a_0 + a_1 x^2_1 + a_2 x_1 + a_3 x_2 + \ldots \quad (5\text{-}27)$$

The third-order regression (multiple variables) can be expressed as follows:

$$\phi = a_0 + a_1 x^3_1 + a_2 x^2_1 + a_3 x_1 + \ldots] \quad (5\text{-}28)$$

3. Change the regression approach from additive to multiplicative.

The following equations are used for this new approach, where the relationship between the independent and dependent variable is exponential:

$$Y = (e^{c_0} * x_1^{c_1} * x_2^{c_2} * x_3^{c_3} \ldots..) \quad (5\text{-}29)$$

$$Y = \exp(c_0 + c_1 x_1 + c_2 x_2 + c_3 x_3 \ldots\ldots) \quad (5\text{-}30)$$

Based on the outcome of the linear regression and the high order, a multivariate analysis approach was chosen for use with the collected data.

In the present study, the following steps were conducted using the above-mentioned approaches:

1. At the beginning, only second-order regression trials were carried out, which showed significant improvement in the $R^2$ values.
2. Based on the initial results, third-order regression trials were carried out, which showed a great improvement with the average $R^2$ values of 0.9.
3. Later, it was seen that the third-order regression was over-fitting the data due to the flexibility in the independent variable terms.

In a similar fashion, over-fitting a regression model occurs when one attempts to estimate too many parameters from a sample that is too small. Regression analysis uses one sample to estimate the values of the coefficients for all the terms in the equation. The sample size limits the number of terms that one can safely include without over-fitting the model. The number of terms in the model includes all of the predictors, interaction effects, and polynomials terms (to model curvature). Larger sample sizes allow one to specify more complex models. For trustworthy results, the sample size must be large enough to support the level of complexity that is required by the research question. If the sample size is not large enough, it will not be able to fit a model that adequately approximates the true model for a response variable. Thus, the results will not be accurate and acceptable.

As an example, Figure 5-4 presents the relationship between $\phi_{actual}$ and $\phi_{model}$ for the dependent variable X1, X2, and X3 in the second order of trials (trial 12 in Table 5-3). Trial 12 was chosen as the best one among the analyses conducted.

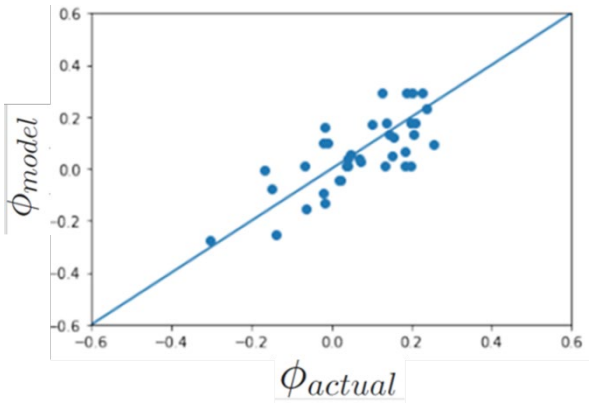


(a) $\phi_\alpha$

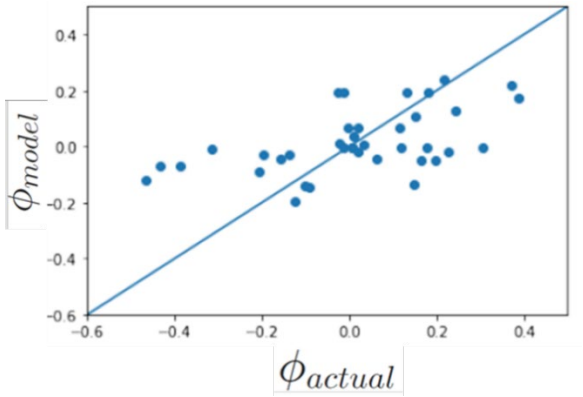


(b) $\phi_\beta$

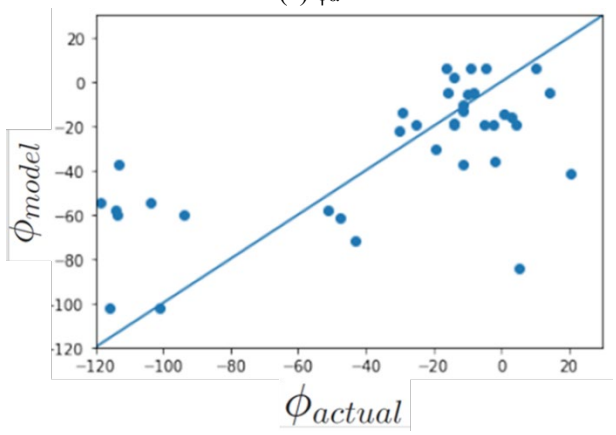


(c) $\phi_\tau$

$R^2$ values for $\phi_\alpha$ = 0.69
$R^2$ values for $\phi_\beta$ =0.29
$R^2$ values for $\phi_\tau$ = 0.43
X1=Replacement, X2=Alumina, X3= alkali,
(trial 12 in Table 5-3)

(d) $R^2$ values

**Figure 5-4. Relationship between $\phi_{actual}$ and $\phi_{model}$ for the dependent variables X1, X2, and X3 in Trial 12**

5.4.2.4. Final Models for Heat Parameters of Slag Hydration Developed from Regression of Literature Data

After many trials (as shown in Appendix D), Figure 5-5 shows that the $R^2$ values of $\phi_\alpha$, $\phi_\beta$, and $\phi_\tau$ all reached 0.88, which is significantly improved when compared with the previous analyses. Therefore, this regression analysis result and its accompanying equations are acceptable as the new slag hydration parameters, which are in second order, for the new slag hydration model. The third-order analysis was rejected due to over-fitting.

The new modeled equations for predicting are as follows:

$$\phi_\alpha = a_1 * X_1 + a_2 * X_3 + a_3 * X_1^2 + a_4 * X_1 * X_3 \quad (5\text{-}31)$$

$$\phi_\beta = b_1 * X_2 + b_2 * X_3 + b_3 * X_1^2 + b_4 * X_2 * X_3 + b_5 * X_3^2 \quad (5\text{-}32)$$

$$\phi_\tau = c_1 * X_2 + c_2 * X_3 + c_3 * X_1^2 + c_4 * X_2 * X_3 + c_5 * X_3^2 \quad (5\text{-}33)$$

where X1 is the slag replacement amount, X2 is the alumina content, X3 is the alkali content, and X4 is the calcium content of the slag used.

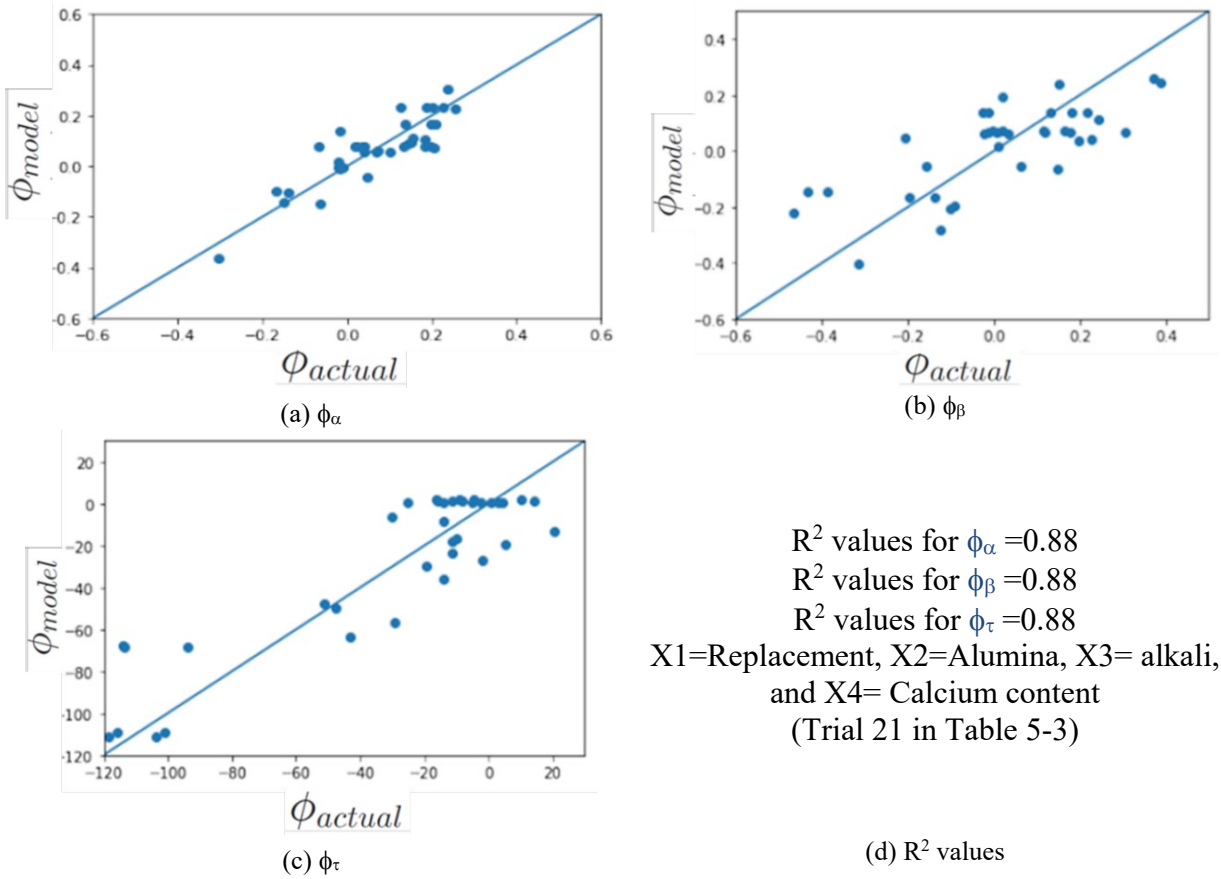


**Figure 5-5. Relationships of $\phi_{actual}$ and $\phi_{model}$ for the dependent variable X1, X2, X3, and X4 in the second-order trial (trial 21 in Table 5-3)**

Knowing $\Phi_\alpha$, $\Phi_\beta$, and $\Phi_\tau$, the new heat parameters $\alpha_u$', $\beta$',$\tau$', of slag cement hydration can be predicted using equations 5-16, 5-17, and 5-18. Together with the activation energy, $E_a$, value calculated from equation 5-15, the new heat parameters can be used for predicting adiabatic temperature of the slag concrete using equations 5-6 and 5-8.

It should be noted that the values of the coefficients ($a_i$, $b_i$, and $c_i$) in equations 5-31 to 5-33 are not presented here because they were further modified during the model validation (as described in Chapter 6). The final equations, after the model validation, are presented in Chapter 7.

## 6. DEVELOPMENT AND VALIDATION OF ATR PREDICTION MODEL (TASK A-6)

As mentioned above, using the heat parameters ($\alpha_u$', $\beta$', and $\tau$') developed in Chapter 5, the true ATR in concrete containing slag can be predicted from equation 5-6. This ATR prediction model needs to be further validated. The temperature data monitored from the laboratory-cast concrete blocks as described in Chapter 4 are designed to serve this purpose.

However, as seen in the previous Figure 4-5, the concrete block temperatures monitored decrease after reaching the peak, indicating a heat loss in the system. That is, they do not represent the true adiabatic temperature profile, where no heat loss or temperature decrease should occur. Thus, the measured concrete block temperature data need to be converted into true adiabatic temperature data with compensation for the heat loss. In this project, 4C software was used to help convert the measured concrete block temperature data into true adiabatic temperatures.

4C has the ability to predict temperature distribution, stress distribution, and distribution of the tensile stress/strength ratio of a concrete element or member. Using the finite element method, 4C computes the thermal stress of a concrete element based upon (1) the differential temperature resulting from thermal analysis, (2) static and geometrical boundary conditions (load, support conditions, etc.), and (3) the development of stiffness, strength, creep, and relaxation properties as a function of maturity. More detailed information can be found in a previous project report (Shaw et al. 2014).

To convert the measured temperature data from the concrete blocks, made with 0%, 25%, 50%, and 75% slag replacement for cement as described in Chapter 4 into true adiabatic temperature, the team's approach was to change the heat parameters ($\alpha$, $\beta$, and $\tau$) in 4C so that the concrete block temperature profile simulated using 4C matches the temperature rise and the maximum temperature profile measured from the large concrete block tests. Since the early-age temperature rise and the maximum temperature are the most important aspect of the temperature profile, the team's focus was on the close match of the early-age temperature profile. Figure 6-1 shows basic steps in the 4C simulation to mimic the concrete block data.

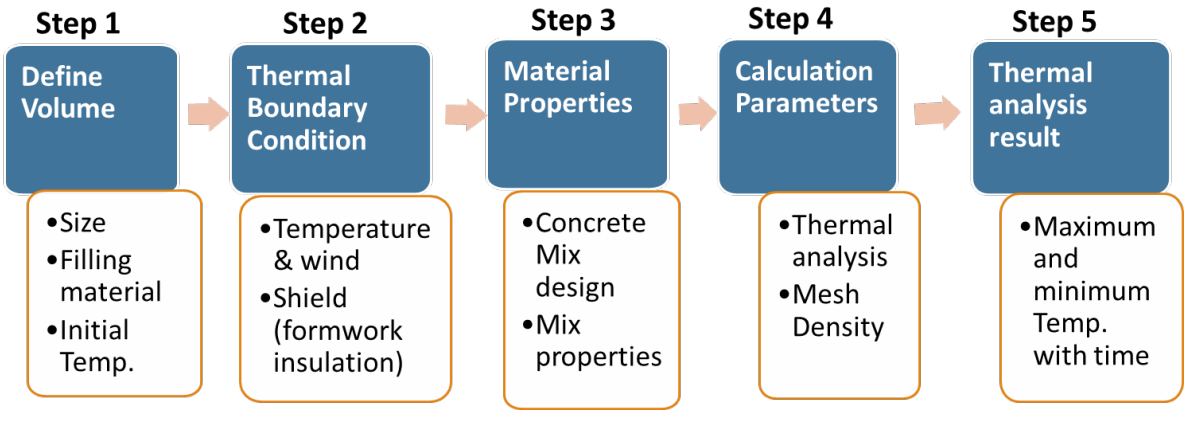


**Figure 6-1. 4C thermal analysis procedure**

As illustrated in Figure 6-1, the input data of 4C include (1) volumetric data of a given concrete element (size, shape, and configuration) (Step 1); (2) the thermal boundary condition (ambient temperature, wind, insulation, and cooling pipes/heating wires) of the concrete element (Step 2); and (3) the material properties (materials used, mix proportion, and placement information) (Step 3). After having these input data, 4C can predict the temperature, maturity, and strength of the concrete, as functions of time (Steps 4 and 5).

The temperature curves provided by 4C are in the form of contour lines, which indicate the temperature development at the cross section of the concrete element. 4C also allows one to input the heat of cementitious hydration, concrete properties (strength/maturity development, thermal properties [specific heat, conductivity, and expansion], initial strain, creep, etc.), construction condition (casting time and temperature), and thermal boundary conditions (insulation, heating mats, cooling pipes, etc.) of the concrete element to be studied manually, according to a prescribed program (under a "surface mode").

## 6.1. 4C Thermal Analysis of Concrete Blocks

### *6.1.1. Input Data*

The input data for the 4C analysis were selected as same as the properties and conditions of the concrete blocks tested in Chapter 4. Detailed inputs are given in the following subsections.

#### 6.1.1.1. Volumetric Parameters (Step 1)

As described in Chapter 4, the concrete blocks cast have a prism shape with a dimension of 3 ft in length, 3 ft in width, and 4 ft in height. The volumetric parameters of 4C include the volume and initial boundary conditions of each face of the analyzed element. The volume consists of shape of geometry, dimensions of the element (only two-dimensional), starting time, and initial temperature. Table 6-1 shows the volumetric parameters of large block mixes for the 4C analysis, as discussed previously.

**Table 6-1. Volumetric parameters of large block for 4C analysis**

| Identification | Material | Size (cm × cm) | Thickness (m) | Start Time (h) | Initial Temperature (°C) |
|---|---|---|---|---|---|
| Large Block (0% slag) | Concrete Mix 0% slag | 91.44 × 91.44 | 1.2 | 0 | 21.2 |
| Large Block (25% slag) | Concrete Mix 25% slag | 91.44 × 91.44 | 1.2 | 0 | 20.16 |
| Large Block (50 % slag) | Concrete Mix 50 % slag | 91.44 × 91.44 | 1.2 | 0 | 16.27 |
| Large Block (75% slag) | Concrete Mix 75% slag | 91.44 × 91.44 | 1.2 | 0 | 10.5 |

6.1.1.2. Thermal Boundary Conditions (Step 2)

The boundary conditions of each face of an analyzed element are significant for thermal analysis. The inputs for thermal boundary conditions required by 4C include initial temperature, wind velocity, shield, heat transfer coefficients, flux, and radiation, where temperature and shield/insulation details are the most essential parameters. The following sections describe the thermal boundary conditions used in the present project.

In this project, a sine function was used to model the fluctuations in ambient temperature to simulate temperature boundary conditions. The temperature boundary parameters of a sine curve include the starting time (*h*) of the initial temperature, minimum temperature (°C), and maximum temperature (°C). Table 6-2 shows the environmental thermal boundary conditions of the various large block mixes.

**Table 6-2. Environmental boundary conditions for large block mixes**

| Identification | Start Time (h) | Min. Temp. (°C) | Max. Temp. (°C) | Temp. Variation | Wind Velocity (m/s) |
|---|---|---|---|---|---|
| Large Block (0% slag) | 0 | 22 | 24 | Sine wave | 0 |
| Large Block (25% slag) | 0 | 22 | 24 | Sine wave | 0 |
| Large Block (50% slag) | 0 | 22 | 24 | Sine wave | 0 |
| Large Block (75% slag) | 0 | 22 | 24 | Sine wave | 0 |

The surface temperature of the concrete blocks studied was assumed to be equal to the average of the seven-day ambient temperature during the whole analysis period, which was inputted using a sine curve format. Wind velocity is assumed constant (zero for our case) during the analysis period instead of varying every day.

The shield information (insulation details) defines the formwork and curing method of the analyzed concrete element. Figure 6-2 shows the insulation conditions of the concrete blocks cast. The large concrete blocks (size 3 ft × 3 ft × 4 ft) were insulated in three layers. The first layer was Styrofoam (2 in. and three layers), the second layer was a steel formwork (0.11 in. thick), and the third layer was an insulation blanket (4 cm and two layers).

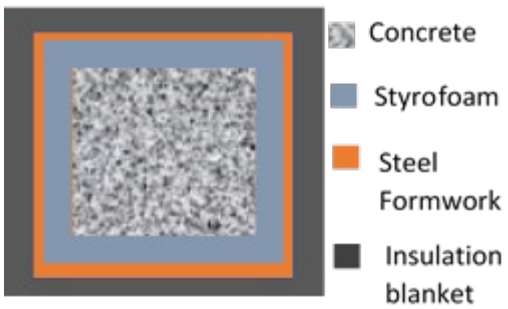


**Figure 6-2. Schematic of concrete block and boundary conditions**

As seen in Figure 6-2, the insulation boundary condition of the concrete blocks cast included the Styrofoam, steel formwork, and insulation blanket on the top. There were three layers of Styrofoam with 2 in. of thickness for each layer. From the R-value of Styrofoam provided by the manufacturer, the thermal conductivity (λ) of the Styrofoam was calculated using the following equation:

$$R = \frac{t}{\lambda} \tag{6-1}$$

where $t$ is the thickness in meters, and λ is thermal conductivity in W/mK.

Similarly, the thermal conductivity of the steel formwork and the insulation blanket were calculated. The thermal conductivity of the overall insulation is presented in Table 6-3.

**Table 6-3 Insulation thermal properties**

| Insulation | Thickness (m) | Thermal conductivity (kJ/m.h.c) |
|---|---|---|
| Styrofoam Sheet **(SS)** | 0.150 | 0.18 |
| Steel Formwork **(SF)** | 0.003 | 200.00 |
| Insulation Blanket **(IB)** | 0.080 | 0.32 |

In this study, the insulation blanket was folded in two layers to cover the large concrete block. Thus, the thickness of the insulation blanket was doubled for the input parameter. Since there is no steel formwork on the top surface of the concrete blocks tested, two separate shield insulation boundary conditions were used for the study. The first one included Styrofoam, steel formwork, and insulation blanket; the second one was for the top surface of concrete block only, which had the Styrofoam and insulation blanket.

It should be noted that 4C does not have any specific consideration for the edges, corners, and places from where the heat may be leaked. The software considers the case where the insulation is 100% perfect, which is clearly not true in a laboratory or field study. The software also does not include reinforcement in concrete.

After the previous information is defined, the heat transfer coefficient and thermal coefficient of concrete can be automatically generated by 4C. Flux and radiation can be left blank depending on the environment.

6.1.1.3. Concrete Materials and Properties (Step 3)

Table 6-4 and Table 6-5 show the list of the input data of concrete materials, proportions, and properties used for the 4C analysis.

**Table 6-4. Concrete mix properties inputs for 4C**

| Concrete Property | 0% Slag | 25% Slag | 50% Slag | 75% Slag | Unit |
|---|---|---|---|---|---|
| Slump | 63.50 | 69.85 | 50.8 | 95.25 | mm |
| Water-cement (w/c) ratio | 0.44 | 0.44 | 0.44 | 0.44 | kg/kg |
| Air content | 6.50 | 6.20 | 5.90 | 2.30 | % |
| Specific heat | 0.88 | 0.87 | 0.86 | 0.86 | kJ/kg/°C |
| Thermal conductivity | 4.0 | 3.8 | 3.8 | 3.8 | kJ/m/h/°C |
| Density | 2,287.44 | 2,299.61 | 2,309.54 | 2,413.98 | $kg/m^3$ |
| Act. energy factor 1 | 33,500 | 33,500 | 33,500 | 33,500 | J/mol |
| Act. energy factor 2 | 1,479 | 1,479 | 1,479 | 1,479 | J/mol/°C |
| Cement | 352 | 264 | 176 | 88 | $kg/m^3$ |
| Cement + mineral additive | 352 | 352 | 352 | 352 | $kg/m^3$ |

**Table 6-5. Material properties inputs for 4C**

| Type | Density ($kg/m^3$) | Specific heat (kJ/kg/°C) | Thermal Conductivity (kJ/m/h/°C) |
|---|---|---|---|
| Cement Type I/II | 3,140 | 1.14 | 1.04 |
| Slag G 100 | 2,930 | 1.05 | 1.01 |
| Coarse aggregate | 2,680 | 0.84 | 4.3 |
| Fine aggregate | 2,650 | 0.77 | 0.71 |
| Euclid WR 91 | 1,050 | 4.185 | 1.04 |
| Water | 1,000 | 4.18 | 2.09 |

The specific heat of cement, aggregates, water, slag, and chemical admixture could be defined by measurements or recommended values. In this study, the specific heat of the materials is shown in Table 6-4. These values were taken from the default data given in 4C for concrete, and some were obtained from the Engineering Toolbox website and literature (Sargam et al. 2020). In the concrete properties input section, activation energy factors were assumed to be 33,500 J/mol, and 1,470 J/mol/°C as default values in 4C.

In the concrete database section of 4C, the current concrete information can be chosen to be used or a new concrete database can be added. Creating a new database requires input information about mixture proportions (cement, water, aggregate, chemical admixture, and their respective properties and quantities such as specific heat and thermal conductivity), properties (slump, w/c ratio, air content, specific heat, thermal conductivity, and density), heat, E-modulus, Poisson ratio, thermal expansion coefficient, initial strain, creep, compressive strength, and tensile strength. These details are listed in Table 6-6.

**Table 6-6. Hardened properties of large concrete block**

| Properties | Values |
|---|---|
| Elastic modulus | Total: 60,000 MPa<br>Time (h): 750<br>Curvature: 0.8 |
| Poisson ratio | Total: 0.17<br>Time (h)<br>Curvature: |
| Thermal expansion coefficient | 0.000008 (1/c) |
| Initial strain | None |
| Creep | None |
| Compressive strength | Total: 60 MPa<br>Time (h): 720<br>Curvature: 0.7 |
| Tensile strength | 1/10th of compressive strength |

*6.1.2. Calculation Parameters (Step 4)*

The main task of this step (Step 4) is to generate mesh for using finite element method to calculate concrete temperature and then thermal stress. In the present study, a general finite element mesh was used to activate the project solver and then to perform temperature calculation. The calculation parameters in 4C include mesh sizes and analysis period, and other calculation parameters include thermal analysis, stress analysis, dimensions, time specifications, nonlinear calculations, mesh node generation, circles, and self-weight.

In the present study, the thermal analysis was kept transient as the default, and the stress analysis was conducted based on the thermal results. There was no structural loading, and two-dimensional with the plain strain was considered. The time specification was the total time (28 days), time step (1 hour, default), and time step factor (0.5 hour, default). The mesh sizes used in the present study were narrow to improve the analysis. The density internal nodes were 3%, minimum distance to border: 0.01%. Mesh node generation was used to make the finite element mash. The higher the percentage of density nodes, the finer the mash. Finer mash gives better results compared to coarser mash.

## 6.2. Results from 4C Thermal Analysis

As mentioned previously, the 4C analysis aims to simulate the temperature profile of the concrete mix cast in the laboratory. The adiabatic experiment included one meter cubic volume of four different concrete mixes (0%, 25%, 50%, and 75% slag replacement). The temperature rise in the block was measured for 30 days, and the temperture profiles at the core and bottom corner of the block were studied specifically. To simulate the measured temperature profile using 4C analyses, the 4C input heat parameters ($Q_\infty$, $\tau_e$, and $\alpha$) were changed for each concrete mix within an expected range so that the 4C simulated temperature profiles match the measured temperature data. Because the early-age temperature profile matching was more crucial in terms

of thermal cracking, the first three to five days of temperature profile matching was prioritized during the 4C analyses. Figures 6-3 through 6-6 show the comparisons of the temperature profile obtained in the laboratory and the 4C analysis.

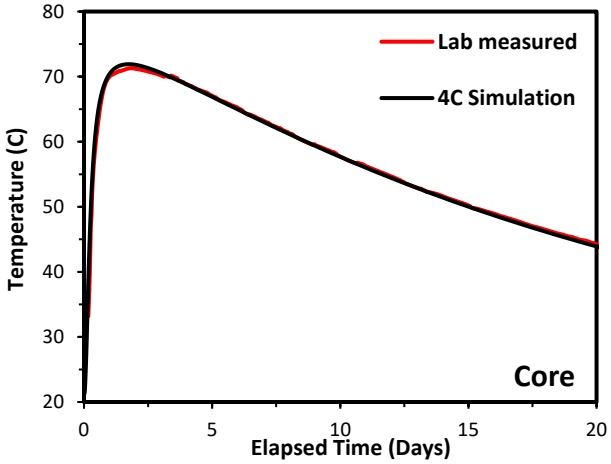


(a) Core temperature

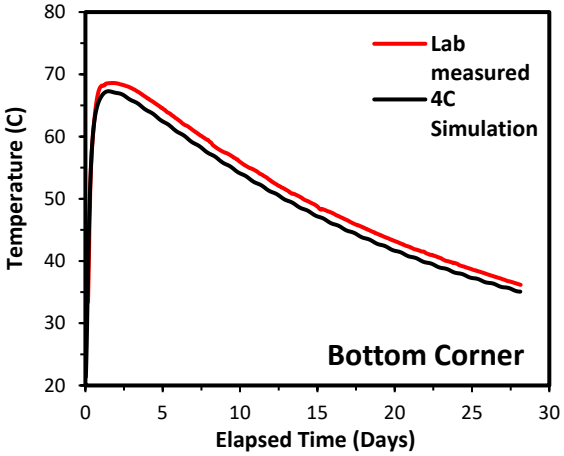


(b) Bottom corner temperature

**Figure 6-3. 4C analysis for the 0% slag concrete mix at (a) core and (b) bottom corner**

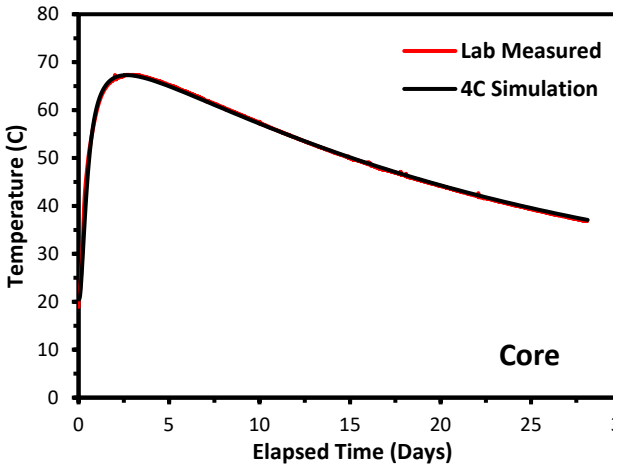


(a) Core temperature

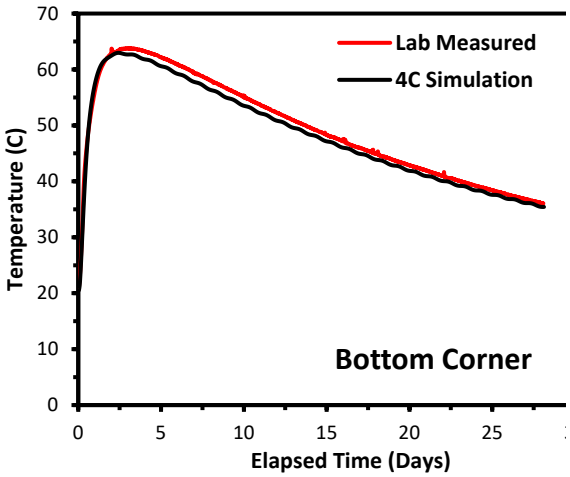


(b) Bottom corner temperature

**Figure 6-4. 4C analysis for the 25% slag concrete mix at (a) core and (b) bottom corner**

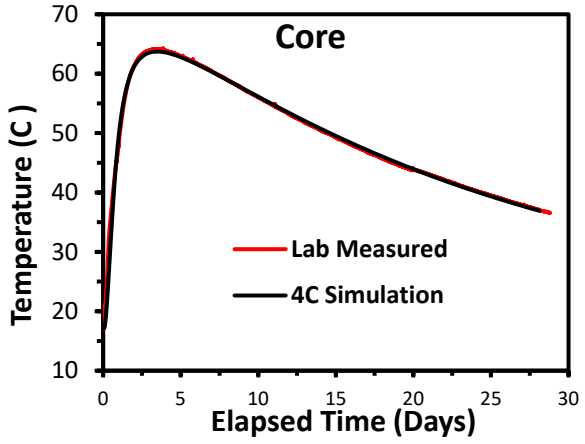


(a) Core temperature

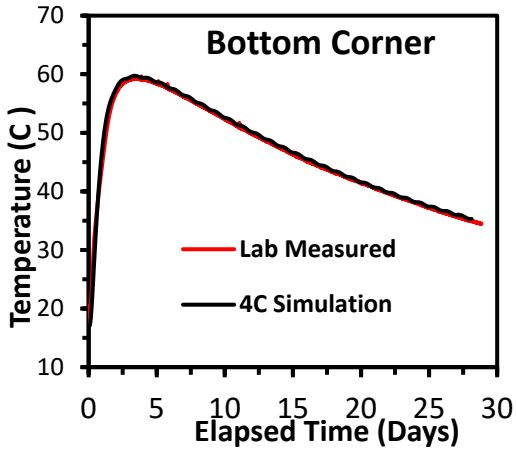


(b) Bottom corner temperature

**Figure 6-5. 4C analysis for the 50% slag concrete mix at (a) core and (b) bottom corner**

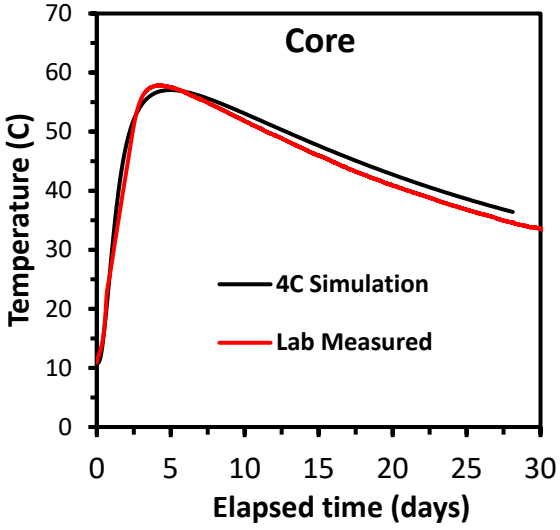


(a) Core temperature

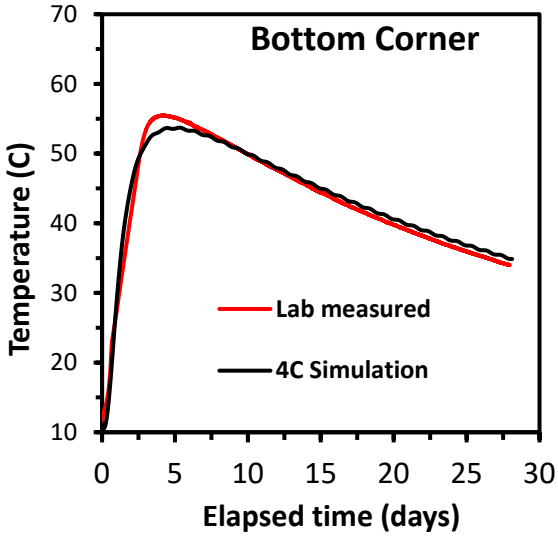


(b) Bottom corner temperature

**Figure 6-6. 4C analysis for the 75% slag concrete mix at (a) core and (b) bottom corner**

It can be seen in Figures 6-3 through 6-6 that the temperature profiles achieved by the 4C simulation almost overlap those obtained from the concrete block temperature measurements, especially for the core temperature profiles and early ages. This indicates a good representation of the accuracy of the 4C simulation. For the 75% slag mix (Figure 6-6), the core temperature profile (Figure 6-6a) from the 4C simulation was slightly overestimated toward the later age (after about 10 days) of the hydration, but this effect was reversed for the bottom corner temperature profile (Figure 6-6b), where the 4C simulation underestimates the maximum temperature by 2°C.

Table 6-7 presents the heat parameters used to obtain the temperature profiles presented in Figures 6-3 through 6-6, where $Q_\infty$ is the ultimate total heat (at $t=\infty$), $\tau_e$ is the time parameter

(time to reach the hydration peak), and α is degree of hydration. It can be seen from Table 6-7 that as the slag replacement increases, the ultimate heat of hydration increases, and the time required to reach the peak of heat also increases.

**Table 6-7. 4C heat parameters for the concrete block mixes**

| | 0% Slag | 25% Slag | 50% Slag | 75% Slag | Unit |
|---|---|---|---|---|---|
| $Q_\infty$ | 300 | 320 | 332 | 350 | KJ/Kg |
| $\tau_e$ | 7.3 | 14.5 | 20 | 25 | Hours |
| α | 0.7 | 0.7 | 0.7 | 0.7 | |

## 6.3. Prediction of True Adiabatic Temperature

Using the heat parameters listed in Table 6-7, 4C program can calculate the true adiabatic temperature of concrete blocks using the following steps:

1. Determine degree of hydration over time:

$$\alpha(t) = 1 - \exp(-t/\tau_e) \quad (6\text{-}1)$$

2. Determine the heat released over time:

$$Q(t) = \alpha(t)Q_\infty \quad (6\text{-}2)$$

Figure 6-7 shows the comparison of the true adiabatic temperature profiles of the large concrete blocks obtained from measurements and 4C predictions. The measured temperature profiles were calculated using equation 5-6 and the heat parameters ($\alpha_u$', β', and τ') developed in Chapter 5, while 4C predicted temperature profiles based on the parameters listed in Table 6-7 and equation 6-2. Figure 6-7 illustrates that except for the concrete mix with 75% slag, the measured profile of most concrete mixes displayed a higher adiabatic temperature than the 4C predicted profile, especially at the early age. The higher measured temperature profile may be related to the accuracy of the heat parameters ($\alpha_u$', β', and τ') developed in Chapter 5 based on literature data.

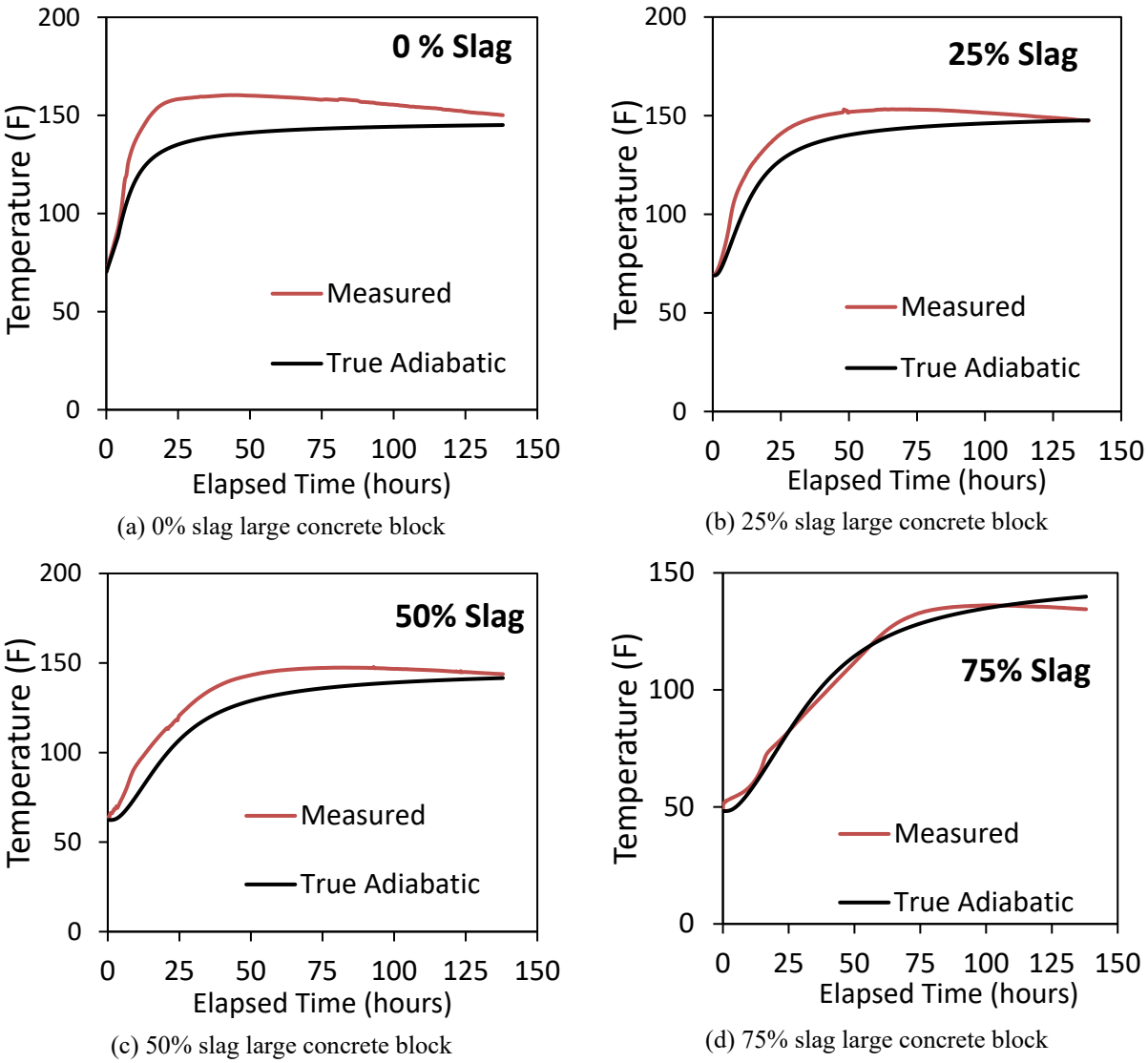


(a) 0% slag large concrete block

(b) 25% slag large concrete block

(c) 50% slag large concrete block

(d) 75% slag large concrete block

**Figure 6-7. Comparison of the adiabatic temperature profiles measured from the large concrete blocks and predicted from 4C**

Therefore, the following steps were taken to validate the newly developed ATR prediction model for mass concrete containing slag:

1. Select new concrete mixes for validation: Six concrete mixes, whose data were not used for the previous model development, were selected for the model validation. Mixes 1 through 3 are the large concrete block mixes containing 25%, 50%, and 75% slag, respectively, and Mixes 4 through 6, as shown in Table 6-8, were from the literature.
2. Validate the newly developed equations for the heat parameters (α', β', and τ'): The effects of the key material parameters of the selected six validation mixes, such as slag replacement percentage, alumina content in slag, alkali content in slag, and calcium content in slag, as listed Table 6-8, on heat parameters were analyzed. Adjustments were made so that the adiabatic temperature profiles of the six mixes were predicted using the refined heat

parameters predicted from the newly developed equations and were comparable to their measured temperature profiles.

3. Evaluate the refined heat parameters using the following steps:
   a. Collect measured true adiabatic temperature profile data: For mixes 1, 2, and 3 (large concrete blocks), the measured profile was achieved using 4C software. For mixes 4, 5, and 6, the data were taken from the literature (Appendix B).
   b. Compute true adiabatic temperature profiles using the new ATR model generated from the new 3P heat parameter equations.
   c. Compare the two sets of the true adiabatic temperature profiles obtained from Steps (a) and (b) by plotting them against each other as shown in Figure 6-8a.
4. Evaluate the heat parameter equations in the existing ConcreteWorks: Similar to Step 3(b), the true adiabatic temperature profiles of the six selected mixes were calculated using the old heat parameter equations in the existing ConcreteWorks. The calculated profiles were also plotted against the measured true adiabatic temperature profile as shown in Figure 6-8b.
5. Determine the acceptance of the new equations/models developed for predicting the heat parameters and ATR profiles of slag concrete.

**Table 6-8. Mixes used for validation of the model with three independent variables**

| No. | Mix ID | Replacement (%) | Alumina (%) | Alkali (%) | Calcium (%) |
|---|---|---|---|---|---|
| 1 | OPC-S25 | 0.25 | 10.05 | 0.54 | 38.90 |
| 2 | OPC-S50 | 0.50 | 10.05 | 0.54 | 38.90 |
| 3 | OPC-S75 | 0.75 | 10.05 | 0.54 | 38.90 |
| 4 | OPC-S50 | 0.50 | 11.00 | 0.50 | 38.90 |
| 5 | OPC-S70 | 0.70 | 9.80 | 0.50 | 38.90 |
| 6 | OPC-S30 | 0.30 | 9.50 | 0.17 | 6.56 |

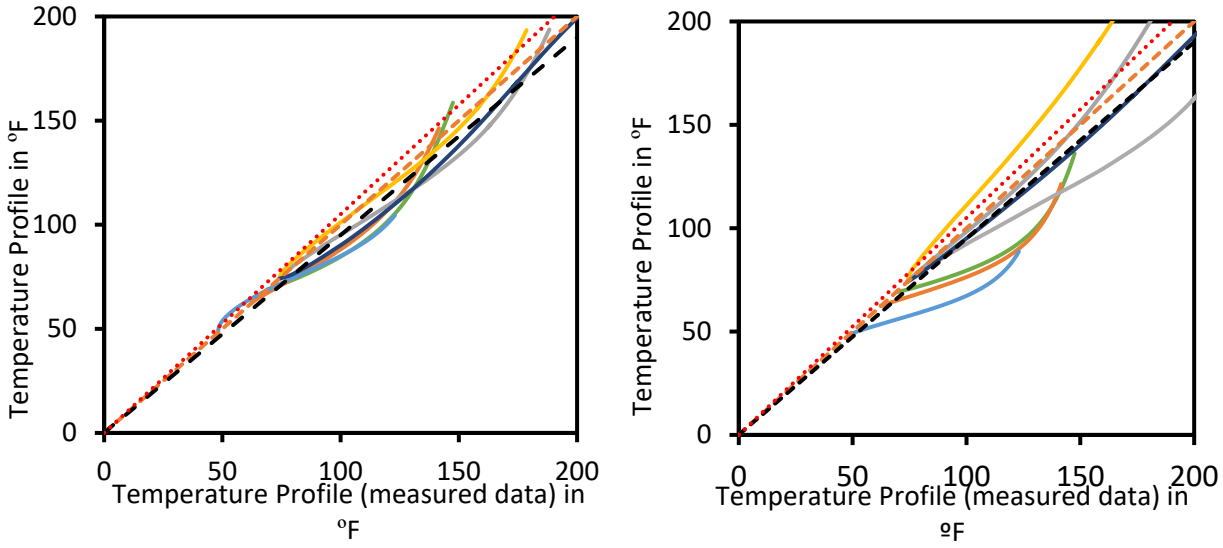


(a) From the newly developed model

(b) From existing ConcreteWorks model

**Figure 6-8. Temperature profile of the measured data from six validation mixes versus (a) proposed new ConcreteWorks model and (b) existing ConcreteWorks model**

It can be observed from Figure 6-8a that the adiabatic temperature data predicted from the newly developed model are much nearer to a 45º straight line, which represents a direct correlation between the measured data and the data predicted by the ConcreteWorks software with the newly developed 3P model for slag hydration. The data predicted by the new models show an error of 15.6% compared to the measured data. Figure 6-8b shows that the existing ConcreteWorks model is very far from the 10% margin line, and many of the relationships between the measured data and the existing ConcreteWorks model temperature profile are not linear. There is a large difference between the measured data and the existing ConcreteWorks model temperature profile. The data predicted by the models in the existing ConcreteWorks show an error of 36.0% compared to the measured data.

Additionally, it appears that as the temperature increases, the difference also increases. This suggests that the existing ConcreteWorks model underestimates the temperature rise in the slag-containing mixtures due to the heat parameter equations. This is mainly because the heat parameter equations in the existing ConcreteWorks model do not take the slag chemical composition into account, thus leading to very different temperature profiles compared to the measured data.

Because of a significant improvement from the existing ConcreteWorks model to the newly developed ATR model, these newly developed heat parameter equations were used to modify the existing ConcreteWorks software. The final equations of the newly developed models are presented in Chapter 7.

## 7. NEW MODEL INCORPORATION AND TRIAL ANALYSES (TASK A-7)

ConcreteWorks version 2.1.0 was modified based on the results obtained from Tasks A-1 through A-6. Modifications made accordingly in the software are discussed in the following sections. Relevant screenshots from the software are also presented. In addition, thermal and sensitivity analyses were conducted using the latest version of ConcreteWorks.

### 7.1. Modification of Inputs

In the existing ConcreteWorks software, the slag chemistry and physical properties are not included in the hydration model, while in the modified ConcreteWorks software, the slag chemistry and physical properties are considered. Therefore, the related default inputs should be updated. These updated default inputs are listed in Tables 7-1 and 7-2. (Note: These data were also used to develop the model, and they are therefore listed here as reference default values.)

**Table 7-1. Updated default input options for the slag and Type I/II physical properties**

| Input Options | Type I/II | Slag |
|---|---|---|
| Specific Gravity | 3.14 | 2.93 |
| Blaine Fineness ($m^2$/kg) | 300 | Grade 100 (443 $m^2$/kg) |

**Table 7-2. Updated default input options for the slag chemical properties**

| Oxide (%) | OPC Type I/II | Slag (Grade100) |
|---|---|---|
| $SiO_2$ | 22.802 | 35.635 |
| $Al_2O_3$ | 5.355 | 10.052 |
| $Fe_2O_3$ | 3.512 | 0.894 |
| CaO | 64.186 | 38.907 |
| MgO | 2.704 | 10.004 |
| $SO_3$ | 1.641 | 0.965 |
| $Na_2O$ | 0.154 | 0.254 |
| $K_2O$ | 0.624 | 0.428 |
| $TiO_2$ | 0.257 | 0.415 |
| $P_2O_5$ | 0.048 | 0.015 |
| $Mn_2O_3$ | 0.082 | 0.293 |
| SrO | 0.099 | 0.038 |
| ZnO | 0.018 | 0.009 |
| BaO | 0.092 | 0.103 |

### 7.2. Modification in the Equations for Heat Parameter Calculations

The following are the modified hydration parameter equations when the Bogue method is used:

$$a_u = 1.031 * \frac{w}{cm0.194} + \frac{w}{cm} + \exp\{-0.0885 - 13.7 * pC4AF * pcem - 283 * pNa2Oeq * pcem - 9.90 * pFA * pFA - CaO - 339 * WRRET - 95.4 * PCHRWR\} + Y_\alpha \quad (7\text{-}1)$$

$$\beta = exp - 0.464 + 3.41 * pC3A * pcem + 107 * WRRET + 33.8 * LRWR + 15.7 * MRWR + 38.3 * PCHRWR + 8.97 * NHRWR + Y\beta \quad (7\text{-}2)$$

$$\tau = \exp\begin{Bmatrix} 2.92 - 0.757 * p_{C3S} * p_{cem} + 98.8 * p_{Na2O} * p_{cem} \\ +4.12 * p_{FA} * p_{FA-CaO} \\ -11.4 * ACCL + 98.1 * WRRET \end{Bmatrix} + Y_\tau \quad (7\text{-}3)$$

where $Y$ is the component corresponding to the slag physical and chemical properties, corresponding to Φ in equations 5-16, 5-17, and 5-18, respectively.

$$\boldsymbol{Y_\alpha} = X_1 * (-2.108 * X_1 + 0.015 * X_2 - 0.534 * X_3 + 0.016 * X_4 \quad (7\text{-}4)$$

$$\boldsymbol{Y_\beta} = X_1 * (2.967 * X_1 + 0.081 * X_2 - 1.819 * X_3 - 0.047 * X_4) \quad (7\text{-}5)$$

$$\boldsymbol{Y_\tau} = X_1 * (-25.403 * X_1 - 1.989 * X_2 - 38.918 * X_3 + 2.154 * X_4 \quad (7\text{-}6)$$

The following are the modified hydration parameter equations when the Rietveld method is used:

$$\mathrm{a_u} = \frac{1.031 * \frac{\mathrm{w}}{\mathrm{cm}}}{0.194 + \frac{\mathrm{w}}{\mathrm{cm}}} + \exp\begin{Bmatrix} -0.297 - 9.73 * \mathrm{p_{C4AF}} * \mathrm{p_{cem}} \\ -325 * \mathrm{p_{Na2Oeq}} * \mathrm{p_{cem}} \\ -8.90 * \mathrm{p_{FA}} * \mathrm{p_{FA-CaO}} \\ -331 * \mathrm{WRRET} - 93.8 * \mathrm{PCHRWR} \end{Bmatrix} + \mathrm{Y_\alpha} \quad (7\text{-}7)$$

$$\beta = \exp\begin{Bmatrix} -0.418 + 2.66 * p_{C3A} * p_{cem} + 108 * WRRET \\ +32 * LRWR + 13.3 * MRWR \\ +42.5 * PCHRWR + 11.0 * NHRWR \end{Bmatrix} + Y_\beta \quad (7\text{-}8)$$

$$\tau = \exp\begin{Bmatrix} 2.95 - 0.972 * \mathrm{p_{C3S}} * \mathrm{p_{cem}} + 152 * \mathrm{p_{Na2O}} * \mathrm{p_{cem}} \\ +4.0 * \mathrm{p_{FA}} * \mathrm{p_{FA-CaO}} \\ -11.8 * \mathrm{ACCL} + 95.1 * \mathrm{WRRET} \end{Bmatrix} + \mathrm{Y_\tau} \quad (7\text{-}9)$$

where $Y$ is the component corresponding to the slag physical and chemical properties.

$$\mathrm{Y_\alpha} = \mathrm{X_1} * (-1.908 * \mathrm{X_1} + 0.007 * \mathrm{X_2} + 0.629 * \mathrm{X_3} + 0.015 * \mathrm{X_4}) \quad (7\text{-}10)$$

$$\mathrm{Y_\beta} = \mathrm{X_1} * (3.031 * \mathrm{X_1} + 0.1 * \mathrm{X_2} - 1.940 * \mathrm{X_3} - 0.051 * \mathrm{X_4}) \quad (7\text{-}11)$$

$$\mathrm{Y_\tau} = \mathrm{X_1} * (-35.54 * \mathrm{X_1} - 0.874 * \mathrm{X_2} - 56.01 * \mathrm{X_3} + 2.102 * \mathrm{X_4}) \quad (7\text{-}12)$$

where X1 is slag replacement (0–1), X2 is alumina content percentage, X3 is alkali content percentage of the slag, and X4 is the calcium content percentage of the slag.

In the older version, the slag cement option has only a "quantity" parameter available. In the newer version, additional options such as alkali, calcium, and alumina content are available, as shown in Figure 7-1.

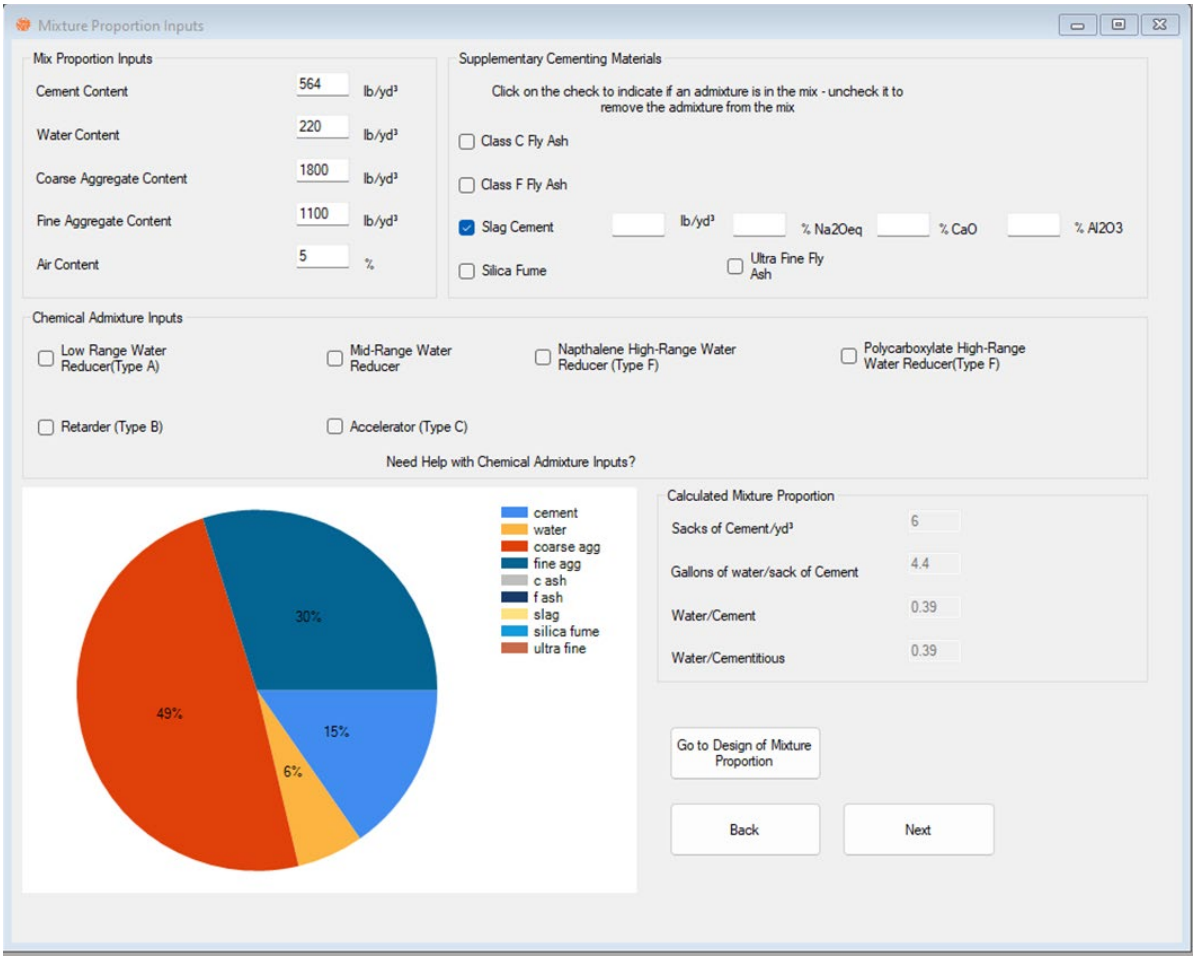


**Figure 7-1. Slag cement chemical properties options**

## 7.3. Sensitivity Analysis of the Modified ConcreteWorks Software

The ATR prediction model in the ConcreteWorks software is based on the 3P statistical model, which focuses on three heat parameters (α, β, and τ), and the efficiency of such a model largely depends on the base data set used in the heat parameter development. Due to a limited data set, and a fixed set of calibration mixes, the updated model has limited accuracy with regard to certain parameters. Thus, the sensitivity of the ConcreteWorks software to each parameter must be analyzed to understand the limitations of the software. To understand this, the important parameters, which significantly affect the thermal analysis, were listed, and a set of trials were prepared to measure the effect of each parameter (within a certain input range) on the thermal

analysis of the mass structure. Table 7-3 provides the input parameters and the corresponding range and intervals used for the analysis. The ranges of input parameters selected cover the values that are generally or practically used.

**Table 7-3. Input parameters and interval range used in the sensitivity analysis**

| Input Parameter | Range | Intervals | No. of Trials | Trial Mix ID |
|---|---|---|---|---|
| Slag Replacement (SR) | 0%–100% | 5% | 20 | SR 0–SR100 |
| Slag Alkali Content (SAiC) | 0%–4% | 0.2% and 0.5% | 10 | SAiC 0–SAiC 4 |
| Slag Calcium Content (SCC) | 10%–60% | 5% | 10 | SCC 10–SCC 60 |
| Slag Alumina Content (SAC) | 0%–20% | 2% | 10 | SAC 0–SAC 20 |
| Insulation R-Value (IRV) | 0–20 | 2 | 10 | IRV 0–IRV 20 |

The trials were conducted to determine the effect of each of the input parameters listed in Table 7-3 on the temperature rise at the core and top corner location for the selected mass concrete structure (7 ft × 7 ft × 7 ft). In the sensitivity analysis, only one parameter varied, and other parameters were kept constant so as to understand the sensitivity of that parameter toward the thermal analysis. Figure 7-2 shows the results from the sensitivity analyses, and the following observations can be made:

- The sensitivity analysis on the slag replacement dosage, ranging from 20 to 60 wt.% of cementitious materials, showed that the largest difference in the maximum core temperature is about 5°C, and the largest difference in the core temperature at the later age (28 days) is about 10°C (Figure 7-2a).
- The sensitivity analysis on the slag alkali content, ranging from 0 to 10 wt.% of slag chemical compositions, showed that the largest difference in the maximum core temperature is about 3°C, and the largest difference in the core temperature at 28 days is about 7°C (Figure 7-2b).
- The sensitivity analysis on the slag calcium content, ranging from 30 to 70 wt.% of slag chemical compositions, showed that the largest difference in the maximum core temperature is about 5°C, and the largest difference in the temperature at 28 days is about 6°C (Figure 7-2c).
- The sensitivity analysis on the slag aluminum content, ranging from 5 to 20 wt.% of slag chemical compositions, showed that the largest difference in the maximum core temperature is about 6°C, and the largest difference in the temperature at 28 days is about 6°C (Figure 7-2d).
- The sensitivity analysis on the concrete insulation R-value, ranging from 0 to 20, showed that the largest difference in the maximum core temperature is about 2.5°C, and the largest difference in the core temperature at 28 days is about 6°C (Figure 7-2e).

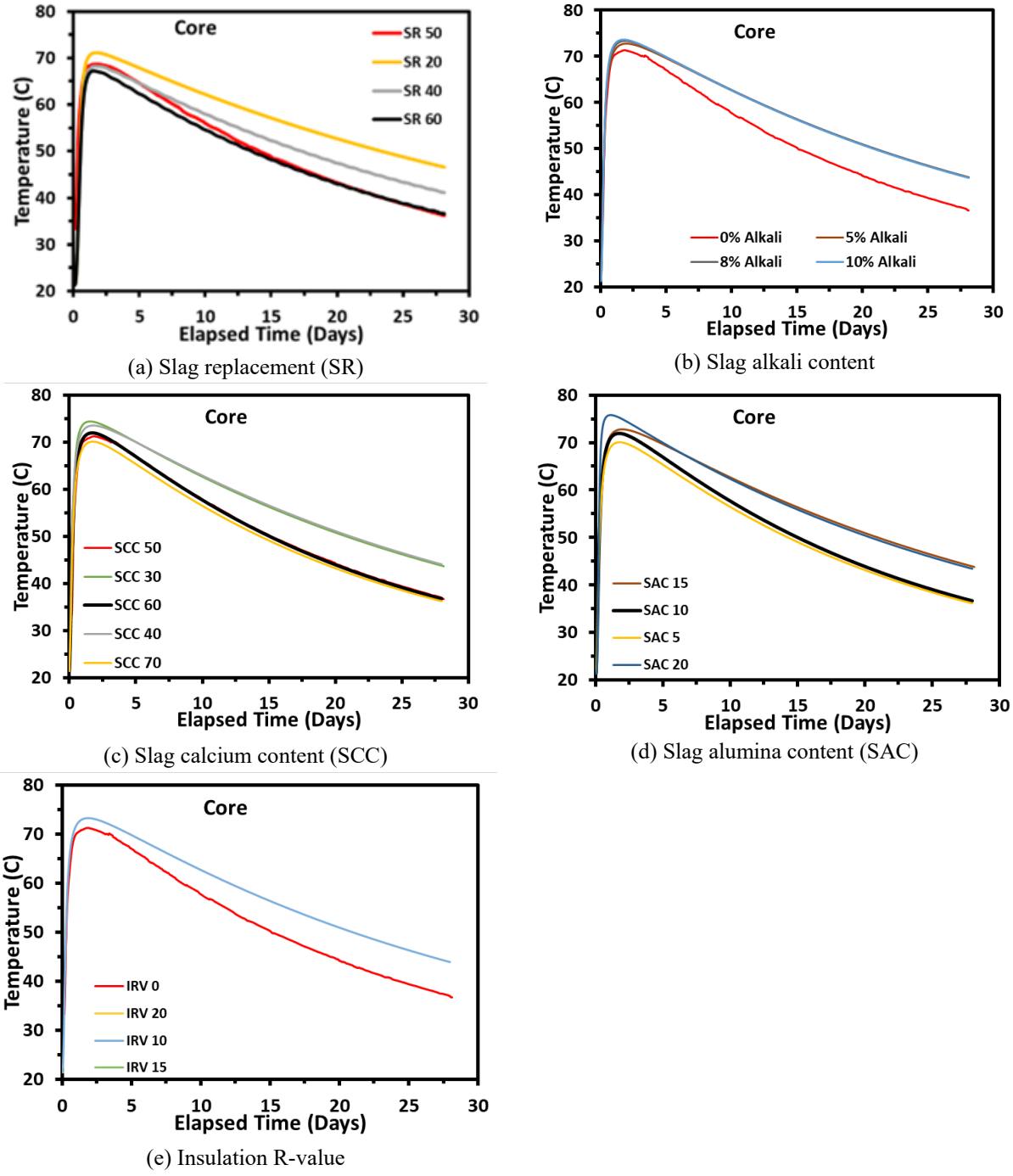


**Figure 7-2. Sensitivity analysis based on the effect of input parameters on the ATR in a selected concrete structure element**

These observations indicate that within the selected parameter ranges, slag replacement dosage clearly influences both the maximum temperature and especially the concrete temperature at later age (28 days). That is, the sensitivity of slag replacement dosage is high for concrete adiabatic temperature. The next most sensitive parameters are slag aluminum and calcium contents, which

more significantly affect the maximum adiabatic temperature of concrete than other parameters (like slag alkali content and the structure insulation R-value).

### 7.4. Limitations

To check the limitations of the ConcreteWorks software, extreme inputs were used to test its response in predicting ATR. As shown in Figure 7-3a, the software provides reasonable maximum concrete temperature predictions at low levels of slag replacement (10% and 20% by weight of the total cementitious materials). However, when the slag replacement dosage reaches 80%, a sudden temperature drop occurs, indicating the software's inability to capture realistic concrete behavior at high slag replacement levels. Similarly, Figure 7-3b shows a sudden temperature drop when the calcium content reaches 80% by weight of the slag compositions, suggesting another instance where the software's response becomes unreliable.

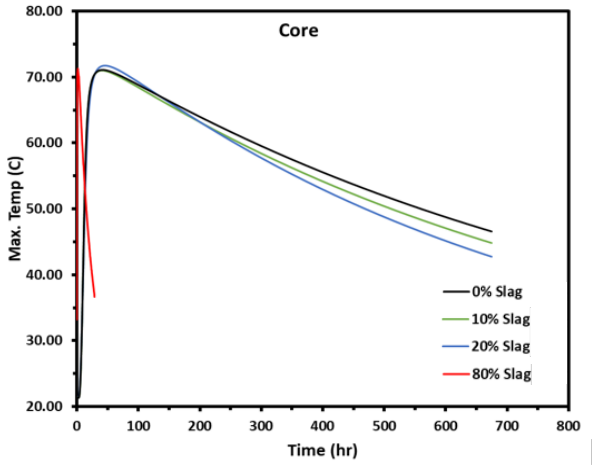


(a) Slag replace dosage

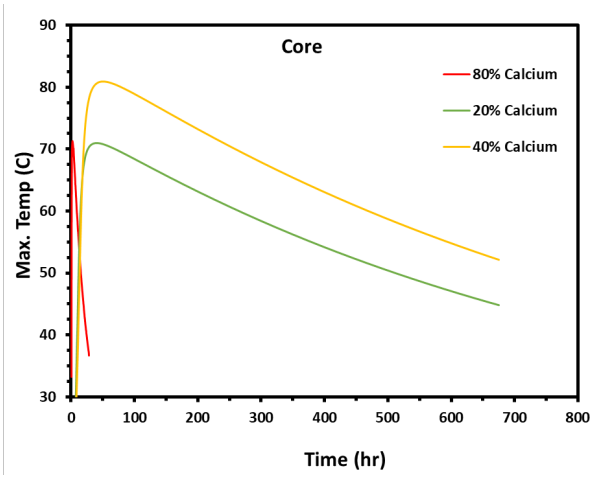


(b) Slag calcium content

**Figure 7-3. Response of ConcreteWorks software to extreme cases**

The occurrence of such a sudden temperature drop reveals the limitation of the models in the software. When a model has only a small amount of data to learn from, it may try to fit the data too closely, capturing noise and randomness in the training set rather than the underlying patterns or relationships that generalize well when new data are entered. This can lead to poor performance when the model is applied to unseen data, because it has essentially memorized the training set rather than learning meaningful patterns.

Another limitation is the lack of statistical power. With limited data, it may be challenging to detect subtle or complex relationships between variables. Statistical tests and inference based on small sample sizes are less reliable and may lead to incorrect conclusions about the population from which the data were drawn. Additionally, limited data can result in high uncertainty and variability in model predictions. Confidence intervals and prediction intervals may be wide, making it difficult to make precise predictions or draw strong conclusions from the model's outputs. Lastly, the generalizability of a model trained on limited data can be questionable. It may perform well on the specific data set it was trained on but struggle to generalize new, unseen data from a different population or time period. This lack of generalizability can limit the model's utility in real-world applications.

Understanding these limitations can help with accurate application, mitigating errors, and managing risks effectively.

# 8. DEVELOPMENT OF A NEW COMPONENT IN CONCRETEWORKS FOR SEAL SLAB–FOOTING THERMAL ANALYSIS (PHASE IIB)

## 8.1. Introduction

Mass concrete is often associated with large structures like bridge foundations. During the construction of bridge foundations or footings, cofferdams are built to form watertight enclosures surrounding excavations. A seal slab is typically placed at or just below the final excavation depth inside the cofferdam, and it provides a stable working surface for the bridge foundations and helps prevent water intrusion during construction.

The Iowa DOT typically implements seal slabs as follows:

1. If it is expected that water flow through the bottom of the cofferdam cannot reasonably be controlled by pumping, it is determined that a seal slab will be necessary to seal off water flow in the bottom of the excavation.
2. The sheet pile cofferdam is installed, and excavation is carried out inside the cofferdam down to the bottom of the seal slab elevation. (During this excavation, the interior of the cofferdam remains flooded.)
3. The seal slab concrete is placed, using a tremie pipe, into the flooded cofferdam (underwater concrete placement). The seal slab extends fully to the edge of the sheet pile cofferdam to provide the best chance of achieving a watertight seal.
4. The seal slab is then left to cure underwater until the time the seal develops sufficient strength to resist the uplift and bending at the base of the excavation caused by the differential water pressure. It is common for the seal to remain submerged for three or more days. During this time, the water in the cofferdam provides the curing protection for the seal slab concrete.
5. After the seal develops sufficient strength, the cofferdam is dewatered, and the seal slab is cleaned and prepared to receive footing concrete. Dewatering and seal slab surface preparation may take several days.
6. After the seal slab surface is prepared, the footing concrete is placed in the dry cofferdam.

Figure 8-1 shows a schematic of a seal slab–footing structure within a cofferdam. (Note that deep foundation elements are not shown in the drawing but may be present on certain projects.)

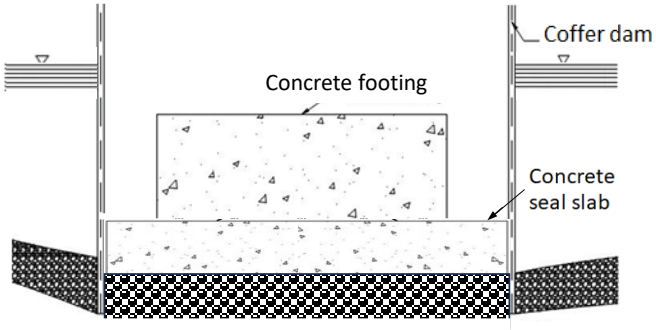


**Figure 8-1. Schematic of the seal slab–footing structure within a cofferdam**

Although not in all cases, a lean concrete mix is typically used for the seal coat slab so that thermal cracking due to the heat of cement hydration would not be much of a concern in this concrete component. Therefore, concrete mixes used for the seal slabs are generally not considered to be mass concrete, and no temperature control of the seal coat slab concrete is believed to be necessary. However, one concern raised by the Iowa DOT is whether the heat development in a seal coat slab can consequently affect the early-age temperature development in the footing placed above it, and the current ConcreteWorks software does not have a component for predicting the concrete temperature of the seal coat slabs.

Therefore, Phase IIB of the ConcreteWorks project aimed to develop a new component in the ConcreteWorks software that enables the prediction of the temperature profiles of bridge foundations influenced by the temperature development of concrete seal slabs.

Originally, the team proposed to achieve the project goal by conducting a field investigation, where a bridge construction site would be selected and the temperature profiles of its concrete seal slab and the footing to be placed above this slab would be monitored. The resulting information, together with the thermal properties of the field concrete mixes to be tested, would be used to develop a new component in the ConcreteWorks software to model the temperature of seal coat concrete slabs. However, a suitable bridge construction site was not available during the project timeframe. Therefore, the team simply developed a new component capable of modeling concrete seal slabs placed underneath rectangular footings without field data. This new component has been added to the ConcreteWorks software.

The sections below describe the modeling approach, procedure, boundary conditions, and inputs of the new component as well as some analysis results from the use of the updated ConcreteWorks software.

## 8.2. Seal Slab Modeling in ConcreteWorks (Task B-1)

In this study, seal slabs were modeled only in two-dimensional analysis cases for rectangular footings.

Before the footing is virtually placed on the seal slab, the seal slab is modeled in the same way as a rectangular footing without a seal slab placed underneath. Curing of the seal slab can be specified in the ConcreteWorks software based on the preferred construction practice. Because seal slabs in Iowa DOT projects are often cured underwater in a flooded cofferdam, in this project a new feature was added that allows the seal slab to cure under water.

The rectangular footing is cured according to user-selected methods with the seal slab directly underneath the footing. If the footing is placed soon after seal slab placement, the concrete in the seal slab underneath the footing may still generate heat from the heat of its cement hydration, which could subsequently influence the temperature development in the footing.

### 8.3. Boundary Conditions and Input Parameters (Task B-1)

To select the use of a seal slab under a rectangular footing, the user checks a box on the Rectangular Footing Dimensions input form, as shown in Figure 8-2. This then displays the seal slab dimension inputs required, as shown in Figure 8-3.

When the user increases the width of the rectangular footing, the minimum width of the seal slab is automatically increased to 1 ft greater than the width of the selected rectangular footing. If the width of the rectangular footing decreases, the required minimum width of the seal slab also decreases to 1 ft greater than the width of the rectangular footing.

If the seal slab is cured under water, the box labeled “Seal Slab Cured Underwater?” can be selected, as shown in Figure 8-3. Otherwise, ConcreteWorks assumes that the same curing used on top of the footing is used on top of the seal slab before the footing concrete is placed.

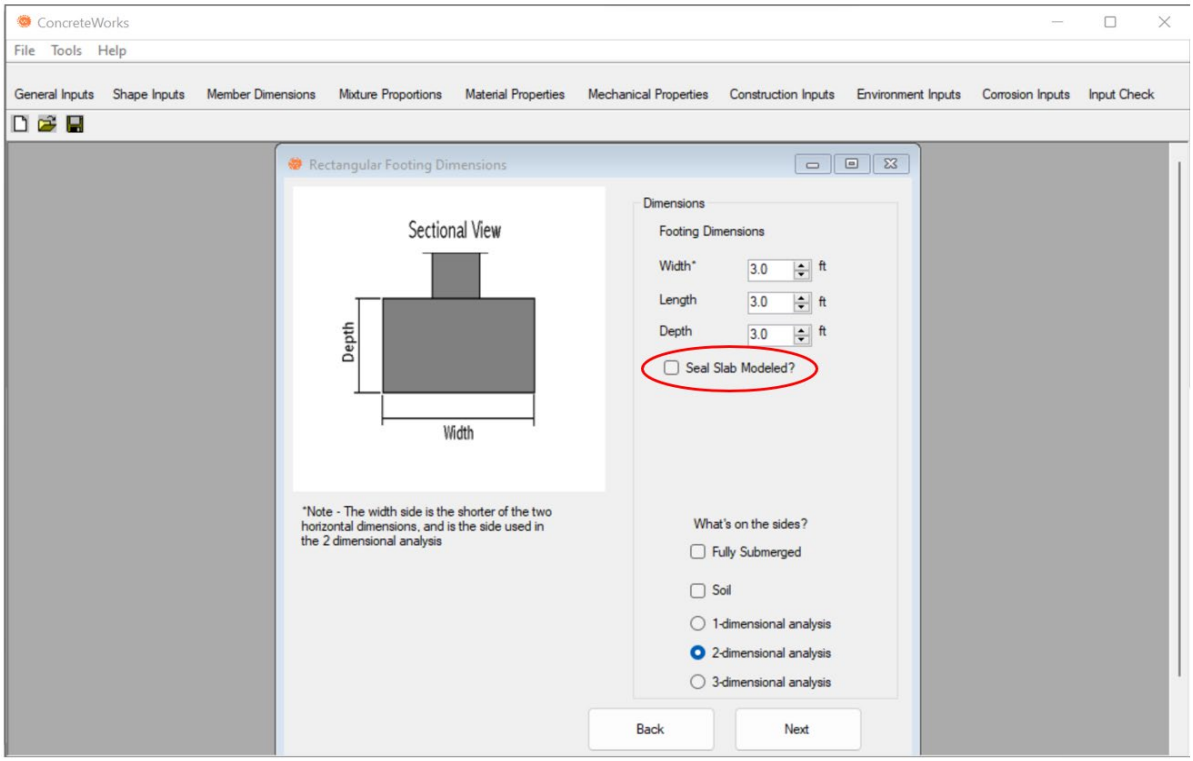


**Figure 8-2. ConcreteWorks screenshot showing seal slab checkbox**

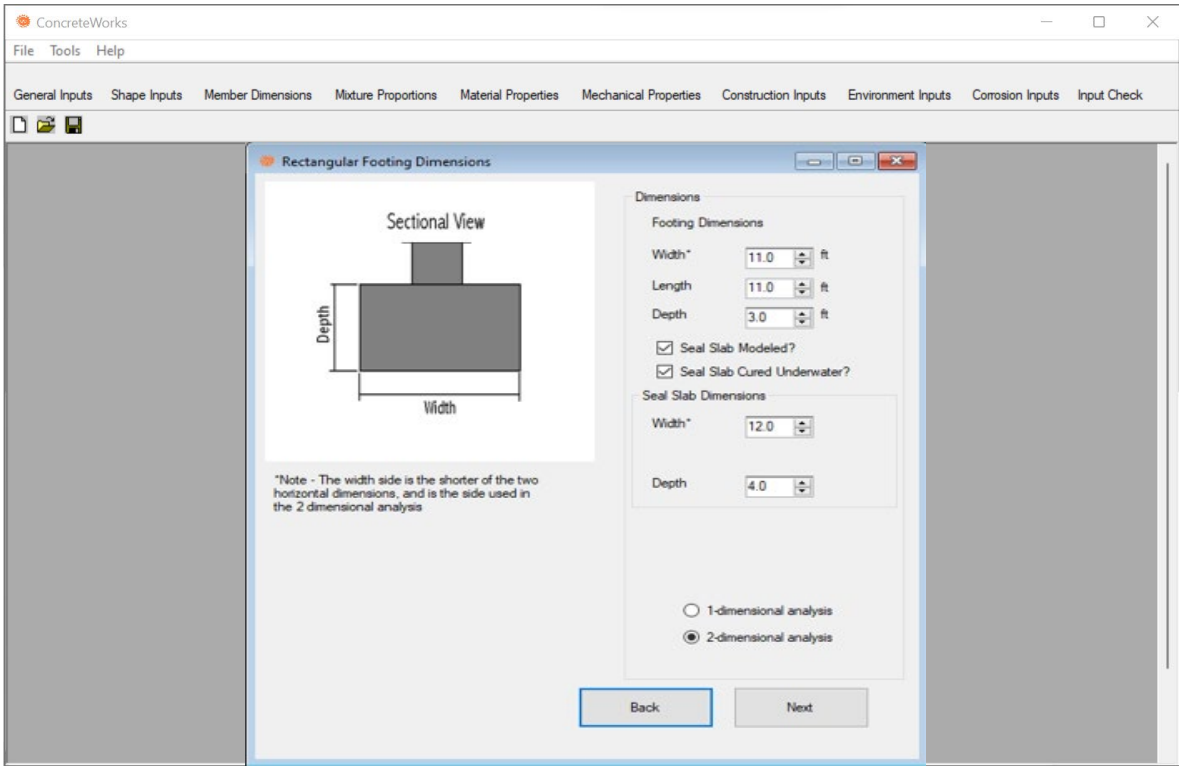


**Figure 8-3. ConcreteWorks screenshot showing seal slab dimension inputs**

Upon entering the mixture proportions input window, the user sees a button labeled “Click to Change Seal Slab Mixture Proportions” when the user has elected to use a seal slab, as shown in Figure 8-4. If the user wishes to use a different concrete mixture in the seal slab than in the footing, the user clicks this button. After clicking this button, the user is brought to a screen where the seal slab mixture proportions can be entered. If the user does not change the seal slab concrete mixture proportions, the mixture proportions will default to the default concrete mixture proportions.

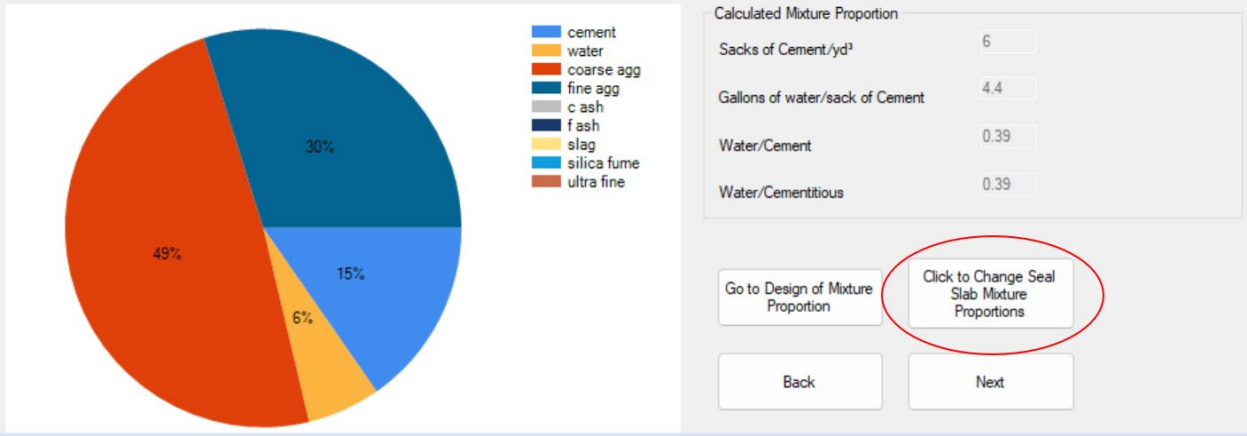


**Figure 8-4. Screenshot of button that allows the user to input seal slab mixture proportions if different than those of the rectangular footing**

When the user elects to use a seal slab, concrete heat of hydration parameter inputs will appear on the Material Properties input form, as shown in Figure 8-5. These parameters are used to calculate the concrete heat generation over time for the seal slab. The default heat of hydration parameters for the seal slab concrete are calculated from the seal slab concrete mixture proportions entered. The user can check the box labeled “Check to manually enter hydration properties” to manually override the calculated default hydration properties.

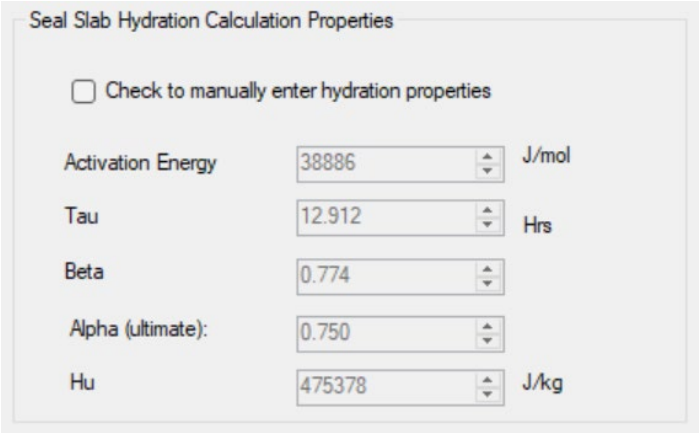


**Figure 8-5. Heat of hydration inputs for seal slab concrete**

When a seal slab is used, the input for "Type of footing subbase" refers to the material underneath the seal slab. The required construction input for the seal slab is the age of the seal slab (for example, 48 hours after seal slab casting) when the footing is placed on top, as shown in Figure 8-6.


**Figure 8-6. Screenshot of construction input needed for the seal slab**

After the concrete temperature developments in the seal slab and footing are calculated, the temperatures shown on the max-min graph in the output window are for the overall seal slab before the footing is placed. During this period, the minimum temperature in the seal slab may be considered as the placement temperature for the footing. After placement, the maximum and minimum temperatures shown are selected from both the footing and seal slab concrete. On the thermocouple points tab, the user can only select from among concrete points on the footing to be included in the graph. Because of this, the concrete maximum and minimum temperatures selected are only shown after the footing is placed, as shown in Figure 8-7.

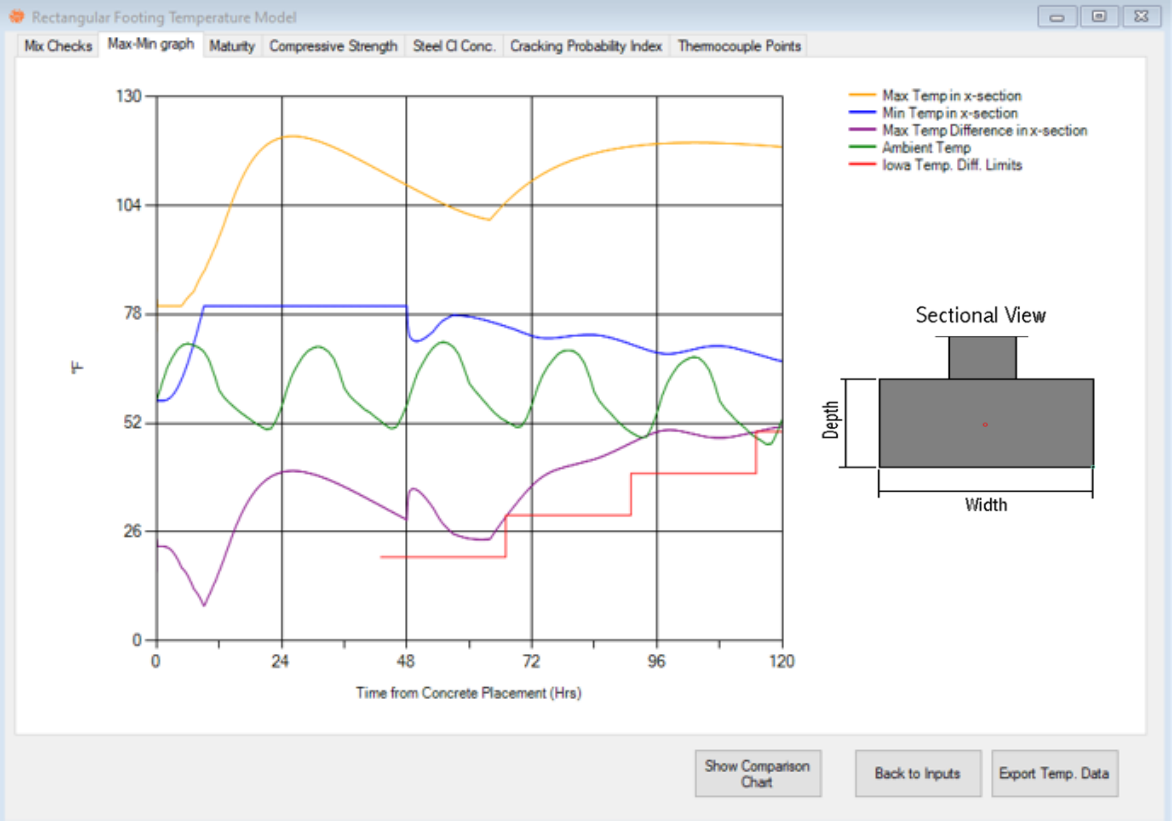


**Figure 8-7. Screenshot of ConcreteWorks graphs for rectangular footing thermocouple points when a seal slab is used**

## 8.4. Trial Analyses of the Effects of Seal Slab on the Temperature Profile of the Footing Above (Task B-2)

In this study, the updated ConcreteWorks software was used to analyze the temperature profile of a footing placed on a seal slab 2, 3, 7, and 14 days after the seal slab was cast, where the effect of the heat of hydration of the seal slab on the heat of the bridge foundation above was considered. The results were then compared with the temperature profile of a corresponding footing placed with no seal slab underneath. Through this comparison, the effects of seal slab temperature evolution on the thermal behavior of the footing were revealed.

The trial input data used in the temperature profile calculation in ConcreteWorks are listed in Tables 8-1 and 8-2. For the trials, the seal slab and foundation mix designs were considered to be the same, although it is possible for the user to input different concrete mix designs for the seal slab and foundation. The same curing used on top of the footing was used on top of the seal slab before the footing concrete was placed. After a user-defined seal slab curing period, the curing material on top of the seal slab was removed, and the footing was virtually placed on top of the seal slab.

**Table 8-1. Concrete mix design for the seal slab and foundation**

| | |
|---|---|
| **Cement Content (lb/yd$^3$)** | 564 |
| **Water Content (lb/yd$^3$)** | 220 |
| **Coarse Aggregate Content (lb/yd$^3$)** | 1800 |
| **Fine Aggregate Content (lb/yd$^3$)** | 1100 |
| **Air Content (%)** | 5.0 |

**Table 8-2. Footing sizes and seal slab sizes used in the ConcreteWorks trials**

| | | | |
|---|---|---|---|
| **Footing Size (w*l*d)** | 3.0 feet | 9.0 feet | 4.0 feet |
| **Seal Slab Size (w*d)** | 10.0 feet | 3.0 feet | |

*8.4.1. Effects of Seal Slab on the Footing Temperature Profile*

Using the input data shown in Tables 8-1 and 8-2 and the abovementioned ConcreteWorks software with the new seal slab component, temperature profiles for the same footing with and without a seal slab were analyzed. The results are presented in Figure 8-8a and 8-8b. For this trial, the footing was placed 48 hours (2 days) after seal slab placement. The core temperature refers to the temperature at the core of the footing, which is the maximum temperature profile of the footing. This temperature is greatly affected by the concrete mix design and footing size. The edge temperature is the minimum temperature profile recorded in the outer periphery of the footing during the hydration process. This temperature is largely affected by the environmental (outside) temperature.

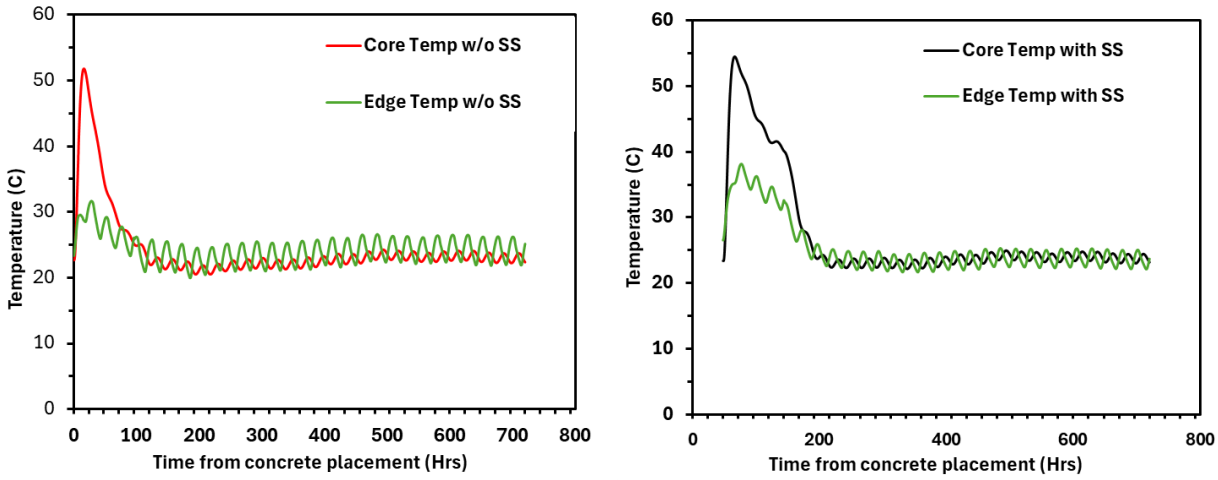


(a) Without Seal Slab (b) With Seal Slab

**Figure 8-8. Temperature profile at the core and edge of the footing**

The effect of the seal slab on the maximum temperature profile of the footing is shown in Figure 8-9. Based on Figure 8-9, the following key observations are made:

- The maximum (core) temperature of the footing with a seal slab is 3ºC higher compared to that of the footing without a seal slab.
- The rates of the core temperature rise of the footings with and without a seal slab are very similar, indicating that the heat development of the seal slab does not significantly affect the rate of cement hydration of the footing.
- Once the maximum temperature is achieved, the temperature drop is much slower, and the heat remains much higher in the footing with a seal slab compared to the footing without a seal slab.

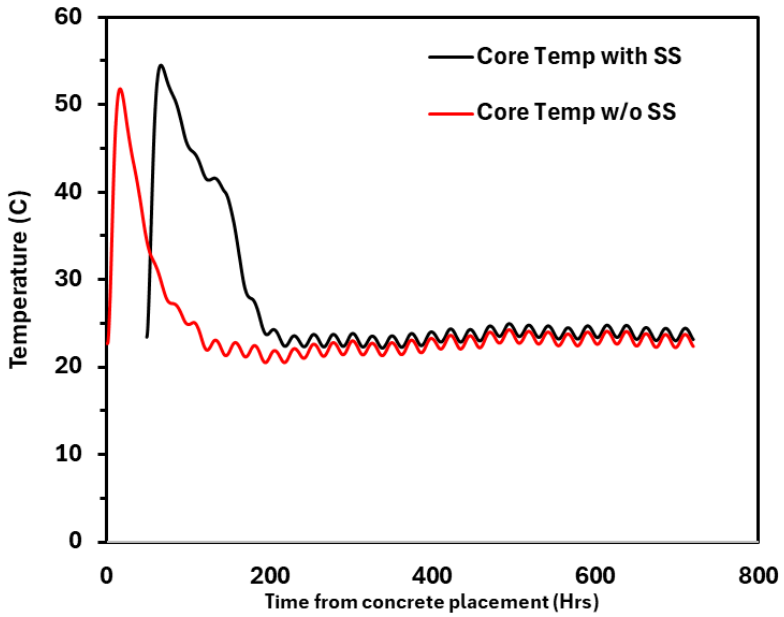


**Figure 8-9. Effect of the seal slab on the maximum temperature profile in the footing**

*8.4.2. Effect of Time of Footing Placement*

To understand the effect of the time of footing placement—or the seal slab age when the footing is placed—on the temperature profile of the footing, several trials were conducted involving the same seal slab and the same footing but with the footing placed on the seal slab at 2 days, 3 days, 7 days, and 14 days after seal slab construction. The core temperature profiles of these footings are shown in Figure 8-10.

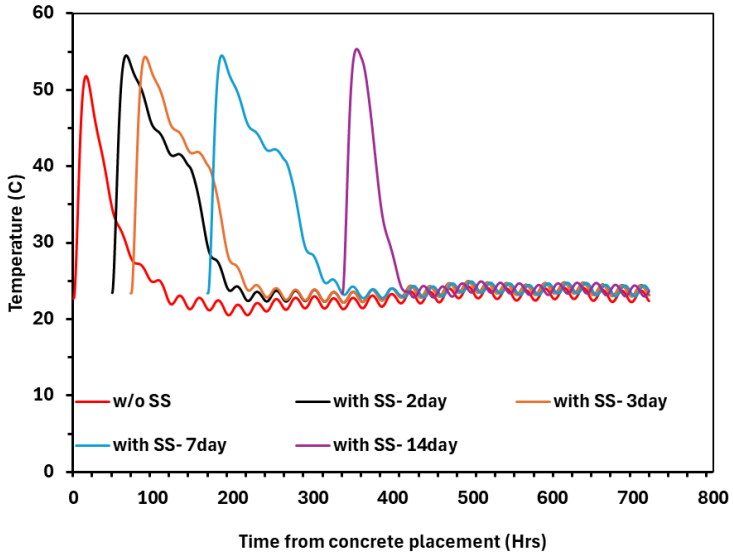


**Figure 8-10. Core temperature profiles of footings at different placement times after seal slab placement**

Based on Figure 8-10, the following key observations are made:

- When the footings are placed on the seal slab at 2, 3, and 7 days after seal slab construction, the temperature behavior of all of the footings looks similar. That is, the maximum core temperatures of the footings are all about 3°C higher than that of the corresponding footing without a seal slab. The heat of all the footings drops slowly, and the heat retention lasts about 4 days (~100 hours).
- The trend in the temperature profile of the footing placed 14 days after seal slab construction looks very similar to that of the footing without a seal slab. Although the maximum core temperature of this footing is still about 3°C higher than that of the footing without a seal slab, there is no heat retention in the footing placed at 14 days after seal slab construction.

*8.4.3. Effects of Environmental Temperature of Seal Slab*

The effect of the environmental temperature was studied by keeping the mix design and structural dimension inputs the same as those used in the previous analysis and assuming that the seal slab was placed in Iowa on June 1, 2024, or October 1, 2024, respectively, and that the footings were placed two days after seal slab construction. Figures 8-11a and 8-11b show the weather conditions at the time of construction. Figures 8-12a and 8-12b show the results of the footing temperature analysis.

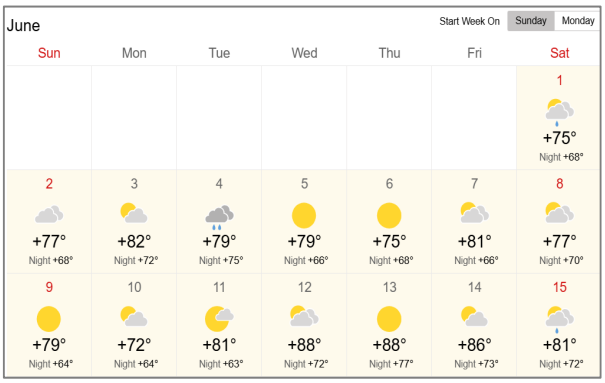


(a) Early June Forecast

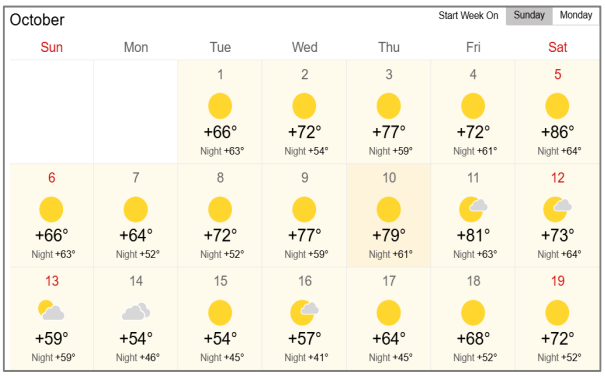


(b) Early October Forecast

*https://world-weather.info/forecast/usa/des_moines/june-2024/* and *https://world-weather.info/forecast/usa/des_moines/october-2024*

**Figure 8-11. Weather conditions on assumed construction dates**

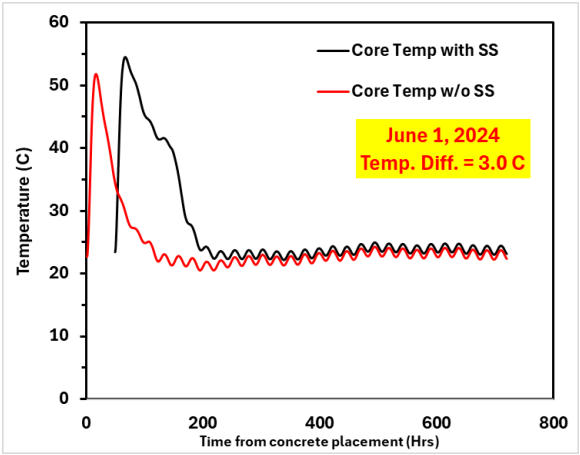


(a) Concrete placement on June 1, 2024

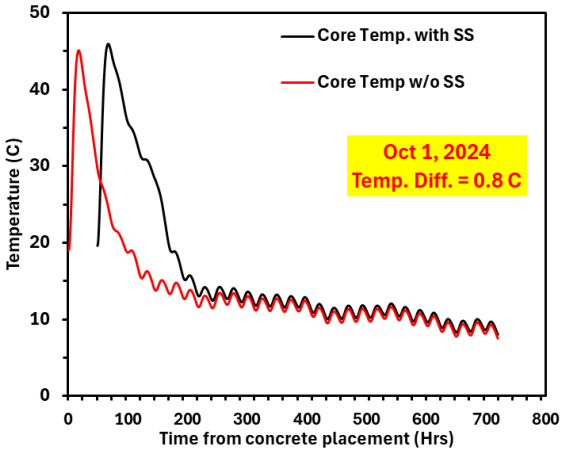


(b) Concrete placement on Oct 1, 2024

**Figure 8-12. Effect of the environmental temperature on the influence of the seal slab on the increase in footing temperature**

As observed in Figure 8-12, when the seal slab construction date is June 1, 2024, the maximum core temperature of the footing placed on the seal slab is 3°C higher than that of the footing without a seal slab. The heat retention in the footing placed on the seal slab is very clear. When the seal slab construction date is October 1, 2024, the maximum core temperature of the footing placed on the seal slab is only 0.8°C higher than that of the footing without a seal slab. The heat retention in the footing placed on the seal slab is significantly reduced.

### *8.4.4. Effects of Seal Slab and Footing Size*

To investigate the effect of seal slab and footing size on the footing temperature profile, the following case studies were conducted.

Case Study 1: Study of different footing sizes, with the seal slab size kept as 10 ft x 3 ft and the footing placed two days after seal slab construction:

- Footing Size 1 (F1): 3 ft x 9 ft x 4 ft, Volume (V1): 108 $ft^3$
- Footing Size 2 (F2): 4 ft x10 ft x 5 ft, Volume (V2): 200 $ft^3$
- Footing Size 3 (F3): 5 ft x 10 ft x 6 ft, Volume (V3): 300 $ft^3$
- Footing Size 4 (F4): 4 ft x 10 ft x 8 ft, Volume (V4): 400 $ft^3$

Case Study 2: Change in the sizes of both footing and seal slab:

A. Footing Size (F1): 3 ft x 9 ft x 4 ft, Volume (V1): 108 $ft^3$; Seal Slab (SS1): 10 ft x 3 ft, Area: 30 $ft^2$
B. Footing Size (F2): 4 ft x 10 ft x 5 ft, Volume (V2): 200 $ft^3$; Seal Slab (SS2):15 ft x 4 ft, Area: 60 $ft^2$
C. Footing Size (F2): 4 ft x 10 ft x 5 ft, Volume (V2): 200 $ft^3$; Seal Slab (SS1): 10 ft x 3 ft, Area: 30 $ft^2$

The footings are placed at 2, 3, 7, and 14 days after seal slab construction.

For the case studies listed above, the mix design of the concrete footing and seal slab (see Table 8-1) and the environmental conditions (June 1, 2024) were kept the same. The core temperature profiles of the footings were analyzed, and the results are presented in Figure 8-13.

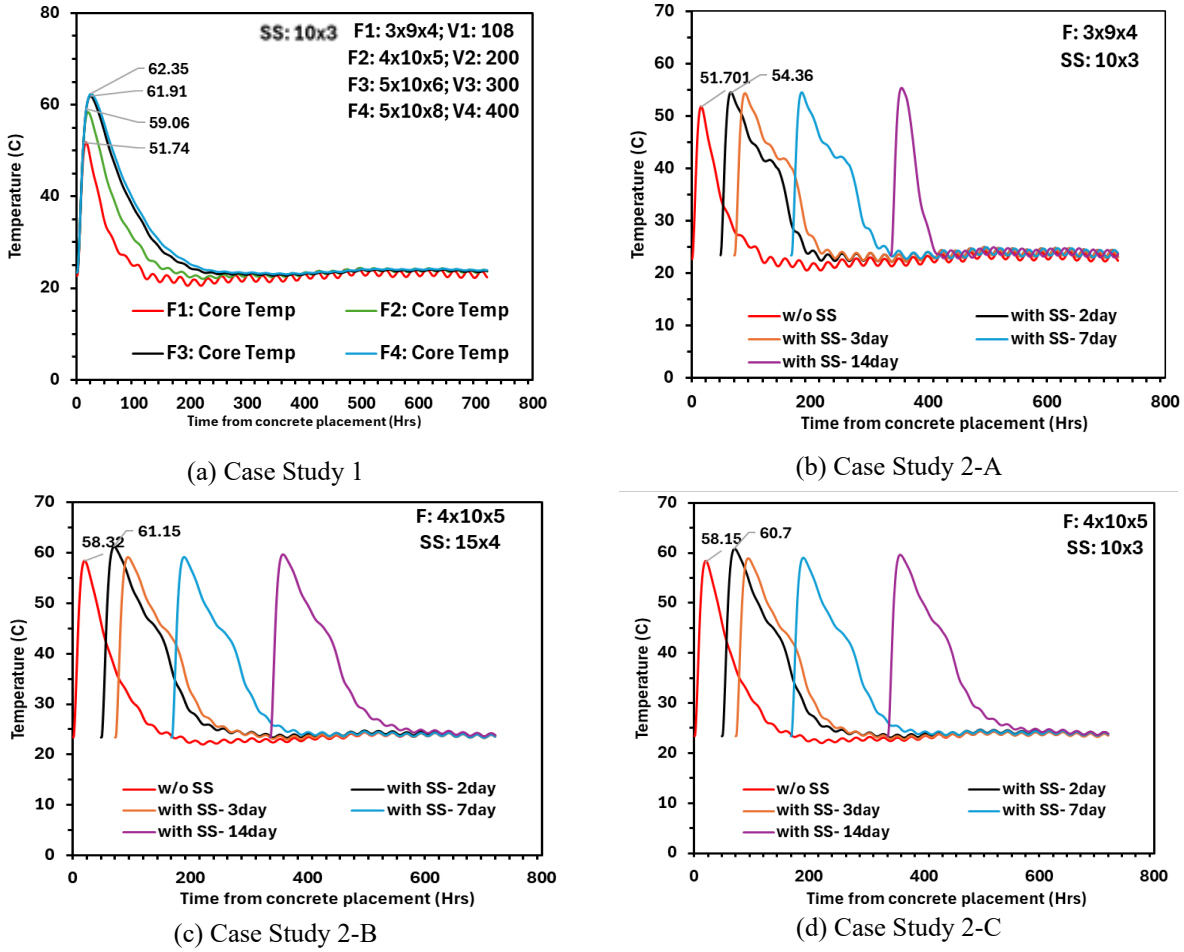


(a) Case Study 1

(b) Case Study 2-A

(c) Case Study 2-B

(d) Case Study 2-C

**Figure 8-13. Effect of seal slab size and footing size on the temperature profile of the footing**

The following observations can be made from Figure 8-13:

- As the size of the footing increases (Case Study 1, Figure 8-13a) from 108 to 300 $ft^3$, the maximum core temperature of the footing increases. When the volume of the footing changes from 108 to 200 $ft^3$, the core temperature increases 7.3°C. When the volume of the footing changes from 200 to 300 $ft^3$, the core temperature increases 2.85°C. When the volume of the footing changes from 300 to 400 $ft^3$, the core temperature increases only 0.44°C. This shows a nonlinear relationship between the temperature rise and the footing size, which reaches a plateau after a certain size of footing.
- For a smaller footing placed on a smaller seal slab (Case Study 2-A, Figure 8-13b), heat retention is observed when the footing is placed within 7 days after seal slab construction. However, the heat retention disappears when the footing is placed 14 days after seal slab construction. For a larger footing placed on a larger seal slab (Case Study 2- B, Figure 8-13c), a maximum core temperature increase is only clear for the early footing placement, 2 days after seal slab construction, but heat retention is observed when the footing is placed within 14 days after seal slab construction.

- As the seal slab size changes while the footing size is kept constant (Case Study 2-B versus Case Study 2-C), the differences in the temperature profiles of the footings are limited (Figure 8-13c versus 8-13d).

### 8.5. Summary of Seal Slab–Footing Analysis

In this study, a new component that enables modeling of the temperature rise in a footing placed on a concrete seal slab was developed and added to the existing ConcreteWorks software. The new component is simple, user friendly, and well-integrated with the existing ConcreteWorks software.

Using the updated ConcreteWorks software with the new seal slab component, several trial analyses were performed. The following conclusions can be made from the cases evaluated:

- The maximum core temperature of a footing placed on a seal slab is generally higher than that of a footing with no seal slab (by approximately 3°C).
- The maximum core temperature of a footing placed on a seal slab drops much more slowly than that of a footing without a seal slab. That is, a seal slab enhances the capacity for heat retention in the footing, keeping the core temperature high for a longer period.
- The temperature profile of a footing placed on a seal slab can be affected by factors like seal slab and footing dimensions, time of footing placement, environmental temperature, the mix design of the seal slab and footing, and so on. Additional sensitivity studies can be conducted to investigate the effects of various seal slab mix designs on the temperature profile of the footings placed above.

# 9. CONCLUSIONS AND RECOMMENDATIONS

## 9.1. Summary and Conclusions from Part A

The previous version of ConcreteWorks did not consider slag chemical and physical properties but dosage in the cement hydration model, and therefore its prediction for thermal properties, like the adiabatic temperature, of mass concrete containing slag is not accurate. In this project, the corresponding physical and chemical properties of slag were identified, and corresponding data were collected from the literature. The key chemical properties were slag replacement percentage, alkali content, alumina content, and calcium content; while fineness may be another key property, the information on slag fineness is limited in the available literature. Using these additional factors and regression analysis on the collected literature data, a new hydration model was developed. The newly developed model was validated using large concrete blocks (with four different concrete mixes) in the laboratory and some literature data. A trial-run thermal analysis was conducted on the modified ConcreteWorks (new) software and the previous ConcreteWorks (older) software to verify the improvements in temperature prediction.

A summary of the features in the modified ConcreteWorks software includes the following:

1. The default input values in the ConcreteWorks software have been updated to contain slag chemical compositions based on the results obtained from this research project (both laboratory and modeling). They are available for use when analyzing Iowa mass concrete and can also be changed when measured data are available.
2. The new slag hydration model includes the chemical properties of the slag, which makes the predictions of the new version of ConcreteWorks more accurate.
3. The temperature prediction of the concrete has improved in the newly modified ConcreteWorks software, when compared with the previous version of ConcreteWorks. The absolute error has decreased from 35% to 15.6%.
4. The newly developed model includes the hydration parameter equations for both the Bogue and Rietveld methods, and these equations are easy to implement.

The following observations were made from the Part A study:

1. Based on the isothermal calorimetry measurements, it was observed that slag replacement does not necessarily decrease the total heat of hydration. When the slag replacement increases from 25% to 75%, the initial rate of heat generation (about 7–20 hours of testing) decreases. However, at a later age (40–80 hours), depending on the temperature and percent replacement), the rate of heat generation and the accumulated heat of slag mixes surpassed that of the control mix (0% slag replacement for cement), indicating the late-age reactivity of slag is high. The surpassing effect occurred earlier as the testing temperature increased.
2. The slag fineness (physical properties) showed great influence on the rate of heat and total heat of hydration. The finer slag (Grade 120) had a significantly higher rate of heat and total heat of hydration compared to Grade 100 slag mixes. This effect was increased at higher temperatures, showing that the mass concrete slag physical properties (such as fineness) can be a key factor that influences the maximum temperature rise.

3. Literature data were collected for the mass concrete structure to get the ATR, slag and cement compositions, and mix designs. These data were used in the 3P and 6P models to get the best-fit hydration parameters. Based on the fit ($R^2$ value), the 3P model was chosen for further advancement.
4. The previous ConcreteWorks model was modified using regression analysis to include slag chemical and physical properties. Slag fineness was excluded due to the lack of availability in the literature data. A second-order polynomial regression was fitted to get the best $R^2$ fit, and cases of over-fitting (on higher order polynomial) were avoided.
5. The model was verified using 4C analysis and large concrete block measurements. The true adiabatic temperature was obtained using the 4C software, and then it was plotted in the 3P model. The new model was also used to model the temperature rise. Both results were compared, and the newly developed model showed a 20% reduction in the absolute error.
6. Overall, the new ConcreteWorks model predicts the early-age temperature profile with higher accuracy and predicts the maturity and strength of Iowa mass concrete quite well.

### 9.2. Summary and Conclusions from Part B

In the Part B study, seal slabs were simply modeled in two-dimensional analysis cases for rectangular footings. Before the footing is virtually placed on the seal slab, the seal slab is modeled the same as a rectangular footing without a seal slab placed underneath. Curing of the seal slab can be specified in the ConcreteWorks software based on the preferred construction practice. Because seal slabs in Iowa DOT projects are often cured underwater in a flooded cofferdam, in this project a new feature was added that allows the seal slab to cure under water. If the underwater curing option is not selected, ConcreteWorks assumes that the same curing used on top of the footing is used on top of the seal slab before the footing concrete is placed. After a user-defined seal slab curing period, the curing material on top of the seal slab is removed, and the footing is virtually placed on top of the seal slab. The input parameters of the seal slab component include seal slab and footing dimensions, mix design, time of footing placement, environmental conditions, and so on. The output parameters are the same as those for a footing with no seal slab. In the software, the user can select a footing with or without a seal slab for temperature analysis. By comparing the temperature profiles of the footing with and without a seal slab, the user can understand the effect of the seal slab on the temperature profile of the footing above.

Using the updated ConcreteWorks software, a series of trial analyses was conducted to investigate the effects of (1) the time of footing placement, (2) the sizes of the seal slab and footing, and (3) the construction season or environmental temperature on the temperature profile of a footing with a seal slab.

The following observations were made from the Part B study:

- A new feature has been added to the ConcreteWorks software that allows the seal slab to cure underwater in a flooded cofferdam if the option is selected.
- The new component is simple, user friendly, and well-integrated with the existing ConcreteWorks software.

- The maximum core temperature of a footing placed on a seal slab is generally higher than that of a footing with no seal slab (by approximately 3°C)
- The maximum core temperature of a footing placed on a seal slab drops much more slowly than that of a footing without a seal slab. That is, a seal slab enhances the capacity for heat retention in the footing, keeping the core temperature high for a longer period.
- The temperature profile of a footing placed on a seal slab can be affected by factors like seal slab and footing dimensions, time of footing placement, environmental temperature, the mix design of the seal slab and footing, and so on. Additional sensitivity studies can be conducted to investigate the effects of various seal slab mix designs on the temperature profile of the footings placed above.

### 9.3. Recommendations

Recommendations for effective use of the modified ConcreteWorks software and for further research are as follows:

1. This study shows that within the selected parameter ranges, slag replacement dosage clearly influences both the maximum temperature and especially the concrete temperature at later age (28 days). That is, the sensitivity of slag replacement dosage is high for concrete adiabatic temperature, followed by slag aluminum and calcium contents. These sensitive parameters should be considered in future mass concrete material selection, mix design, and thermal control.
2. The modified ConcreteWorks software offers reliable predictions for concrete containing up to 75% slag replacement for cement. Caution is advised when predicting the temperature of concrete with higher slag content, as limited data are available for such mixtures, and the statistical power may not be sufficient for developing a reliable model.
3. The modified ConcreteWorks software has a newly developed hydration model, which includes slag chemical properties, but it still does not include slag physical properties (fineness). In the future, this model can be modified by considering fineness as an input parameter (when enough literature data are available to conduct the analysis).
4. The modified version of ConcreteWorks does not take the chemical properties of any other SCMs, such as fly ash and silica fume, into account. In the future, based on literature and available data, the model can be further improved, and a new model can be developed for tertiary cementitious systems.
5. In this study, only binary slag cement with slag was studied. Low-carbon cements, such as portland limestone cement (PLC), which has been increasingly used in Iowa, and calcined clay-containing binary and ternary cements, such as limestone calcined clay cement (LC3), which are increasingly used in the United States, have not been included in the present study. Investigation into the thermal behavior of mass concrete containing low-carbon cement, especially limestone cement, may be necessary in the very near future.
6. The modified version of ConcreteWorks can be used to generate a temperature development profile at any point and the temperature differential between any two points in the mass concrete member. In the future, the generated results can be compared with the Iowa DOT temperature differential limits, and the information on the comparison can be incorporated into the software.

7. While the newly developed seal slab model provides valuable insights, further studies incorporating field data are necessary to validate its accuracy and enhance its practical applicability.

## REFERENCES


Abeka, H., S. Agyeman, and M. Adom-Asamoah. 2017. Thermal effect of mass concrete structures in the tropics: Experimental, modelling and parametric studies. *Cogent Engineering*, Vol. 4, No. 1.

Ballard, J. W., H. M. Jennings, R. A. Livingston, A. Nanat, G. W. Scherer, J. S. Schweitzer, K. L. Srivener, and J. J. Thomas. 2011. Mechanisms of Cement Hydration. *Cement and Concrete Research*, Vol. 41, pp. 1208–1223.

Barnett, S. J., M. N. Soutsos, J. H. Bungey, and S. G. Millard. 2005. The effect of ground granulated blast furnace slag on the strength development and adiabatic temperature rise of concrete mixes. *Cement Combinations for Durable Concrete*. ICE Publishing, London, UK. pp. 165–172.

Bas, B. E. 2020. Study on the Thermal Properties of Concrete Containing Ground Granulated Blast Furnace Slag, Fly Ash, and Steel Reinforcement. MS thesis. West Virginia University, Morgantown, WV.

Chen, H.-L. R., S. Mardmomen, and G. Leon. 2021. On-site measurement of heat of hydration of delivered mass concrete. *Construction and Building Materials*, Vol. 269.

Chini, A. R., and A. Parham. 2005. *Adiabatic Temperature Rise of Mass Concrete in Florida*. Florida Department of Transportation, Tallahassee, FL.

Coole, M. 1998. Heat release characteristics of concrete containing ground granulated slag in simulated large pours. *Magazine of Concrete Research*, Vol. 40, No. 144, pp. 152–158.

Dabarera, A., W. Saengsoy, K. Kaewmanee, K. Mori, and S. Tangtermsirikul. 2017. Models for predicting hydration degree and adiabatic temperature rise of mass concrete containing ground granulated blast furnace slag. *Engineering Journal*, Vol. 21, No. 3, pp. 157–171.

da Silva, W. R. L., V. Šmilauer, and P. Štemberk. 2015. Upscaling semi-adiabatic measurements for simulating temperature evolution of mass concrete structures. *Materials and Structures*, Vol. 48, pp. 1031–1041.

Gajda, J., M. Weber, and I. Diaz-Loya. 2014. A low temperature rise mixture for mass concrete. *Concrete International*, Vol. **36, No.** 8, pp. 48–53.

Gajda, J., and M. Vangeem. 2002. Controlling temperatures in mass concrete. *Concrete International*, Vol. 24, No. 1, pp. 58–62.

Ge, Z., K. Wang, P. Sandberg, and J. Ruiz. 2009. Characterization of cement-based materials using a simple isothermal calorimeter. *Journal of Advanced Concrete Technology*, Vol. 7, No. 3, pp. 355–366.

Ge, Z., and K. Wang. 2009. Modified heat of hydration and strength models for concrete containing fly ash and slag. *International Journal of Computers and Concrete*, Vol. 6, No. 1, pp. 19–40.

Gruyaert, E., N. Robeyst, and B. N. De. 2010. Study of the hydration of portland cement blended with blast furnace slag by calorimetry and thermogravimetry. *Journal of Thermal Analysis and Calorimetry*, Vol. 102, No. 3, pp. 941–951.

Hamid, H., and M. G. Chorzepa. 2020. Quantifying maximum temperature in 17 mass concrete cube specimens made with mixtures including metakaolin and/or slag. *Construction and Building Materials*, Vol. 252.

Han, S. 2020. Assessment of curing schemes for effectively controlling thermal behavior of mass concrete foundation at early ages. *Construction and Building Materials*, Vol. 230.

Lawrence, A. M., M. Tia, C. C. Ferraro, and M. Bergin. 2012. Effect of early-age strength on cracking in mass concrete containing different supplementary cementitious materials: Experimental and finite-element investigation. *Journal of Materials in Civil Engineering*, Vol. 24, No. 4, pp. 362–372.

Luan, Y., T. Ishida, T. Nawa, and T. Sagawa. 2012. Enhanced model and simulation of hydration process of blast furnace slag in blended cement. *Journal of Advanced Concrete Technology*, Vol. 10, No. 1, pp. 1–13.

Koo, K.-M., G. Kim, J.-K. Yoo, and E.-B. Lee. 2014. Properties of adiabatic temperature rise on concrete considering cement content and setting time. *Indian Journal of Engineering and Materials Sciences*, Vol. 21, No. 5, pp. 527–535.

Moon, H., S. Ramanathan, P. Suraneni, C.-S. Shon, C.-J. Lee, and C.-W. Chung. 2018. Revisiting the effect of slag in reducing heat of hydration in concrete in comparison to other supplementary cementitious materials. *Materials*, Vol. 11, No. 10, p. 1847.

Poole, J. L. 2007. Modeling Temperature Sensitivity and Heat Evolution of Concrete. MS Thesis. The University of Texas at Austin, Austin, TX.

Poole, J. L K. A. Riding, K. J. Folliard, M. C. G. Juenger, and A. K. Schindler. 2007. Methods for calculating activation energy for portland cement. *ACI Materials Journal*, Vol. 104, No. 1, pp. 303–311.

Riding, K. A. 2007. Early-Age Concrete Thermal Stress Measurement and Modeling. MS Thesis. The University of Texas at Austin, Austin, TX.

Riding, K. A., J. L. Poole, A. K. Schindler, M. C. G. Juenger, and K. J. Folliard. 2006. Evaluation of temperature prediction methods for mass concrete members. *ACI Materials Journal*, Vol. 103, No. 5, pp. 357–365.

Riding, K. A., J. L. Poole, A. K. Schindler, M. C. G. Juenger, and K. J. Folliard. 2007. Temperature boundary condition models for concrete bridge members. *ACI Materials Journal*, Vol. 104, No. 4, pp. 379–387.

Riding, K. A., J. L. Poole, K. J. Folliard, M. C. G. Juenger, and A. K. Schindler. 2011. New model for estimating apparent activation energy of cementitious systems. *ACI Materials Journal*, Vol. 108, No. 5, pp. 550–557.

Riding, K.A., J. L. Poole, K. J. Folliard, M. C. G. Juenger, and A. K. Schindler. 2012. Modeling hydration of cementitious systems. *ACI Materials Journal*, Vol. 109, No. 2, pp. 225–234.

Riding, K., J. Vosahlik, K. Bartojay, C. Lucero, A. Sedaghat, A. Zayed, and C. C. Ferraro. 2019. Methodology comparison for concrete adiabatic temperature rise. *ACI Materials Journal*, Vol. 116, No. 2, pp. 45–53.

Sargam, Y., K. Wang, and J. E. Alleman. 2020. Effects of modern concrete materials on thermal conductivity. *Journal of Materials in Civil Engineering*, Vol. 32, No. 4.

Schindler, A. K., and K. J. Folliard. 2003. Influence of supplementary cementing materials on the heat of hydration of concrete. *Proceedings, Advances in Cement and Concrete IX Conference, Copper Mountain Conference Resort, Frisco, CO*.

Schindler, A. K., and K. J. Folliard. 2005. Heat of hydration models for cementitious materials. *ACI Materials Journal*, Vol. 102, No. 1, pp. 24–33.

Shaw, J., C. T. Jahren, K. Wang, and J. Li. 2014. *Iowa Mass Concrete for Bridge Foundations Study – Phase II*. InTrans Project 10-384. Institute for Transportation, Iowa State University, Ames, IA.

Tam, C., Y. Loo, K. Choong. 1994. Adiabatic temperature rise in concrete with and without GGBFS. *ACI Symposium Papers*, Vol. 149, pp. 649–664.

Tang, K., J. Khatib, and G. Beattie. 2017. Effect of partial replacement of cement with slag on the early-age strength of concrete. *Proceedings of the Institution of Civil Engineers - Structures and Buildings*, Vol. 170, No. 6, pp. 451–461.

Tia, M., C. Ferraro, A. Lawrence, S. Smith, and F. Ochiai. 2010. *Development of Design Parameters for Mass Concrete Using Finite Element Analysis*. Florida Department of Transportation, Tallahassee, FL.

Wang, K., Y. Sargam, K. Riding, M. Faytarouni, C. Jahren, and J. Shen. 2020. *Evaluate, Modify, and Adapt the ConcreteWorks Software for Iowa's Use*. Institute for Transportation, Ames, IA.

Wang, X.-Y., and H.-S. Lee. 2010. Modeling the hydration of concrete incorporating fly ash or slag. *Cement and Concrete Research*, Vol. 40, No. 7, pp. 984–996.

Woo, H.-M., C.-Y. Kim, and J.H. Yeon. 2018. Heat of hydration and mechanical properties of mass concrete with high-volume GGBFS replacements. *Journal of Thermal Analysis and Calorimetry*, Vol. 132, pp. 599-609.

Yikici, T. A., and H.-L. R. Chen. 2015. Use of maturity method to estimate compressive strength of mass concrete. *Construction and Building Materials*, Vol. 95, pp. 802–812.

Zayed, A., K. Riding, C. C. Ferraro, A. Bien-Aime, N. Shanahan, D. Buidens, T. Meagher, V. Tran, J. D. Henika, J. M. Paris, C. M. Tibbetts, and B. E. Watts. 2015. *Long-Life Slab Replacement Concrete*. Florida Department of Transportation, Tallahassee, FL.

Zhu, H., D. G. Mapa, C. Lucero, K. A. Riding, and A. Zayed. 2022. Effect of slag characteristics on adiabatic temperature rise of blended concrete. *ACI Materials Journal*, Vol. 119, No. 1.

## APPENDIX A. SEMI-ADIABATIC CALORIMETER CALIBRATION PROCEDURE

The use of boiling water is a simple, practical approach to semi-adiabatic calorimeter calibration, as boiling water has a stable and known temperature (100°C at standard atmospheric pressure). Below is the calibration process.

1. **Setup:**
   - Fill a container with boiled water and place the container inside the semi-adiabatic chamber.
   - Seal the chamber properly to minimize external influences.
2. **Record Temperature:**
   - The temperature of the water was recorded for 160 hours at intervals of 15 minutes using Type T sensors installed in the semi-adiabatic chamber (shown in Figure 4-3a as MID, EXT1, and EXT2).
3. **Calculate Heat Input:**
   - Calculate the total heat input: $Q_{input} = m_{water} \cdot C_{water} \cdot \Delta T_{water}$
   - Where $Q_{input}$ is the total heat input; $m_{water}$ is the mass of the water; $C_{water}$ is the specific heat capacity of water ($C_{water}$ =4.186 J/g°C); and $\Delta T_{water}$ is the temperature difference from 100°C to the final temperature.
4. **Determine Temperature Rise:**
   - The temperature rise inside the chamber ($\Delta T_{chamber}$) is $T_{chamber,\ initial} - T_{chamber,\ final}$.
5. **Estimate Apparent Heat Capacity:**
   - The apparent heat capacity ($C_{app}$) of the chamber can be estimated from: $C_{app} = Q_{input}/\Delta T_{chamber}$.
6. **Develop Heat Loss Model Using Solver Function:**
   - List the experimental data and plot the heat input ($Q_{input}$ versus corresponding temperature rise ($\Delta T_{chamber}$) in an Excel spreadsheet.
   - Use the regression analysis with the Solver function to model the heat loss of the water: $Q_{loss} = C_{f1} \cdot \Delta T_{chamber} + C_{f2} \cdot (\Delta T_{chamber})^4$, thus generating the best-fit calibration factors ($C_{f1}$ and $C_{f2}$).
7. **Apply the Calibration Data in Concrete:**
   - For concrete tested using a semi-adiabatic calorimetry, use the formula $Q_{loss} = C_{f1} \cdot \Delta T_{sa} + C_{f2} \cdot (\Delta T_{sa})^4$, where $\Delta T_{sa}$ is the recorded semi-adiabatic temperature rise of the concrete sample.
   - The total heat generated ($Q_{gen}$) in concrete will be calculated as $Q_{gen} = Q_{loss} + (m \cdot C \cdot \Delta T_{sa})$, where $m$ is the mass of concrete sample and $C$ is the specific heat capacity of concrete (approximately 0.84 J/g°C or 840 J/kg°C).
   - The true adiabatic temperature rise ($\Delta T_{true\ ATR}$) can be calculated as $\Delta T_{true\ ATR} = Q_{gen}/(m \cdot C)$.

## APPENDIX B. LIST OF PAPERS REVIEWED FOR HYDRATION MODEL

Table B-1 presents the list of papers where data were extracted for the slag cement hydration model.

**Table B-1. List of papers included in slag cement hydration model data extraction**

| Paper No. | Reference | Paper Title | Acceptance of final data | Reason for non-acceptance |
|---|---|---|---|---|
| 1 | Han 2020 | Assessment of curing schemes for effectively controlling thermal behavior of mass concrete foundation at early ages | No | Not sufficient |
| 2 | Tang et al. 2017 | Effect of partial replacement of cement with slag on the early-age strength of concrete | No | Not true Adiabatic |
| 3 | Zayed et al. 2015 | Long-life slab replacement concrete | Yes | |
| 4 | Wang and Lee 2010 | Modeling the hydration of concrete incorporating fly ash or slag | Yes | |
| 5 | Chen et al. 2021 | On-site measurement of heat of hydration of delivered mass concrete | Yes | |
| 6 | Schindler and Folliard 2003 | Influence of supplementary cementing materials on the heat of hydration of concrete | No | Not true adiabatic |
| 7 | Riding et al. 2019 | Methodology comparison for concrete adiabatic temperature rise | Yes | |
| 8 | Hamid and Chorzepa 2020 | Quantifying maximum temperature in 17 mass concrete cube specimens made with mixtures including metakaolin and/or slag | Yes | |
| 9 | Luan et al. 2012 | Enhanced model and simulation of hydration process of blast furnace slag in blended cement | No | No cement composition |
| 10 | Tia et al. 2010 | Development of design parameters for mass concrete using finite element analysis | No | No composition |
| 11 | Woo et al. 2018 | Heat of hydration and mechanical properties of mass concrete with high-volume GGBFS replacements | Yes | |
| 12 | Bas 2020 | Study on the thermal properties of concrete containing ground granulated blast furnace slag, fly ash, and steel reinforcement | No | Not True Adiabatic |
| 13 | Koo et al. 2014 | Properties of adiabatic temperature rise on concrete considering cement content and setting time | No | No composition |
| 14 | Abeka et al. 2017 | Thermal effect of mass concrete structures in the tropics: Experimental, modelling and parametric studies | No | No composition |
| 15 | Coole 1998 | Heat release characteristics of concrete containing ground granulated slag in simulated large pours | No | Not True Adiabatic |
| 16 | da Silva et al. 2015 | Upscaling semi-adiabatic measurements for simulating temperature evolution of mass concrete structures | No | No composition |
| 17 | Yikici and Chen 2015 | Use of maturity method to estimate compressive strength of mass concrete | No | Not True Adiabatic |
| 18 | Lawrence et al. 2012 | Effect of early-age strength on cracking in mass concrete containing different supplementary cementitious materials: Experimental and finite-element investigation | No | No composition |
| 19 | Zhu et al. 2022 | Effect of slag characteristics on adiabatic temperature | Yes | |
| 20 | Riding et al. 2012 | Modeling hydration of cementitious systems | Yes | |

## APPENDIX C. PROPERTIES OF SLAGS COLLECTED FROM THE LITERATURE

The chemical and physical properties of the slag used in selected mixes are presented in Tables C-1 through C-3.

**Table C-1. Chemical properties of slag used in selected mixes**

| No. | Slag Replacement | Alumina % | Alkali % | Mg % | Ca % | $E_a$ (J/mol) | Hu (j/kg) | Hu*Au (J/kg) |
|---|---|---|---|---|---|---|---|---|
| 1 | 0.500 | 7.730 | 0.501 | 10.400 | 39.42 | 37009 | 478135 | 403366 |
| 2 | 0.700 | 7.730 | 0.501 | 10.400 | 39.42 | 44302 | 471271 | 346695 |
| 3 | 0.700 | 20.500 | 0.429 | 4.200 | 38.50 | 43988 | 458713 | 412841.7 |
| 4 | 0.800 | 20.500 | 0.429 | 4.200 | 38.50 | 45442 | 459476 | 385959.84 |
| 5 | 0.500 | 10.050 | 0.532 | 10.000 | 38.90 | 41486 | 461762 | 369409.6 |
| 6 | 0.700 | 10.050 | 0.532 | 10.000 | 38.90 | 43502 | 461457 | 355321.89 |
| 7 | 0.500 | 11.400 | 0.400 | 7.300 | 41.70 | 41392 | 462000 | 444444 |
| 8 | 0.470 | 11.400 | 0.400 | 7.300 | 41.70 | 42168 | 453000 | 447111 |
| 9 | 0.480 | 11.400 | 0.363 | 7.300 | 41.70 | 42176 | 453000 | 426726 |
| 10 | 0.300 | 11.400 | 0.363 | 7.300 | 41.70 | 40315 | 471000 | 454986 |
| 11 | 0.400 | 11.400 | 0.363 | 7.300 | 41.70 | 41097 | 469000 | 458682 |
| 12 | 0.500 | 11.400 | 0.363 | 7.300 | 41.70 | 42008 | 468000 | 468000 |
| 13 | 0.500 | 11.400 | 0.363 | 7.300 | 41.70 | 41624 | 461000 | 398304 |
| 14 | 0.300 | 11.400 | 0.363 | 7.300 | 41.70 | 39597 | 476000 | 423164 |
| 15 | 0.400 | 11.400 | 0.363 | 7.300 | 41.70 | 40200 | 474000 | 435132 |
| 16 | 0.500 | 11.400 | 0.363 | 7.300 | 41.70 | 40960 | 472000 | 346920 |
| 17 | 0.300 | 11.400 | 0.363 | 7.300 | 41.70 | 31532 | 475000 | 475000 |
| 18 | 0.500 | 11.400 | 0.363 | 7.300 | 41.70 | 32824 | 471000 | 426255 |
| 19 | 0.300 | 11.400 | 0.363 | 7.300 | 41.70 | 39924 | 432000 | 432000 |
| 20 | 0.400 | 11.400 | 0.363 | 7.300 | 41.70 | 40644 | 436000 | 436000 |
| 21 | 0.500 | 11.400 | 0.363 | 7.300 | 41.70 | 41502 | 440000 | 440000 |
| 22 | 0.300 | 11.200 | 0.600 | 10.100 | 36.60 | 38060 | 468000 | 444600 |
| 23 | 0.150 | 9.200 | 0.600 | 10.200 | 37.10 | 37129 | 469000 | 365820 |
| 24 | 0.300 | 9.200 | 0.600 | 10.200 | 37.10 | 38060 | 468000 | 402480 |
| 25 | 0.450 | 9.200 | 0.600 | 10.200 | 37.10 | 39281 | 466000 | 433380 |
| 26 | 0.300 | 9.000 | 0.600 | 10.300 | 36.70 | 38060 | 468000 | 407160 |
| 27 | 0.600 | 7.820 | 0.560 | 10.710 | 39.18 | 43765 | 469930 | 337,405 |
| 28 | 0.600 | 10.690 | 0.400 | 10.700 | 39.23 | 45483 | 469930 | 319,391 |
| 29 | 0.600 | 10.090 | 0.520 | 10.810 | 38.33 | 39975 | 469930 | 350,912 |
| 30 | 0.600 | 13.800 | 0.410 | 5.600 | 42.00 | 37641 | 469930 | 322,879 |
| 31 | 0.600 | 17.070 | 0.680 | 10.960 | 35.49 | 30220 | 469930 | 347,374 |
| 32 | 0.600 | 7.820 | 0.560 | 10.710 | 39.18 | 38714 | 466174 | 336,447 |
| 33 | 0.600 | 13.800 | 0.410 | 5.600 | 42.00 | 39285 | 466174 | 315,191 |
| 34 | 0.600 | 17.070 | 0.680 | 10.960 | 35.49 | 34476 | 466174 | 357,926 |

**Table C-2. Chemical and physical properties of slag used in selected mixes**

| No. | Au | β | τ (h) | $R^2$ | w/c ratio | $P_{C4AF}$ | $P_{cem}$ | $P_{Na2Oeq}$ |
|---|---|---|---|---|---|---|---|---|
| 1 | 0.844 | 0.54 | 38.7 | 0.98 | 0.4 | 0.1032 | 0.5 | 0.00488 |
| 2 | 0.736 | 0.55 | 36.4 | 0.95 | 0.4 | 0.1032 | 0.3 | 0.00488 |
| 3 | 0.9 | 0.62 | 13.44 | 0.863 | 0.355 | 0.0953 | 0.3 | 0.00878 |
| 4 | 0.84 | 0.53 | 16.84 | 0.883 | 0.355 | 0.0953 | 0.2 | 0.00878 |
| 5 | 0.8 | 0.75 | 40 | 0.97 | 0.4 | 0.09 | 0.5 | 0.0054 |
| 6 | 0.77 | 0.65 | 47 | 0.97 | 0.4 | 0.09 | 0.3 | 0.0054 |
| 7 | 0.962 | 0.46 | 42.656 | 0.93 | 0.44 | 0.1126 | 0.5 | 0.00408 |
| 8 | 0.987 | 0.485 | 39.812 | 0.96 | 0.44 | 0.1156 | 0.53 | 0.004948 |
| 9 | 0.942 | 0.58 | 42.587 | 0.96 | 0.41 | 0.1156 | 0.52 | 0.004948 |
| 10 | 0.966 | 0.482 | 27.483 | 0.95 | 0.44 | 0.10346 | 0.7 | 0.005606 |
| 11 | 0.978 | 0.498 | 28.729 | 0.94 | 0.44 | 0.10346 | 0.6 | 0.005606 |
| 12 | 1 | 0.46 | 39.858 | 0.95 | 0.44 | 0.10346 | 0.5 | 0.005606 |
| 13 | 0.864 | 0.585 | 32.665 | 0.97 | 0.44 | 0.09738 | 0.5 | 0.004632 |
| 14 | 0.889 | 0.638 | 21.291 | 0.94 | 0.44 | 0.0699 | 0.7 | 0.00758 |
| 15 | 0.918 | 0.592 | 26.005 | 0.92 | 0.44 | 0.0699 | 0.6 | 0.00758 |
| 16 | 0.735 | 0.757 | 21.698 | 0.93 | 0.44 | 0.0699 | 0.5 | 0.00758 |
| 17 | 1 | 0.751 | 21.332 | 0.97 | 0.42 | 0.06086 | 0.7 | 0.004948 |
| 18 | 0.905 | 0.685 | 26.534 | 0.98 | 0.42 | 0.06086 | 0.5 | 0.004948 |
| 19 | 1 | 0.497 | 38.991 | 0.95 | 0.44 | 0.1613 | 0.7 | 0.004316 |
| 20 | 1 | 0.478 | 47.914 | 0.94 | 0.44 | 0.1613 | 0.6 | 0.004316 |
| 21 | 1 | 0.439 | 81.595 | 0.94 | 0.44 | 0.1613 | 0.5 | 0.004316 |
| 22 | 0.95 | 0.701 | 29.752 | 0.93 | 0.4 | 0.1065 | 0.7 | 0.005606 |
| 23 | 0.78 | 0.753 | 19.379 | 0.97 | 0.4 | 0.1065 | 0.85 | 0.005606 |
| 24 | 0.86 | 0.579 | 30.093 | 0.95 | 0.4 | 0.1065 | 0.7 | 0.005606 |
| 25 | 0.93 | 0.499 | 49.334 | 0.94 | 0.4 | 0.1065 | 0.55 | 0.005606 |
| 26 | 0.87 | 0.588 | 30.047 | 0.95 | 0.4 | 0.1065 | 0.7 | 0.005606 |
| 27 | 0.718 | 0.792 | 26.523 | 0.96 | 0.4 | 0.077 | 0.4 | 0.0065 |
| 28 | 0.68 | 0.863 | 27.012 | 0.93 | 0.4 | 0.077 | 0.4 | 0.0065 |
| 29 | 0.747 | 0.97 | 26.03 | 0.94 | 0.4 | 0.077 | 0.4 | 0.0065 |
| 30 | 0.687 | 1.039 | 21.26 | 0.98 | 0.4 | 0.077 | 0.4 | 0.0065 |
| 31 | 0.739 | 1.24 | 24.047 | 0.95 | 0.4 | 0.077 | 0.4 | 0.0065 |
| 32 | 0.722 | 0.744 | 34.001 | 0.97 | 0.4 | 0.089 | 0.4 | 0.004 |
| 33 | 0.676 | 0.982 | 24.112 | 0.95 | 0.4 | 0.089 | 0.4 | 0.004 |
| 34 | 0.768 | 1.021 | 26.982 | 0.94 | 0.4 | 0.089 | 0.4 | 0.004 |

**Table C-3. Additional chemical and physical properties of slag used in selected mixes**

| No. | $P_{Na2O}$ | $P_{FA}$ | $P_{C3S}$ | $P_{GGBF}$ | $P_{C3A}$ | WRRET | LRWR | MRWR | NHRWR |
|---|---|---|---|---|---|---|---|---|---|
| 1 | 0.0012 | 0 | 0.6753 | 0.5 | 0.0654 | 0 | 0.0006 | 0 | 0 |
| 2 | 0.0012 | 0 | 0.6753 | 0.7 | 0.0654 | 0 | 0.0006 | 0 | 0 |
| 3 | 0 | 0 | 0.5638 | 0.7 | 0.0835 | 0 | 0 | 0 | 0 |
| 4 | 0 | 0 | 0.5638 | 0.8 | 0.0835 | 0 | 0 | 0 | 0 |
| 5 | 0.00154 | 0 | 0.62 | 0.5 | 0.06 | 0 | 0 | 0 | 0 |
| 6 | 0.00154 | 0 | 0.62 | 0.7 | 0.06 | 0 | 0 | 0 | 0 |
| 7 | 0.002 | 0 | 0.6616 | 0.5 | 0.04 | 0 | 0 | 0 | 0 |
| 8 | 0.001 | 0 | 0.626 | 0.47 | 0.0443 | 0 | 0 | 0.0041 | 0 |
| 9 | 0.001 | 0 | 0.626 | 0.48 | 0.0443 | 0 | 0 | 0.0077 | 0 |
| 10 | 0.001 | 0 | 0.64624 | 0.3 | 0.06704 | 0 | 0 | 0 | 0 |
| 11 | 0.001 | 0 | 0.64624 | 0.4 | 0.06704 | 0 | 0 | 0 | 0 |
| 12 | 0.001 | 0 | 0.64624 | 0.5 | 0.06704 | 0 | 0 | 0 | 0 |
| 13 | 0.002 | 0 | 0.7432 | 0.5 | 0.07307 | 0 | 0 | 0 | 0.0034 |
| 14 | 0.001 | 0 | 0.63346 | 0.3 | 0.10155 | 0 | 0 | 0 | 0 |
| 15 | 0.001 | 0 | 0.63346 | 0.4 | 0.10155 | 0 | 0 | 0 | 0 |
| 16 | 0.001 | 0 | 0.63346 | 0.5 | 0.10155 | 0 | 0 | 0 | 0 |
| 17 | 0.001 | 0 | 0.57375 | 0.3 | 0.10928 | 0 | 0.003 | 0 | 0 |
| 18 | 0.001 | 0 | 0.57375 | 0.5 | 0.10928 | 0 | 0.003 | 0 | 0 |
| 19 | 0.003 | 0 | 0.5057 | 0.3 | 0.01634 | 0 | 0 | 0 | 0 |
| 20 | 0.003 | 0 | 0.5057 | 0.4 | 0.01634 | 0 | 0 | 0 | 0 |
| 21 | 0.003 | 0 | 0.5057 | 0.5 | 0.01634 | 0 | 0 | 0 | 0 |
| 22 | 0.001 | 0 | 0.5232 | 0.3 | 0.06005 | 0.003 | 0 | 0 | 0 |
| 23 | 0.001 | 0 | 0.5232 | 0.15 | 0.06005 | 0.003 | 0 | 0 | 0 |
| 24 | 0.001 | 0 | 0.5232 | 0.3 | 0.06005 | 0.003 | 0 | 0 | 0 |
| 25 | 0.001 | 0 | 0.5232 | 0.45 | 0.06005 | 0.003 | 0 | 0 | 0 |
| 26 | 0.001 | 0 | 0.5232 | 0.3 | 0.06005 | 0.003 | 0 | 0 | 0 |
| 27 | 0.0002 | 0 | 0.54 | 0.6 | 0.056 | 0.003 | 0 | 0 | 0 |
| 28 | 0.0002 | 0 | 0.54 | 0.6 | 0.056 | 0.003 | 0 | 0 | 0 |
| 29 | 0.0002 | 0 | 0.54 | 0.6 | 0.056 | 0.003 | 0 | 0 | 0 |
| 30 | 0.0002 | 0 | 0.54 | 0.6 | 0.056 | 0.003 | 0 | 0 | 0 |
| 31 | 0.0002 | 0 | 0.54 | 0.6 | 0.056 | 0.003 | 0 | 0 | 0 |
| 32 | 0.0018 | 0 | 0.445 | 0.6 | 0.037 | 0.003 | 0 | 0 | 0 |
| 33 | 0.0018 | 0 | 0.445 | 0.6 | 0.037 | 0.003 | 0 | 0 | 0 |
| 34 | 0.0018 | 0 | 0.445 | 0.6 | 0.037 | 0.003 | 0 | 0 | 0 |

## APPENDIX D. DETAILED RESULTS FROM REGRESSION ANALYSIS

Table D-1 shows the second-order regression analysis with the $R^2$ fit. The independent variables (X) varied from two to six, and the corresponding $R^2$ fit was calculated. For second-order regression, all the possible combinations of the independent variables were tried as shown in Table D-1. For each combination, a regression analysis was performed to get the $R^2$ fit. It is evident that as the number of variable increases from two to six, the $R^2$ value increases as well. Theoretically, trial 31 (with six independent variables) should be best for regression analysis due to its higher $R^2$ value, but practically that is not accurate, as discussed below.

**Table D-1. Second-order regression trials to achieve the best fit**

| Trial | No. of Var. | Replacement (X1) | Alumina (X2) | Alkali (X3) | Ca (X4) | Mg (X5) | Sulphur (X6) | $R^2$ value | | |
|---|---|---|---|---|---|---|---|---|---|---|
| | | | | | | | | $\phi_\alpha$ | $\phi_\beta$, | $\phi_\tau$ |
| 1 | 2 | Yes | Yes | | | | | 0.54 | 0.45 | 0.38 |
| 2 | | Yes | | Yes | | | | 0.53 | 0.50 | 0.35 |
| 3 | | Yes | | | Yes | | | 0.44 | 0.39 | 0.41 |
| 4 | | Yes | | | | Yes | | 0.42 | 0.38 | 0.37 |
| 5 | | Yes | | | | | Yes | 0.40 | 0.35 | 0.37 |
| **6** | 3 | **Yes** | **Yes** | **Yes** | | | | **0.72** | **0.74** | **0.81** |
| **7** | | **Yes** | **Yes** | | **Yes** | | | **0.74** | **0.72** | **0.82** |
| 8 | | Yes | Yes | | | Yes | | 0.60 | 0.62 | 0.65 |
| 9 | | Yes | Yes | | | | Yes | 0.63 | 0.65 | 0.42 |
| 10 | | Yes | | Yes | Yes | | | 0.60 | 0.62 | 0.44 |
| 11 | | Yes | | Yes | | Yes | | 0.80 | 0.65 | 0.52 |
| 12 | | Yes | | Yes | | | Yes | 0.66 | 0.67 | 0.53 |
| 13 | | Yes | | | Yes | Yes | | 0.74 | 0.77 | 0.49 |
| 14 | | Yes | | | Yes | | Yes | 0.69 | 0.71 | 0.50 |
| 15 | | Yes | | | | Yes | Yes | 0.71 | 0.73 | 0.54 |
| 16 | 4 | Yes | Yes | Yes | Yes | | | 0.78 | 0.76 | 0.78 |
| 17 | | Yes | Yes | Yes | | Yes | | 0.79 | 0.71 | 0.83 |
| 18 | | Yes | Yes | Yes | | | Yes | 0.74 | 0.76 | 0.79 |
| 19 | | Yes | | Yes | Yes | Yes | | 0.64 | 0.67 | 0.74 |
| 20 | | Yes | | Yes | Yes | | Yes | 0.76 | 0.74 | 0.65 |
| 21 | | Yes | Yes | | Yes | Yes | | 0.74 | 0.72 | 0.71 |
| 22 | | Yes | Yes | | Yes | | Yes | 0.73 | 0.75 | 0.78 |
| 23 | | Yes | Yes | | | Yes | Yes | 0.80 | 0.72 | 0.68 |
| 24 | | Yes | | Yes | | Yes | Yes | 0.72 | 0.73 | 0.77 |
| 25 | | Yes | | | Yes | Yes | Yes | 0.70 | 0.68 | 0.74 |
| 26 | 5 | Yes | Yes | Yes | Yes | Yes | | 0.83 | 0.84 | 0.81 |
| 27 | | Yes | Yes | Yes | Yes | | Yes | 0.82 | 0.84 | 0.80 |
| 28 | | Yes | Yes | Yes | | Yes | Yes | 0.74 | 0.75 | 0.83 |
| 29 | | Yes | Yes | | Yes | Yes | Yes | 0.81 | 0.75 | 0.84 |
| 30 | | Yes | | Yes | Yes | Yes | Yes | 0.82 | 0.81 | 0.83 |
| 31 | 6 | Yes | Yes | Yes | Yes | Yes | Yes | 0.85 | 0.95 | 0.78 |

For second-order regression with independent variables two through five, the regression equations are given as follows, where *a* is the coefficient of the independent variable and *c* is a constant for the whole equation.

$$Y = a_1 * X^2{}_1 + a_2 * X_1 + a_3 * X^2{}_2 + a_4 * X_2 + a_5 * X_1 * X_2 + c$$

For second-order regression with two independent variables, the number of coefficients are six, as shown in the previous equation.

$$Y = a_1 * X^2{}_1 + a_2 * X_1 + a_3 * X^2{}_2 + a_4 * X_2 + a_5 * X_1 * X_2 + a_6 * X^2{}_3 + a_7 * X_3 + a_8 * X_1 * X_3 + a_9 * X_2 * X_3 + \mathrm{c}$$

For second-order regression with 3 independent variables, the number of coefficients are 10, as shown in the previous equation.

$$Y = a_1 * X^2{}_1 + a_2 * X_1 + a_3 * X^2{}_2 + a_4 * X_2 + a_5 * X_1 * X_2 + a_6 * X^2{}_3 + a_7 * X_3 + a_8 * X_1 * X_3 + a_9 * X_2 * X_3 + a_{10} * X^2{}_4 + a_{11} * X_4 + a_{12} * X_1 * X_4 + a_{13} * X_2 * X_4 + a_{14} * X_3 * X_4 + c$$

For second-order regression with 4 independent variables, the number of coefficients are 15, as shown in the previous equation.

$$Y = a_1 * X^2{}_1 + a_2 * X_1 + a_3 * X^2{}_2 + a_4 * X_2 + a_5 * X_1 * X_2 + a_6 * X^2{}_3 + a_7 * X_3 + a_8 * X_1 * X_3 + a_9 * X_2 * X_3 + a_{10} * X^2{}_4 + a_{11} * X_4 + a_{12} * X_1 * X_4 + a_{13} * X_2 * X_4 + a_{14} * X_3 * X_4 + a_{15} * X^2{}_5 + a_{16} * X_5 + a_{17} * X_1 * X_5 + a_{18} * X_2 * X_5 + a_{19} * X_3 * X_5 + a_{20} * X_4 * X_5 + c$$

For second-order regression with 5 independent variables, the number of coefficients are 21, as shown in the previous equation.

Similarly, for 6 independent variables, the number of coefficients for the equations are 28. To fit data with 28 coefficients, a second-order polynomial is much easier, as practically one can fit mostly any curve with 28 coefficients. This is called over-fitting, where an analysis that corresponds too closely to a particular set of data and may therefore fail to add data or predict future observation. Thus, any results with more than three variables were not used in the final analysis.

Table D-2 shows the third-order polynomial regression analysis with the $R^2$ fit. The independent variables (X) varied from two to six, and the corresponding $R^2$ fit was calculated. It is evident as the number of variables increases from two to six, the $R^2$ value increases as well. Theoretically, trial 31 (with six independent variables) should be best for regression analysis due to its higher $R^2$ value, but practically that is not accurate, as discussed below.

**Table D-2. Third-order regression trials to achieve the best fit**

| Trial | No. of Var. | Replacement (X1) | Alumina (X2) | Alkali (X3) | Ca (X4) | Mg (X5) | Sulphur (X6) | $R^2$ value | | |
|---|---|---|---|---|---|---|---|---|---|---|
| | | | | | | | | $\phi_\alpha$ | $\phi_\beta$, | $\phi_\tau$ |
| 1 | 2 | Yes | Yes | | | | | 0.75 | 0.72 | 0.71 |
| 2 | | Yes | | Yes | | | | 0.74 | 0.73 | 0.72 |
| 3 | | Yes | | | Yes | | | 0.74 | 0.75 | 0.63 |
| 4 | | Yes | | | | Yes | | 0.78 | 0.72 | 0.64 |
| 5 | | Yes | | | | | Yes | 0.72 | 0.71 | 0.73 |
| 6 | 3 | Yes | Yes | Yes | | | | 0.88 | 0.87 | 0.94 |
| 7 | | Yes | Yes | | Yes | | | 0.87 | 0.89 | 0.88 |
| 8 | | Yes | Yes | | | Yes | | 0.84 | 0.81 | 0.83 |
| 9 | | Yes | Yes | | | | Yes | 0.78 | 0.73 | 0.78 |
| 10 | | Yes | | Yes | Yes | | | 0.81 | 0.83 | 0.84 |
| 11 | | Yes | | Yes | | Yes | | 0.78 | 0.82 | 0.76 |
| 12 | | Yes | | Yes | | | Yes | 0.76 | 0.79 | 0.80 |
| 13 | | Yes | | | Yes | Yes | | 0.77 | 0.72 | 0.79 |
| 14 | | Yes | | | Yes | | Yes | 0.78 | 0.80 | 0.81 |
| 15 | | Yes | | | | Yes | Yes | 0.77 | 0.81 | 0.80 |
| 16 | 4 | Yes | Yes | Yes | Yes | | | 0.98 | 0.98 | 0.97 |
| 17 | | Yes | Yes | Yes | | Yes | | 0.97 | 0.95 | 0.94 |
| 18 | | Yes | Yes | Yes | | | Yes | 0.96 | 0.91 | 0.94 |
| 19 | | Yes | | Yes | Yes | Yes | | 0.95 | 0.96 | 0.93 |
| 20 | | Yes | | Yes | Yes | | Yes | 0.94 | 0.96 | 0.96 |
| 21 | | Yes | Yes | | Yes | Yes | | 0.95 | 0.94 | 0.95 |
| 22 | | Yes | Yes | | Yes | | Yes | 0.93 | 0.94 | 0.94 |
| 23 | | Yes | Yes | | | Yes | Yes | 0.94 | 0.93 | 0.95 |
| 24 | | Yes | | Yes | | Yes | Yes | 0.93 | 0.95 | 0.94 |
| 25 | | Yes | | | Yes | Yes | Yes | 0.92 | 0.94 | 0.91 |
| 26 | 5 | Yes | Yes | Yes | Yes | Yes | | 0.98 | 0.97 | 0.95 |
| 27 | | Yes | Yes | Yes | Yes | | Yes | 0.97 | 0.96 | 0.94 |
| 28 | | Yes | Yes | Yes | | Yes | Yes | 0.96 | 0.95 | 0.94 |
| 29 | | Yes | Yes | | Yes | Yes | Yes | 0.95 | 0.91 | 0.93 |
| 30 | | Yes | | Yes | Yes | Yes | Yes | 0.94 | 0.94 | 0.93 |
| 31 | 6 | Yes | Yes | Yes | Yes | Yes | Yes | 0.98 | 0.98 | 0.98 |

The following equation shows a general expression of the analysis with two independent variables.

$$Y = a_1 * X^3{}_1 + a_2 * X^2{}_1 + a_3 * X_1 + a_4 * X^3{}_1 + a_5 * X^2{}_1 + a_6 * X_1 + a_7 * X^2{}_1 * X_2 + a_8 * X_1 * X^2{}_2 + a_9 * X_1 * X_2 + \mathrm{c}$$

For third-order regression with 2 independent variables, the number of coefficients are 10 as shown in the previous equation. Similarly, the number of coefficients with 3 independent variables would be 20, as shown in the following equation.

$$Y = a_1 * X^3{}_1 + a_2 * X^2{}_1 + a_3 * X_1 + a_4 * X^3{}_1 + a_5 * X^2{}_1 + a_6 * X_1 + a_7 * X^2{}_1 * X_2 + a_8 * X_1 * X^2{}_2 + a_9 * X_1 * X_2 + a_{10} * X^3{}_3 + a_{11} * X^2{}_3 + a_{12} * X_3 + a_{13} * X^2{}_1 * X_3 + a_{14} * X^2{}_2 * X_3 + a_{15} * X_1 * X^2{}_3 + a_{16} * X_2 * X^2{}_3 + a_{17} * X_1 * X_2 * X_2 + a_{18} * X_1 * X_3 + a_{19} * X_2 * X_3 + \mathrm{c}$$

Thus, the third-order analysis was rejected due to over-fitting, and further analysis was limited to second-order with a maximum of three to four variables (depending on the number of coefficients).

## APPENDIX E. HYDRATION PARAMETERS

The hydration parameters (total Q, β, and τ) were obtained by fitting the temperature profile of selected mixes in the 4C software by changing these parameters to achieve the best fit.

Tables E-1 through E-4 show the 4C fitting results, where the hydration parameters Q_∞ (total heat), τ (time for hydration peak), and β (curvature) are calculated by mimicking the laboratory-measured temperature for the large concrete block mixes. To achieve the best fit, several combinations of the hydration parameter values were used. Some of these combinations are presented in Tables E-1 through E-4.

**Table E-1. 4C trials with hydration parameters to imitate the 0% slag laboratory-measured temperature profile**

| Trial No. | $Q_\infty$ (KJ/kg) | τ (time in h) | β (curvature) | Fit ($R^2$) |
|---|---|---|---|---|
| 1 | 300 | 6 | 1.2 | 0.84 |
| 2 | 300 | 7 | 0.8 | 0.89 |
| 3 | 300 | 7 | 0.9 | 0.86 |
| 4 | 300 | 7 | 0.6 | 0.91 |
| 5 | 300 | 7 | 0.7 | 0.94 |
| 6 | 300 | 7 | 0.75 | 0.93 |
| 7 | 300 | 6 | 0.7 | 0.91 |
| 8 | 300 | 7.2 | 0.7 | 0.97 |
| 9 | 300 | 7.1 | 0.7 | 0.95 |
| **10** | **300** | **7.3** | **0.7** | **0.99 (Best)** |
| 11 | 300 | 7.3 | 0.72 | 0.97 |
| 12 | 290 | 7 | 1.5 | 0.85 |
| 13 | 270 | 7 | 2 | 0.65 |
| 14 | 250 | 7 | 0.5 | 0.87 |
| 15 | 295 | 7.2 | 0.7 | 0.92 |
| 16 | 300 | 7.2 | 0.75 | 0.94 |
| 17 | 295 | 8 | 0.68 | 0.90 |
| 18 | 300 | 8.0 | 0.65 | 0.91 |
| 19 | 300 | 8.5 | 0.65 | 0.93 |
| 20 | 320 | 8.0 | 0.7 | 0.88 |
| 21 | 295 | 8.1 | 0.73 | 0.87 |
| 22 | 300 | 7.5 | 0.7 | 0.93 |
| 23 | 310 | 7.2 | 0.71 | 0.95 |
| 24 | 300 | 7.3 | 0.65 | 0.93 |

**Table E-2. 4C trials with hydration parameters to imitate the 25% slag laboratory-measured temperature profile**

| Trial No. | $Q_\infty$ (KJ/kg) | τ (time in h) | β (curvature) | Fit ($R^2$) |
|---|---|---|---|---|
| 1 | 300 | 15.0 | 1.00 | 0.82 |
| 2 | 400 | 15.0 | 0.80 | 0.84 |
| 3 | 350 | 15.0 | 0.90 | 0.88 |
| 4 | 300 | 25.0 | 0.60 | 0.86 |
| 5 | 325 | 20.0 | 0.70 | 0.84 |
| 6 | 330 | 10.0 | 0.70 | 0.89 |
| 7 | 330 | 15.0 | 0.70 | 0.94 |
| 8 | 320 | 20.0 | 0.70 | 0.92 |
| 9 | 350 | 12.0 | 0.70 | 0.85 |
| 10 | 330 | 18.0 | 0.70 | 0.88 |
| 11 | 330 | 15.0 | 0.70 | 0.94 |
| 12 | 350 | 12.0 | 0.65 | 0.91 |
| 13 | 340 | 15.0 | 0.68 | 0.92 |
| 14 | 335 | 14.0 | 0.75 | 0.91 |
| 15 | 325 | 14.0 | 0.80 | 0.93 |
| 16 | 315 | 15.0 | 0.70 | 0.96 |
| 17 | 320 | 15.0 | 0.70 | 0.97 |
| **18** | **320** | **14.5** | **0.70** | **0.99 (Best)** |
| 19 | 320 | 14.5 | 0.72 | 0.97 |
| 20 | 330 | 14.5 | 0.70 | 0.96 |
| 21 | 325 | 14.5 | 0.68 | 0.96 |
| 22 | 325 | 14.0 | 0.75 | 0.95 |
| 23 | 320 | 14.0 | 0.75 | 0.96 |
| 24 | 310 | 15.0 | 0.75 | 0.93 |
| 25 | 330 | 14.0 | 0.70 | 0.95 |

**Table E-3. 4C trials with hydration parameters to imitate the 50% slag laboratory-measured temperature profile**

| Trial No. | $Q_\infty$ (KJ/kg) | τ (time in h) | β (curvature) | Fit ($R^2$) |
|---|---|---|---|---|
| 1 | 400 | 25.0 | 0.50 | 0.70 |
| 2 | 300 | 25.0 | 0.50 | 0.73 |
| 3 | 350 | 25.0 | 0.50 | 0.80 |
| 4 | 350 | 25.0 | 0.60 | 0.83 |
| 5 | 325 | 25.0 | 0.60 | 0.81 |
| 6 | 375 | 25.0 | 0.60 | 0.88 |
| 7 | 330 | 25.0 | 0.60 | 0.93 |
| 8 | 330 | 25.0 | 0.70 | 0.95 |
| 9 | 330 | 20.0 | 0.75 | 0.96 |
| 10 | 330 | 18.0 | 0.75 | 0.95 |
| 11 | 330 | 20.0 | 0.72 | 0.97 |
| 12 | 332 | 20.0 | 0.72 | 0.98 |
| **13** | **332** | **20.0** | **0.70** | **0.99 (Best)** |
| 14 | 335 | 20.0 | 0.70 | 0.98 |
| 15 | 340 | 19.0 | 0.70 | 0.95 |
| 16 | 330 | 19.0 | 0.70 | 0.97 |
| 17 | 330 | 19.0 | 0.72 | 0.98 |
| 18 | 330 | 19.0 | 0.75 | 0.97 |
| 19 | 340 | 20.0 | 0.68 | 0.96 |
| 20 | 340 | 20.0 | 0.65 | 0.94 |
| 21 | 325 | 20.0 | 0.75 | 0.95 |
| 22 | 325 | 22.0 | 0.80 | 0.91 |
| 23 | 330 | 22.0 | 0.85 | 0.93 |
| 24 | 325 | 25.0 | 0.80 | 0.91 |
| 25 | 325 | 25.0 | 0.70 | 0.94 |

**Table E-4. 4C trials with hydration parameters to imitate the 75% slag laboratory-measured temperature profile**

| Trial No. | $Q_\infty$ (KJ/kg) | τ (time in h) | β (curvature) | Fit ($R^2$) |
|---|---|---|---|---|
| 1 | 400 | 30.0 | 0.50 | 0.74 |
| 2 | 300 | 30.0 | 0.50 | 0.71 |
| 3 | 350 | 30.0 | 0.50 | 0.82 |
| 4 | 350 | 30.0 | 0.60 | 0.88 |
| 5 | 350 | 20.0 | 0.60 | 0.90 |
| 6 | 360 | 20.0 | 0.60 | 0.94 |
| 7 | 360 | 20.0 | 0.70 | 0.96 |
| 8 | 360 | 30.0 | 0.70 | 0.94 |
| 9 | 350 | 30.0 | 0.65 | 0.93 |
| 10 | 355 | 30.0 | 0.70 | 0.95 |
| 11 | 355 | 30.0 | 0.72 | 0.96 |
| 12 | 355 | 25.0 | 0.72 | 0.97 |
| 13 | 350 | 25.0 | 0.72 | 0.98 |
| 14 | 350 | 25.0 | 0.71 | 0.98 |
| **15** | **350** | **25.0** | **0.7** | **0.99 (Best)** |
| 16 | 350 | 25.0 | 0.69 | 0.98 |
| 17 | 340 | 24.0 | 0.70 | 0.96 |
| 18 | 360 | 28.0 | 0.70 | 0.95 |
| 19 | 340 | 22.0 | 0.70 | 0.94 |
| 20 | 355 | 25.0 | 0.70 | 0.98 |
| 21 | 360 | 28.0 | 0.70 | 0.91 |
| 22 | 360 | 26.0 | 0.70 | 0.95 |
| 23 | 355 | 26.0 | 0.70 | 0.97 |
| 24 | 355 | 24.0 | 0.70 | 0.98 |
| 25 | 350 | 24.0 | 0.70 | 0.97 |

Table E-1 shows some of the 4C trial combinations for the 0% slag replacement concrete mix. The total heat, tau, and beta were varied over a range to achieve the best fit. To start the fit, initially the maximum temperature at the center was mimicked by changing the $Q_\infty, \tau,$ and $\beta$. Once the maximum temperature was close enough, the slope of the temperature rise and fall were duplicated. Using the same parameters, the bottom corner temperature profile was also mimicked with little variation. The best fit for the temperature at the core and bottom corner were considered. As seen in Table E-1, trial 10 showed the best fit (also reported in Table 6-7).

The same steps were followed for 25%, 50%, and 75% slag replacement mixes, and the respective trials to achieve the best fit are shown in Tables E-2, E-3, and E-4. The best fit results ($Q_\infty, \tau,$ and $\beta$) for each concrete mix are presented in Table 6-7.

Figure E-1 shows some of the selected trials for the 0% slag concrete mix where the temperature profile of the trials is plotted along with the laboratory-measured trials for the core (Figure E-1a) and bottom corner (Figure E-1b) locations.

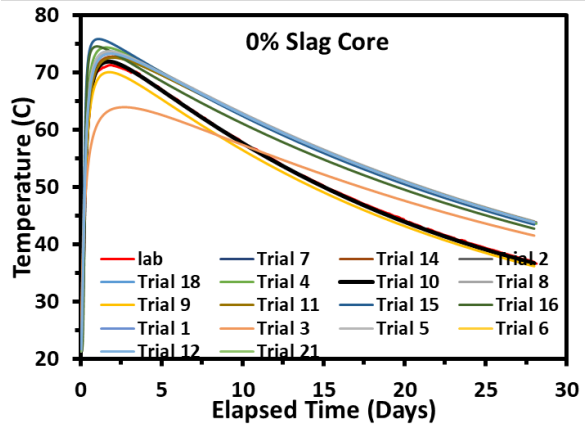


(a) 4C trials for 0% slag mix lab data (at core)

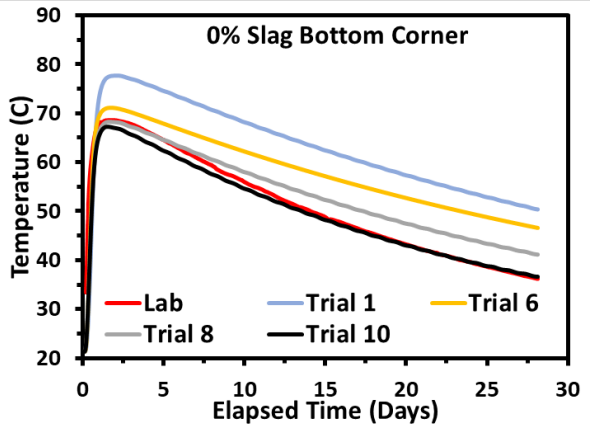


(b) 4C trials for 0% slag mix lab data (at bottom corner)

**Figure E-1. 4C trials to get the best fit for laboratory-observed concrete block data**

For the 0% slag mix, trial 10 seems to be best fit as seen from Figure E-1. To understand the effect of each hydration parameter ($Q_\infty$, $\tau$, and $\beta$) on the temperature profile in 4C, a sensitivity analysis was done for the 0% slag concrete mix (shown in Figure E-2). Figure E-2a shows the effect of the total heat ($Q_\infty$) on the temperature profile, Figure E-2b shows the effect of the time parameter ($\tau$) on the temperature profile, and Figure E-2c shows the effect of curvature parameter ($\beta$) on the temperature profile.

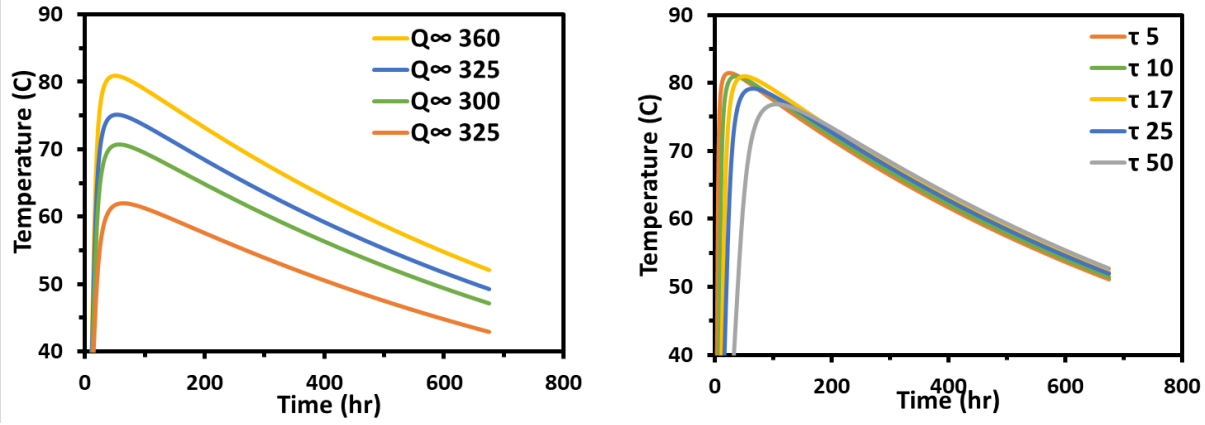


(a) Sensitivity analysis for total heat parameter

(b) Sensitivity analysis for time (τ) parameter

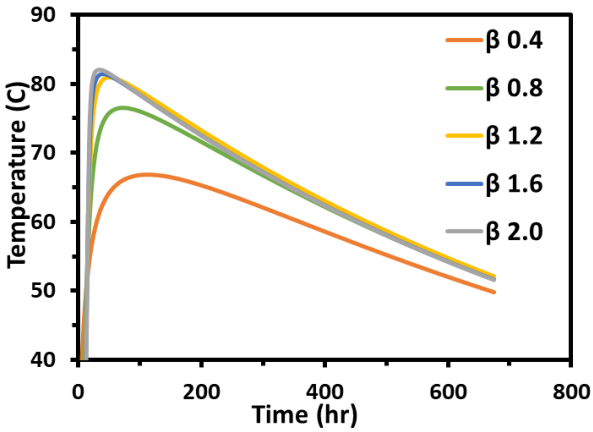


(c) Sensitivity analysis for curvature (β) parameter

**Figure E-2. 4C sensitivity analysis for the hydration parameters (Q∞, τ, β)**

As seen in Figure E-2a, when the total heat increases in the model, the maximum temperature also increases, and the curve shifts slightly to the left, showing a rapid temperature gain. It can be interpreted that a higher temperature concrete mix will have higher total heat released.

As seen in Figure E-2b, when tau (time parameter) increases, the curve shifts to the right, and the maximum temperature decreases. It can be interpreted that a concrete mix with a slow hydration rate (i.e., the time to achieve the hydration peak is longer) would result in a lower maximum temperature, and the time to achieve the maximum temperature would also increase. Also, the total heat and tau did not show any significant effect on the curvature of the temperature profile. Figure E-2c shows that as the curvature parameter (beta) increases, the temperature profile of the concrete mix shifts to the left and the maximum temperature increases. As seen from the plot, the slight variation in beta shows a significant effect on the maximum temperature and time to achieve the hydration peak. Thus, it shows the maximum temperature is affected by all three hydration parameters ($Q_\infty, \tau,$ and β) and is very sensitive to the change in the curvature parameter.

**THE INSTITUTE FOR TRANSPORTATION IS THE FOCAL POINT FOR TRANSPORTATION AT IOWA STATE UNIVERSITY.**

**InTrans** centers and programs perform transportation research and provide technology transfer services for government agencies and private companies;

**InTrans** contributes to Iowa State University and the College of Engineering's educational programs for transportation students and provides K–12 outreach; and

**InTrans** conducts local, regional, and national transportation services and continuing education programs.


IOWA STATE UNIVERSITY

Visit **InTrans.iastate.edu** for color pdfs of this and other research reports.